Contribution of Interface Acoustic Phonons and Remote-polar Phonons in the Hole Mobility of Diamond

BY

GIORGIO BONOMO
B.S, Politecnico di Torino, Turin, Italy, 2017

THESIS

Submitted as partial fulfillment of the requirements
for the degree of Master of Science in Electrical and Computer Engineering
in the Graduate College of the
University of Illinois at Chicago, 2019

Chicago, Illinois

Defense Committee:

Michael Stroscio, Chair and Advisor

Junxia Lucy Shi

Fabrizio Bonani, Politecnico di Torino

ACKNOWLEDGMENTS

First of all, I would like to thank Prof. Michael Stroscio, to have introduced me to these interesting and stimulating topics. His profound knowledge of the subject, together with its teachings and suggestions have been fundamental through the entire writing of this work.

I would like to thank Prof. Mitra Dutta as well, for the suggestions and clarifications that came during each meeting, allowing me to gain a more conscious point of view of the matter.

I am grateful to Prof. Fabrizio Bonani, for his support during the entire thesis development. Thanks to his class, my interest for the subject actually spread, leading to the will of gaining a deeper knowledge on the topic.

I would also like to thank Prof. Dutta and Prof. Stroscio's group students: the meeting together had been of great inspiration, giving me the chance to get in touch with new and stimulating research projects and allowing me to have a glance at the challenges of their research activities.

A sincere gratitude goes to my friends and colleagues Giorgio Carnevali, Marco Montagna and Francesca Pistilli, for the patience and affection shown during this entire experience at Chicago and especially during the writing of the thesis.

I will always be grateful to my friends and former colleagues Giacomo Borraccini and Riccardo Sciuto: despite the distance, the chance to discuss with them has always been a great help in the process of obtaining a more clear point of view on my work.

ACKNOWLEDGMENTS (continued)

Finally, a special thank goes to my family, that always supported me in any forward step, and my friends in Catania, Turin and Chicago, who have always been by my side.

GB

TABLE OF CONTENTS

TABLE OF CONTENTS (continued)

LIST OF TABLES

LIST OF FIGURES

LIST OF FIGURES (continued)

FIGURE **PAGE**

LIST OF ABBREVIATIONS

AlN	Aluminium Nitride
BN	Boron Nitride
FET	Field Effect Transistor
MISFET	Metal-Insulator FET
MOSFET	Metal-Oxide FET
MESFET	Metal-Semiconductor FET
HFET	Heterojunction FET
SCFET	Surface Channel FET
SAW	Surface Acoustic Wave
FCC	Face-Centered Cubic
2DHG	2-D Hole gas

SUMMARY

The present work is focused on the formulation of the relaxation time due to the hole–surface-acoustic phonon and hole–remote-polar phonon scattering mechanisms in mesoscopic diamond-based devices.

First of all, an introduction on the promising role of diamond in the realization of high power and high frequency devices is given, together with a focus on the current difficulties and attempts in the understanding and fabrication of devices based on this material.

An extensive study on the existence of surface waves in such structures follows, in order to understand which surface-acoustic modes are possible; this is followed by the quantization of these waves in order to take into account the reduced number of phonons in a nanoscale structure, the formulation of the interaction Hamiltonian, and the final calculation of the relaxation time through Fermi Golden Rule.

Then, the insertion of an upper layer constituted by a wide-band gap material such as AlN or BN on top of diamond is analyzed. This procedure, performed for the realization of various types of FETs, causes a potential due to the interface-optical phonon modes in the upper layer, usually constituted by a polar material, that decays into diamond, resulting in the existence of a remote polar phonon potential in the material. This leads to an interaction Hamiltonian in diamond due to its decaying phonon potential, which facilitates the formulation of an expression for the relaxation time due to this phenomenon.

CHAPTER 1

INTRODUCTION

Diamond, with its outstanding physical properties such as high breakdown voltage, high thermal conductivity, high carrier mobility and high acoustic wave velocity, represents an interesting material for the realization of both high frequency and high power devices.

However, the realization of such devices became possible only in recent years due to major improvements in the lithography and fabrication techniques, leading to a recent renovated interest for the material. Several examples of Field Effect Transistor (FET) and Surface Acoustic Wave (SAW) devices are available in literature [1] [2] [3]: attempts for the realization of Surface Channel Metal-Semiconductor FETs (SC-MESFETs) directly depositing the gate metal on the diamond substrate, Metal-Insulator FETs (MISFETs) depositing the gate metal on top of a gate dielectric realized through an AlN layer [4], and Heterostructure FETs (HFETs) exploiting an AlN [5] or h-BN [6] -diamond heterojuction are reported, confirming the current research interest in the material.

1.1 Diamond Doping

One of the main topics still under investigation concerns the doping mechanisms that can be applied to diamond: in fact, the conventional substitutional doping is challenging because of the high activation of dopants such Boron (acceptor) or Phosphorus (donor), leading to relatively low carrier densities at room temperature.

Alternatively, surface transfer doping of H-terminated diamond seems a promising solution. A good starting point in the comprehension of the mechanisms leading to the formation of a high mobility 2-D Hole Gas (2DHG) under the surface of H-terminated diamond is reported in [7], in which it is found that the presence of H-terminated diamond is only one necessary requirement for the appearance of the surface conductivity: exposure to atmospheric agents is essential in order to provide a water layer on the surface of diamond, necessary for the creation of the 2DHG, according to the physical phenomenon depicted in Figure 1. For a correct understanding of the mechanism depicted in Figure 1, it is important to recall H-terminated diamond is characterized by a negative electron affinity [8]: this causes its vacuum level to be at a lower energy than the conduction band, as is apparent from the diagram.

This important result, explaining the appearance of the surface conductivity as the result of an exchange of interfacial charges between the valence band (E_V) of diamond and the available energetic states of atmospheric water, balancing the Fermi Energy of the first with the chemical potential (μ_e) of the latter, represents a milestone for the comprehension and the development of more controlled and stable doping techniques on diamond.

Further researches demonstrated the possibility of exploiting the fullerene molecule C_{60}[9] and its fluorinated variants [10], or transition metal-oxides characterized by an high electron affinity such as vanadium oxide V_2O_5[11] or molybdenum trioxide MoO_3[12] to induce surface transfer doping, improving the thermal stability and carrier concentration in respect to the doping obtained by atmospheric adsorbates.

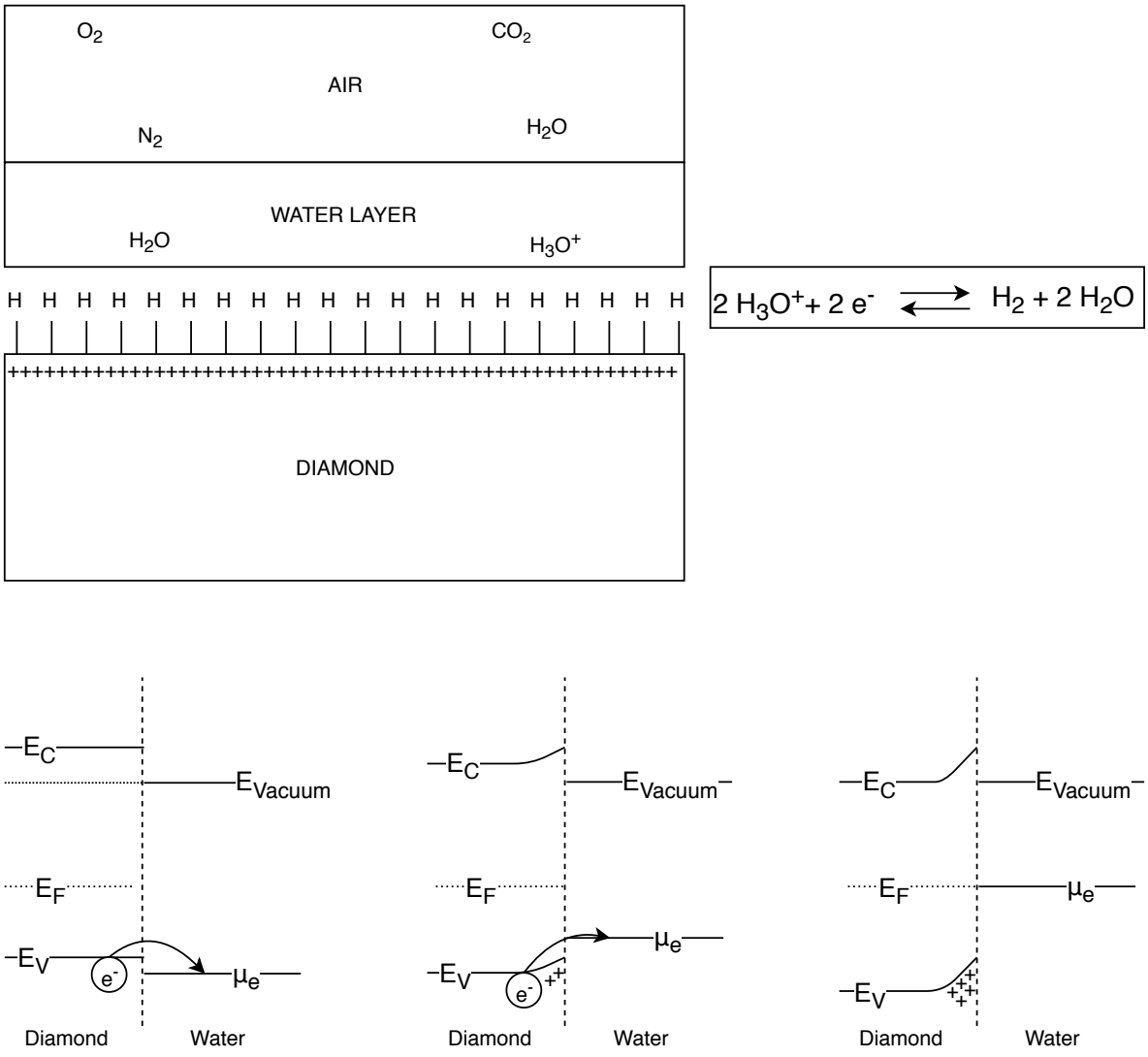

Figure 1: Surface channel charge creation mechanism in H-terminated diamond.

Moreover, further increasing in the hole concentrations is observed after the exposure of the diamond surface to gases as O_3 [13] and NO_2 [14].

1.2 Diamond Passivation

Another serious limitation preventing the introduction of this type of SC-FET in high power and frequency applications is the sensibility of their electrical properties to their surrounding environment due to propensity of the 2DHG to degrade when exposed to high operating temperatures or vacuum; this issue is discussed directly in [15] and [4], in which respectively Al_2O_3 and AlN are proposed as exploitable materials for the fabrication of a passivation layer, able to encapsulate the 2DHG. Other solutions contemplate the insertion of oxygen-terminated diamond, characterized by an highly insulated surface, able to provide the required passivation; this method, proposed in [6], is depicted in Figure 2; the entire diamond surface, with the exception of the part covered by h-BN, is O-terminated to provide insulation.

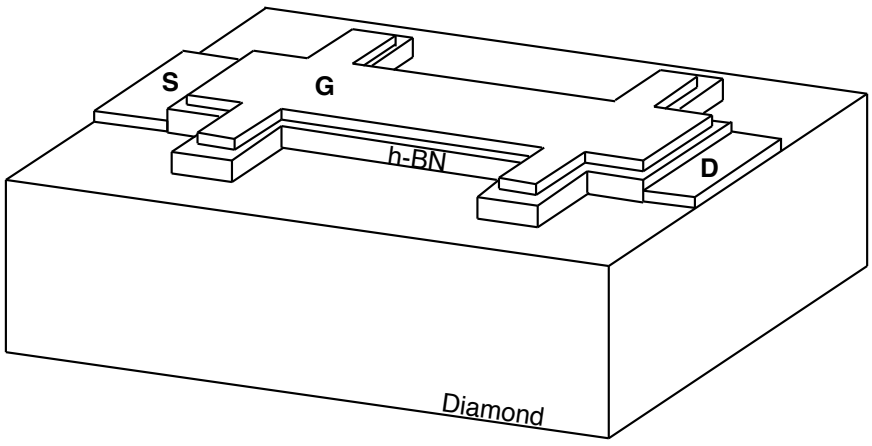

Figure 2: Diamond-FET with h-BN exploited as gate dielectric.

1.3 Current Work

The aim of this work concerns the study and formulation of the contribution of two interactions mechanisms such as hole–interface (IF) acoustic-phonon interaction due to the surface waves in the structure, and hole–remote interface polar-phonon interaction due to the insertion of a polar material on top of the diamond substrate; these effects, often neglected during the study of the mobility in diamond-based devices, are under investigation to understand their effectiveness and importance.

In order to describe these two mechanisms, both the elastic continuum model and the dielectric continuum model [16] are exploited; the first model describes acoustic phonons in terms of elastic waves in a continuum medium, and is used for the description of the surface-acoustic phonons, while the second is based on the idea that lattice vibrations give rise to an electrostatic polarization that can be described through the classical equations of electrostatics, and is used to model remote-interface polar-phonons.

After this initial step, second quantization is performed, to take into account the reduced number of phonons in the structure; finally, the interaction Hamiltonian is formulated, and the scattering rate is calculated through the Fermi Golden Rule approximation.

As a matter of fact, Fermi Golden Rule provides a compact result for the calculation of carrier–phonon scattering rates, modelled as weak perturbations of the Hamiltonian describing the system in absence of interactions. Its derivation, reported in Ref.[16], is based on the assumption $t << \frac{2\hbar}{E_f - E_i}$, where t represents the transit time in the device and $E_f - E_i$ represents the energy difference between final and initial states. However in many cases the obtained

result constitutes a reasonable approximation even if this condition is not met, especially compared to the alternative methods based on Feynman path integral, whose high computational requirements make those solutions rarely exploited in practice.

By the mathematical formulation of the two mechanisms, these contributions are finally taken into account, in an effort to obtain a complete picture of the phenomena determining the mobility inside nanoscale diamond-based devices, and giving new guidelines for their development.

CHAPTER 2

PREVIOUS WORK

2.1 Diamond Mobility

Due to the already mentioned properties of the material, several studies have been performed on the holes mobility in diamond. In Ref.[17], the Hall hole mobility of homoepitaxial boron-doped diamond is discussed, taking into account ionized impurities, neutral impurities, bulk acoustic phonons and non-polar optical phonons. Ref.[17] considers both intraband and interband processes in describing hole scattering mechanisms. By comparison with the measured Hall mobility, an estimation of the acoustic deformation potential is given, together with the observation that at room temperature the mobility is completely limited by acoustic phonon scattering. Ref.[17] also gives an interesting comparison of holes mobility for diamond, Si and 4H-SiC, that finds as motivations for the higher mobility of diamond its high optical phonon energy, that causes the optical phonons branch to be poorly populated at room temperature.

Another interesting work is Ref.[18], in which the mobility of a two-dimensional hole gas (2DHG) in H-terminated diamond is calculated, considering surface impurities, acoustic deformation potential, bulk non-polar optical phonon and surface/interface roughness as scattering mechanisms. The novelty in the proposed approach concerns the approximation of the hole accumulation layer as a 2DHG described through the Fang-Howard wave function. The results

reported by these authors are in good agreement with the experimental data, confirming the validity of the approximations.

Furthermore, in both of these works a simplified model to describe the dispersion of the topmost valence bands is taken into account. Based on the result obtained in Ref.[19] applying ab initio calculations exploiting a linear-muffin-tin-orbital model, the small energy separation between the two uppermost bands (referred to as light hole (lh) and heavy hole (hh)) and the third one (referred to as split-off (so)) in diamond is neglected, considering the three bands degenerate in the Γ point of the Brillouin zone. In this way, the three valence bands are considered to be a single parabolic band, characterized by effective masses whose values are reported in Table I, in which m_{hh} refers to the heavy holes, m_{lh} for the light holes and m_{so} for the spin-orbit holes, with m_0 representing the electron rest mass. The obtained values for the density-of-state mass, calculated as $m^*_{hh} = \left[(m^{*110}_{hh})^2\, m^{*100}_{hh}\right]^{\frac{1}{3}}$ and $m^*_{lh} = \left[(m^{*110}_{lh})^2\, m^{*100}_{lh}\right]^{\frac{1}{3}}$, are reported in the final column of the table, together with the total density-of-state mass $m^* = (m^{*3/2}_{lh} + m^{*3/2}_{hh} + m^{*3/2}_{so})^{\frac{2}{3}}$.

This useful model is adopted also in this work, in order to take into account the existence of both intraband and interband processes and the almost degeneracy of the valence band.

TABLE I: ADOPTED EFFECTIVE MASSES FOR DIAMOND

m^{*100}_{hh}	$0.427\, m_0$	m^{*110}_{hh}	$0.69\, m_0$	m^*_{hh}	$0.588\, m_0$
m^{*100}_{lh}	$0.366\, m_0$	m^{*110}_{lh}	$0.278\, m_0$	m^*_{lh}	$0.303\, m_0$
m^*_{so}	$0.394\, m_0$	m_0	9.11×10^{-31}	m^*	$0.908\, m_0$

2.2 Confined phonon modes

It is well known that, when dealing with devices realized through nanoscale structures, the dimensional confinement modifies the phase space of phonons, giving rise to confined and interface phonon modes, whose interaction with the carriers should be taken into account.

As a matter of fact, several works are available in the literature showing the significance of acoustic phonon-carriers interactions in nanoscale devices such as quantum wires [20] [21], quantum wells [22] and Si nanolayers [23], proving that their influence on carrier transport may differ from that obtained solely from bulk modes.

On the other hand, the importance of scattering of carriers by remote-interface polar phonons has already been proved in literature [24] [25] as well: in these works, the effect of remote phonons coming from the SiO_2 gate oxide and scattering with the inversion layer charges in Si in a MOSFET structure is calculated, showing the importance of the phenomenon in the determination of the mobility in these devices, especially in the case of large inversion population densities.

Based on this results, the investigation of these phenomena in diamond-based FETs devices represents an interesting research topic for the understanding of the mechanisms involved in the limitation of holes mobility.

CHAPTER 3

ACOUSTIC INTERFACE PHONON MODES QUANTIZATION AND RELAXATION TIME

In order to take into account the interaction between acoustic-IF phonon modes and the 2DHG at the diamond surface, a preliminary step concerns the identification of the possible surface modes in the diamond structure.

In particular, the study of Rayleigh surface waves is performed, analyzing the possible existence of symmetric (M1) and antisymmetric (M2) surface modes. To start this analysis, the structure depicted in Figure 3 is considered.

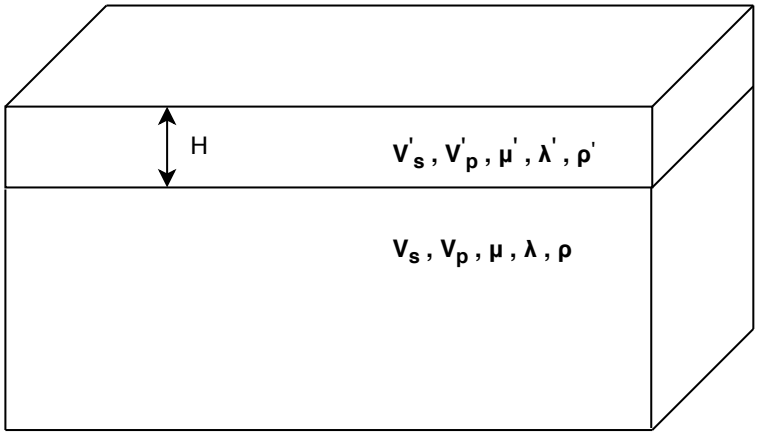

Figure 3: Elastic surface layer over a semi-infinite elastic solid.

A useful recapitulation of diamond's fundamental constants adopted through the entire work is reported in Table II.

TABLE II: ADOPTED DIAMOND CONSTANTS

Crystal density	$\rho = 3515\,kg\,m^{-1}$	[18]
Bandgap	$5.47\,eV$	[26]
Static dielectric constant	5.7	[26]
Thermal conductivity	$2000\,W\,m^{-1}\,K^{-1}$	[27]
Holes mobility	$1600\,cm^2\,V^{-1}\,s^{-1}$	[27]
Hole saturation velocity	$1.0 \times 10^7\,cm\,s^{-1}$	[27]
Young modulus	$1220\,GPa$	[27]
Longitudinal wave velocity	$V_l = 18210\,m\,s^{-1}$	[28]
Transverse wave velocity	$V_s = 12300\,m\,s^{-1}$	[28]
Acoustic deformation potential	$E_a = 8.7\,eV$	[28]

3.1 Rayleigh Waves and Higher Modes Existence

Considering the general case of generalized Lamb waves, it is well-known that if the shear velocity V_s in the substrate and the shear velocity V_s' in the plate are significantly different ($V_s' >> V_s$), a single generalized Lamb wave solution exists, that reduces to a Rayleigh wave on the substrate in the case in which $\beta H \to 0$, where β is the wave propagation constant and H is the thickness of the elastic plate placed above the diamond structure. This Rayleigh wave exists only for a range in which the product βH leads to the fulfillment of the relation $\frac{\omega}{\beta} < V_s$, with ω the angular frequency of the wave.

However, when $V_s' << V_s$, an infinite number of solutions are possible, that are divided into two families of modes, often known as the M_1 and M_2 series. The first modes of both the series are characterized by interesting properties: in the case in which the thickness H of the plate goes to 0, the M_{11} mode tends to a Rayleigh surface wave in the substrate, while higher M_1 modes and all the M_2 modes are leaky waves. Increasing the thickness H of the plate, the first mode to become possible is the M_{21} mode, also known as Sezawa wave (whose quantization is performed in **APPENDIX A**). Finally, for very high frequencies or thick plates ($\beta H \to \infty$). the M_{11} mode tends to a Rayleigh surface wave on the upper boundary of the plate, while all the higher modes (from M_{21} and M_{22} above) degenerate into almost completely vertically polarized shear waves in the plate; on the other hand, the behavior of the Sezawa waves depends strongly on the relative material properties of the substrate and the plate. In particular, for certain combinations of material parameters, the Sezawa wave tends to a Stoneley wave tightly bound to the plate-substrate interface.

These results, reported in the detailed analysis performed by Auld [29] and in agreement with the outcome of the extended study performed by Kanai [30], are summarized in Figure 4. It is observed that, for $\beta H \to \infty$, all the modes from M_{21} above, tend to the shear velocity in the plate V_s' as predicted, while for $\beta H \to 0$, only the Rayleigh wave (M11 mode) exists in the substrate.

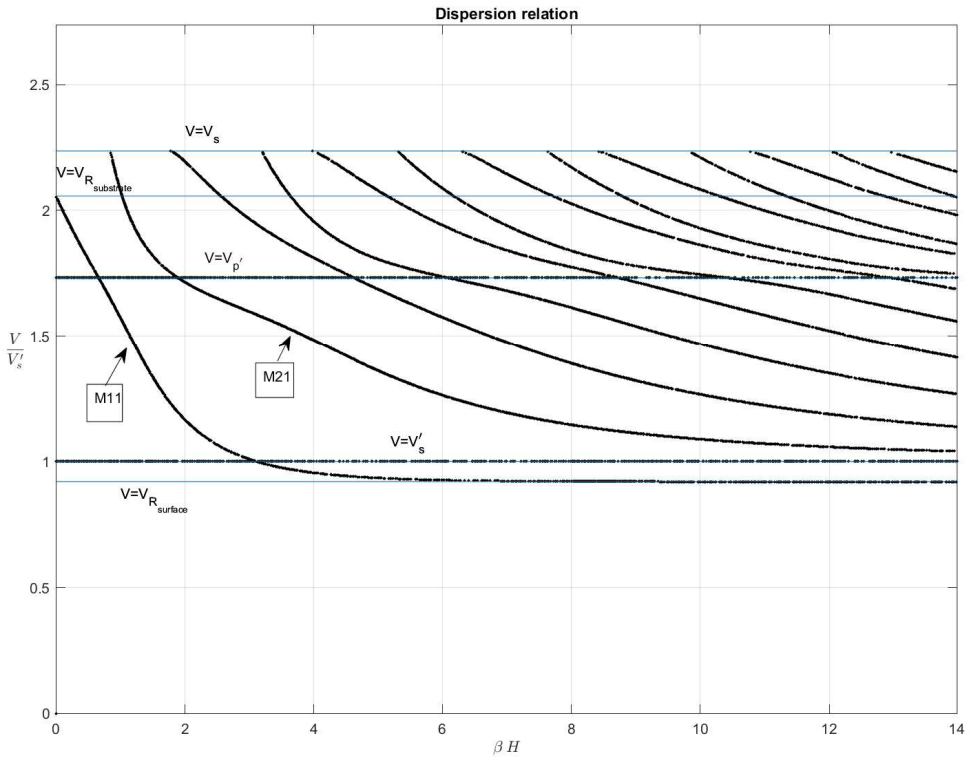

Figure 4: SAWs dispersion relation for $\mu/\mu' = 5$, $\rho/\rho' = \lambda/\mu = \lambda'/\mu' = 1$; modes exist only between V_s and $V_{R\,surface}$.

The expression for the dispersion relation, obtained by forcing the determinant of the 6x6 matrix reported in Ref.[31] to be null, somewhat differs from the one reported in the same and following papers from the authors, that probably contain errors due to the propagation of misprints. The results obtained confirm the existence of a single surface acoustic mode (the Rayleigh wave indeed) in a structure such as the one depicted in Figure 5.

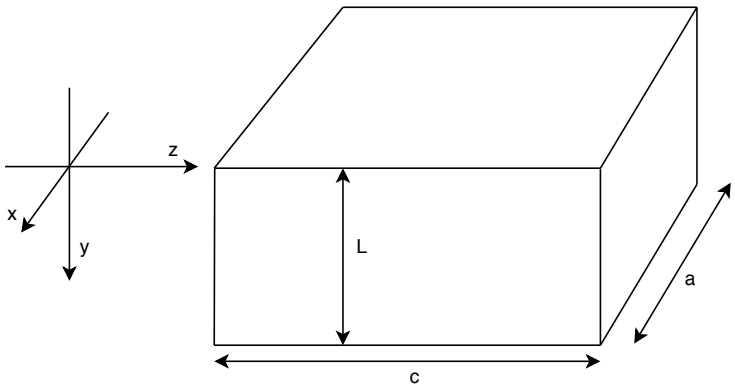

Figure 5: Diamond film structure under analysis for Rayleigh waves.

For this reason, in the following description, Rayleigh waves in a diamond structure are going to be analyzed solely.

3.2 Quantization of Acoustic Modes

Starting from the particle displacement expression, the second quantization procedure is carried out, in order to take into account the strong reduction in the number of phonons inside the structure due to the scaling down of the dimensions.

Recalling the analysis performed by Graff [32] for Rayleigh waves, it is possible to formulate the displacement of the particles for a wave traveling to the right on an isotropic substrate along the z axis:

$$u_y = -A\left(\alpha_{tl}e^{-\alpha_{tl}y} - 2\frac{\alpha_{tl}\beta_R^2}{\beta_R^2 + \alpha_{ts}^2}e^{-\alpha_{ts}y}\right)e^{i(\beta_R z - \omega t)} \tag{3.1}$$

$$u_z = iA\beta_R\left(e^{-\alpha_{tl}y} - 2\frac{\alpha_{ts}\alpha_{tl}}{\beta_R^2 + \alpha_{ts}^2}e^{-\alpha_{ts}y}\right)e^{i(\beta_R z - \omega t)} \tag{3.2}$$

where β_R, α_{tl} and α_{ts} represent respectively the Rayleigh wave propagation constant and the imaginary parts of the transverse wave vector components for the longitudinal and shear partial waves. For these waves:

$$\begin{cases} \beta_R^2 - \alpha_{tl}^2 = (\frac{\omega}{V_l})^2 \\ \beta_R^2 - \alpha_{ts}^2 = (\frac{\omega}{V_s})^2 \\ V_R = \frac{\omega}{\beta_R} \end{cases} \tag{3.3}$$

where V_R is the Rayleigh wave velocity, V_s is the shear wave velocity in the substrate and V_l is the longitudinal wave velocity in the substrate.

The characteristic equation of Rayleigh waves in the structure can be expressed as:

$$4\beta_R^2\alpha_{ts}\alpha_{tl} = (\alpha_{ts}^2 + \beta_R^2)^2 \tag{3.4}$$

often approximated for simplicity as:

$$\frac{V_R}{V_s} = \frac{0.87 + 1.12\sigma}{1 + \sigma} \tag{3.5}$$

where σ is the *Poisson's ratio* for the material. A comparison of the two expressions is shown in Figure 6, confirming the validity of the approximation.

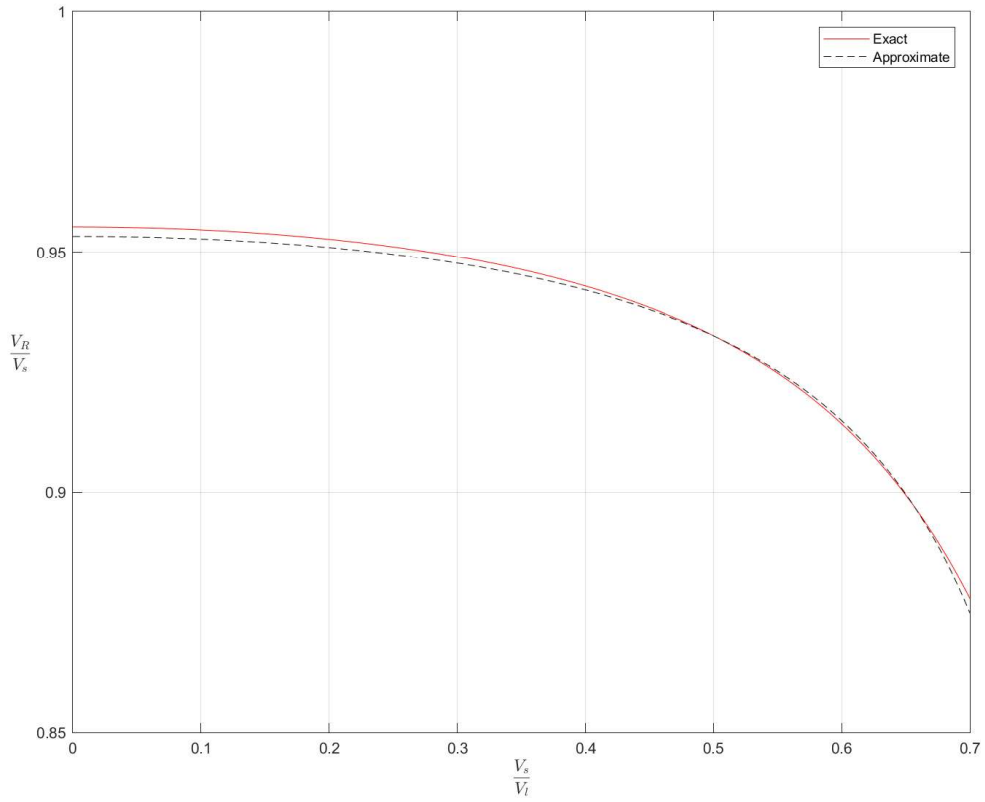

Figure 6: Rayleigh velocity V_R as a function of V_s and V_l.

Other useful relations that come from standard elastic theory are recalled here:

$$\begin{aligned} V_s &= \sqrt{\frac{\mu}{\rho}} \\ V_l &= \sqrt{\frac{\lambda + 2\mu}{\rho}} \\ \sigma &= \frac{\lambda}{2(\mu + \lambda)} = \frac{1 - 2(V_s/V_l)^2}{2[1 - (V_s/V_l)^2]} \end{aligned} \tag{3.6}$$

where λ and μ represent respectively the first and second Lamé parameter, while ρ is the material density. Finally, the dispersion relation for Rayleigh Wave is reported in Figure 7.

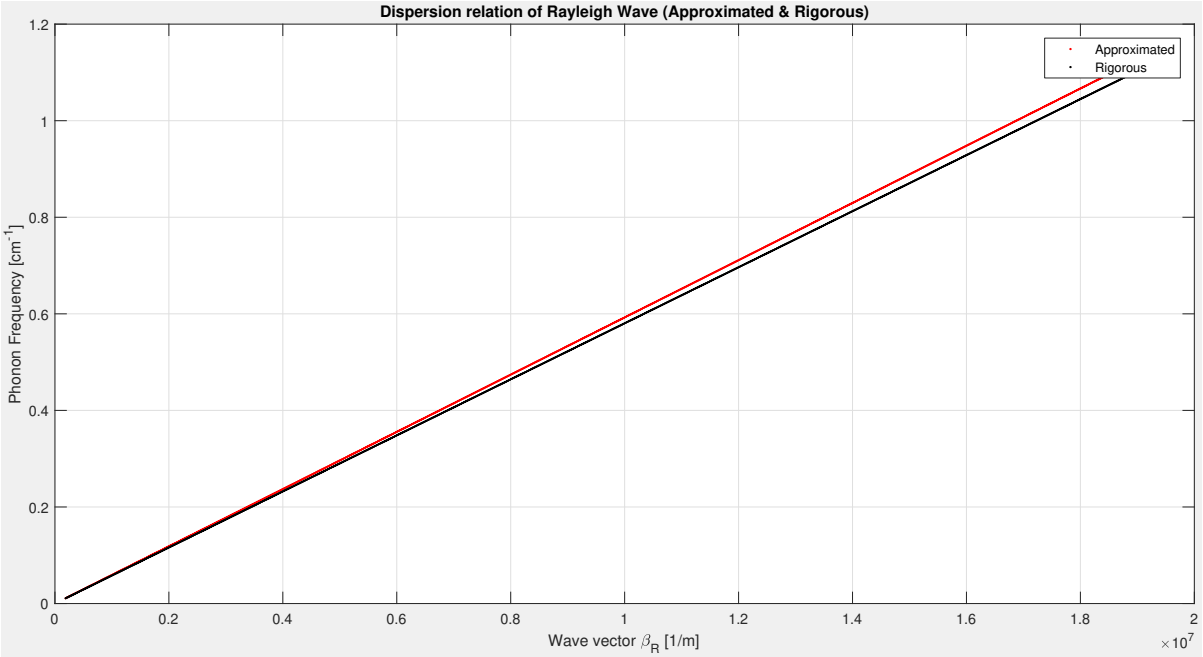

Figure 7: Dispersion relation for Rayleigh Wave for a substrate thickness of 100 μm

It is now convenient to introduce the representation of the displacement vector through the scalar potentials ϕ and Ψ. For these, it holds:

$$\begin{aligned} \nabla^2\phi \,-\, \frac{1}{V_l^2}\frac{\partial^2\phi}{\partial t^2} \,&=\, 0 \\ \nabla^2\Psi \,-\, \frac{1}{V_s^2}\frac{\partial^2\Psi}{\partial t^2} \,&=\, 0 \\ \phi \,=\, A\, e^{-\alpha_{tl}y} e^{i(\beta_R z - \omega t)}) \,&=\, \phi(y) e^{i(\beta_R z - \omega t)} \\ \Psi \,=\, A\left(-\frac{2i\alpha_{tl}\beta_R}{\alpha_{ts}^2 \,+\, \beta_R^2}\right) e^{-\alpha_{ts}y} e^{i(\beta_R z - \omega t)}) \,&=\, \Psi(y) e^{i(\beta_R z - \omega t)} \end{aligned} \tag{3.7}$$

Therefore, the displacements can be expressed as:

$$\boldsymbol{u}(x,y,z) \,=\, \nabla\phi \,+\, \nabla \times (\Psi \cdot \hat{x}) \tag{3.8}$$

Proceeding with the quantization procedure reported in Ref.[16], the orthonormality of the displacements is enforced. First of all, it is useful to compute:

$$\begin{aligned} u_y \cdot u_y^* = A^2\alpha_{tl}^2 \left(e^{-\alpha_{tl}y} \,-\, 2\frac{\beta_R^2}{\beta_R^2 \,+\, \alpha_{ts}^2} e^{-\alpha_{ts}y}\right)^2 \,= \\ A^2\alpha_{tl}^2 \left(e^{-2\alpha_{tl}y} \,-\, \frac{4\beta_R^2}{\beta_R^2 \,+\, \alpha_{ts}^2} e^{-(\alpha_{tl}\,+\,\alpha_{ts})y} \,+\, \frac{4\beta_R^4}{\left(\beta_R^2 \,+\, \alpha_{ts}^2\right)^2} e^{-2\alpha_{ts}y}\right) \end{aligned} \tag{3.9}$$

Similarly,

$$\begin{aligned} u_z \cdot u_z^* = A^2\beta_R^2 \left(e^{-\alpha_{tl}y} \,-\, 2\frac{\alpha_{ts}\alpha_{tl}}{\beta_R^2 \,+\, \alpha_{ts}^2} e^{-\alpha_{ts}y}\right)^2 \,= \\ A^2\beta_R^2 \left(e^{-2\alpha_{tl}y} \,-\, \frac{4\alpha_{ts}\alpha_{tl}}{\beta_R^2 \,+\, \alpha_{ts}^2} e^{-(\alpha_{ts}\,+\,\alpha_{tl})y} \,+\, \frac{4\alpha_{ts}^2\alpha_{tl}^2}{\left(\beta_R^2 \,+\, \alpha_{ts}^2\right)^2} e^{-2\alpha_{ts}y}\right) \end{aligned} \tag{3.10}$$

The quantization integral, for a film without any dependency along the x-axis, becomes:

$$\frac{1}{cL}\int_0^c dz \int_0^{+\infty} dy\, u(\beta_R, y, z)\cdot u^*(\beta_R, y, z) \;=\; 1 \tag{3.11}$$

where L is the normalization length along the vertical axis of the film, c is the normalization length along the horizontal axis of the film, and the formalism ω_{β_R} has been introduced to refer to the angular frequency of the mode with wave vector β_R.

As shown in Equation 3.9 and Equation 3.10, the dependency along the z-axis cancels out, leading to:

$$\frac{1}{c}\int_0^c dz = \frac{1}{c}\cdot c = 1$$

Therefore, the quantization integral becomes:

$$\begin{aligned}\frac{1}{L}\int_0^{+\infty} A^2\alpha_{tl}^2\left(e^{-2\alpha_{tl}y} \;-\; \frac{4\beta_R^2}{\beta_R^2 \;+\; \alpha_{ts}^2}e^{-(\alpha_{tl}+\alpha_{ts})y} \;+\; \frac{4\beta_R^4}{\left(\beta_R^2 \;+\; \alpha_{ts}^2\right)^2}e^{-2\alpha_{ts}y}\right)dy + \\ \frac{1}{L}\int_0^{+\infty} A^2\beta_R^2\left(e^{-2\alpha_{tl}y} \;-\; \frac{4\alpha_{ts}\alpha_{tl}}{\beta_R^2 \;+\; \alpha_{ts}^2}e^{-(\alpha_{ts}+\alpha_{tl})y} \;+\; \frac{4\alpha_{ts}^2\alpha_{tl}^2}{\left(\beta_R^2 \;+\; \alpha_{ts}^2\right)^2}e^{-2\alpha_{ts}y}\right)dy \;=\; 1\end{aligned} \tag{3.12}$$

This leads to:

$$\frac{A^2\alpha_{tl}^2}{L}\Big[\frac{e^{-2\alpha_{tl}y}}{-2\alpha_{tl}}\Big|_0^{+\infty} - \frac{4\beta_R^2}{\beta_R^2+\alpha_{ts}^2}\frac{e^{-(\alpha_{tl}+\alpha_{ts})y}}{-(\alpha_{tl}+\alpha_{ts})}\Big|_0^{+\infty} + \frac{4\beta_R^4}{(\beta_R^2+\alpha_{ts}^2)^2}\frac{e^{-2\alpha_{ts}y}}{-2\alpha_{ts}}\Big|_0^{+\infty}\Big] +$$
$$+\frac{A^2\beta_R^2}{L}\Big[\frac{e^{-2\alpha_{tl}y}}{-2\alpha_{tl}}\Big|_0^{+\infty} - \frac{4\alpha_{tl}\alpha_{ts}}{\beta_R^2+\alpha_{ts}^2}\frac{e^{-(\alpha_{tl}+\alpha_{ts})y}}{-(\alpha_{tl}+\alpha_{ts})}\Big|_0^{+\infty} + \frac{4\alpha_{ts}^2\alpha_{tl}^2}{(\beta_R^2+\alpha_{ts}^2)^2}\frac{e^{-2\alpha_{ts}y}}{-2\alpha_{ts}}\Big|_0^{+\infty}\Big] = 1$$

$$\frac{A^2\alpha_{tl}^2}{L}\Big[\frac{1}{2\alpha_{tl}} - \frac{4\beta_R^2}{\beta_R^2+\alpha_{ts}^2}\frac{1}{\alpha_{tl}+\alpha_{ts}} + \frac{4\beta_R^4}{(\beta_R^2+\alpha_{ts}^2)^2}\frac{1}{2\alpha_{ts}}\Big] +$$
$$+\frac{A^2\beta_R^2}{L}\Big[\frac{1}{2\alpha_{tl}} - \frac{4\alpha_{tl}\alpha_{ts}}{\beta_R^2+\alpha_{ts}^2}\frac{1}{\alpha_{tl}+\alpha_{ts}} + \frac{4\alpha_{ts}^2\alpha_{tl}^2}{(\beta_R^2+\alpha_{ts}^2)^2}\frac{1}{2\alpha_{ts}}\Big] = 1$$

It is now possible to rearrange the expression as:

$$A^2\left[\frac{\alpha_{tl}}{2} - \frac{4\beta_R^2\alpha_{tl}^2}{(\beta_R^2+\alpha_{ts}^2)(\alpha_{tl}+\alpha_{ts})} + \frac{2\beta_R^4\alpha_{tl}^2}{\alpha_{ts}(\beta_R^2+\alpha_{ts}^2)} + \right.$$
$$\left. + \frac{\beta_R^2}{2\alpha_{tl}} - \frac{4\alpha_{tl}\alpha_{ts}\beta_R^2}{(\beta_R^2+\alpha_{ts}^2)(\alpha_{tl}+\alpha_{ts})} + \frac{2\beta_R^2\alpha_{ts}\alpha_{tl}^2}{(\beta_R^2+\alpha_{ts})^2}\right] = 1$$

where S is the area of the structure, and ρ is the diamond density.

Equivalently, recalling Equation 3.3,

$$A^2\left[\frac{\alpha_{tl}}{2} - \frac{(\beta_R^2+\alpha_{ts}^2)\alpha_{tl}}{\alpha_{ts}(\alpha_{tl}+\alpha_{ts})} + \frac{2\beta_R^2\alpha_{tl}}{4\alpha_{ts}^2} + \frac{\beta_R^2}{2\alpha_{tl}} - \frac{\left(\alpha_{ts}^2+\beta_R^2\right)}{(\alpha_{tl}+\alpha_{ts})} + \frac{\alpha_{tl}}{2}\right] = 1$$

Thus:

$$A^2\left[\frac{2\alpha_{ts}^2\alpha_{tl}^2\,(\alpha_{ts}+\alpha_{tl})}{2\alpha_{ts}^2\alpha_{tl}\,(\alpha_{ts}+\alpha_{tl})} - \frac{2(\beta_R^2+\alpha_{ts}^2)\alpha_{tl}^2\alpha_{ts}}{2\alpha_{ts}^2\alpha_{tl}\,(\alpha_{ts}+\alpha_{tl})} + \frac{\beta_R^2\alpha_{tl}^2(\alpha_{ts}+\alpha_{tl})}{2\alpha_{ts}^2\alpha_{tl}\,(\alpha_{ts}+\alpha_{tl})} + \frac{\beta_R^2\alpha_{ts}^2(\alpha_{tl}+\alpha_{ts})}{2\alpha_{ts}^2\alpha_{tl}\,(\alpha_{ts}+\alpha_{tl})} + \right.$$
$$\left. - \frac{2\alpha_{tl}\alpha_{ts}^2(\alpha_{ts}^2+\beta_R^2)}{2\alpha_{ts}^2\alpha_{tl}\,(\alpha_{ts}+\alpha_{tl})}\right] = 1$$

or equivalently:

$$A^2\left[\frac{2\alpha_{ts}^2\alpha_{tl}^2}{2\alpha_{ts}^2\alpha_{tl}} - \frac{2(\beta_R^2 + \alpha_{ts}^2)\alpha_{tl}\alpha_{ts}}{2\alpha_{ts}^2\alpha_{tl}} + \frac{\beta_R^2\alpha_{tl}^2}{2\alpha_{ts}^2\alpha_{tl}} + \frac{\beta_R^2\alpha_{ts}^2}{2\alpha_{ts}^2\alpha_{tl}}\right] = 1 \tag{3.13}$$

and after further simplifications, it is finally determined that:

$$A = \sqrt{\frac{2\alpha_{ts}^2\alpha_{tl}}{\beta_R^2\left(\alpha_{tl} - \alpha_{ts}\right)^2 + 2\alpha_{ts}^2\alpha_{tl}\left(\alpha_{tl} - \alpha_{ts}\right)}} \tag{3.14}$$

3.3 Hole–acoustic-phonon Interaction Hamiltonian and Relaxation Time

It is now possible to compute the divergence of the displacement, which will be useful for the following calculations of the relaxation time. Recalling Equation 3.7 and Equation 3.8:

$$\nabla \cdot \mathbf{u}(\mathbf{r}) = \nabla \cdot (\nabla\phi + \nabla \times (\Psi \cdot \hat{x})) = \nabla^2\phi = \frac{1}{V_l^2}\frac{\partial^2\phi}{\partial t^2} = -\left(\frac{\omega^2}{V_l^2}\right)\phi \tag{3.15}$$

Thus, it is now possible to write the Hamiltonian of the hole–acoustic-phonon interactions:

$$H_{def} = \sum_{\boldsymbol{q}} E_a \, div\, \hat{\boldsymbol{U}}(\boldsymbol{r}, t) \tag{3.16}$$

where E_a is known as the *acoustic deformation potential*, $\boldsymbol{r} = (x, y, z)$, $\boldsymbol{q} = (q_x, q_z)$ and $\hat{\boldsymbol{U}}(\boldsymbol{r}, t)$ is expressed in terms of the annihilation and creation operators $a_{\boldsymbol{q}}$ and $a_{-\boldsymbol{q}}^{\dagger}$ as:

$$\hat{\boldsymbol{U}}(\boldsymbol{r}, t) = \sqrt{\frac{\hbar}{2\rho\omega}}\mathbf{u}(\boldsymbol{r})\left(a_{\boldsymbol{q}} + a_{-\boldsymbol{q}}^{\dagger}\right) \tag{3.17}$$

Therefore, the Hamiltonian may be expressed as,

$$H_{def} \;=\; -E_a \sum_{\boldsymbol{q}} \frac{\omega^2}{V_l^2} \sqrt{\frac{\hbar}{2\rho\omega S}}\, \phi(y) \left(a_{\boldsymbol{q}} \;+\; a^{\dagger}_{-\boldsymbol{q}}\right) e^{i\boldsymbol{q}\cdot\boldsymbol{r}_{||}} \tag{3.18}$$

where $\boldsymbol{r}_{||} \;=\; (x, z)$ and the displacements are taken as plane waves in the (x, z) directions. It is emphasized that the time-dependent factor $e^{i\omega t}$ is not included in this initial formulation, since it will be included in the energy-conserving δ-function in the Fermi Golden Rule.

The 2DHG wave function is described through the Fang-Howard variational function [33]:

$$\Psi(\boldsymbol{r}) = |\boldsymbol{k}\rangle = \sqrt{\frac{b^3}{2}}\,(y \;-\; l)\, e^{-\frac{1}{2}b(y-l)} \cdot \frac{e^{i\boldsymbol{k}_{||}\boldsymbol{r}_{||}}}{\sqrt{S}}, \quad y \;-\; l \;>\; 0 \tag{3.19}$$

where l is the distance of the 2DEG from the surface, $\boldsymbol{r} \;=\; (x, y, z)$, $\boldsymbol{k}_{||} \;=\; (k_x, k_z)$ and b is a variational parameter determined by minimizing the total energy of the system, whose value is reported in [34] and in [35] to be:

$$b = \left(\frac{33 m^* e_h^2 N_h}{8\epsilon_0 \epsilon_r \hbar^2}\right)^{\frac{1}{3}} \tag{3.20}$$

with e_h representing the positive hole charge and N_h representing the 2DHG sheet density.

Before continuing, the Fermi Golden Rule formulation is recalled:

$$\frac{1}{\tau} \;=\; \frac{2\pi}{\hbar} \sum_{q} \left|M^{\{e,a\}}(q)\right|^2 \delta(E(k') - E(k) \pm \hbar\omega) \tag{3.21}$$

The matrix element $M^{\{e,a\}}(q)$ for both emission and absorption from an initial electron state $|\boldsymbol{k}\rangle$ to a final electron state $\langle \boldsymbol{k'}|$ can be computed as:

$$\begin{aligned} M^{\{e,a\}}(q) = \langle \boldsymbol{k'}, N_q + \frac{1}{2} \pm \frac{1}{2} | H_{def} | \boldsymbol{k}, N_q \, + \, \frac{1}{2} \mp \frac{1}{2} \rangle = \\ -E_a \, \frac{\omega^2}{V_l^2} \sqrt{\frac{\hbar}{2\rho\omega S}} \, A \, \langle \boldsymbol{k'} \Big| e^{-\alpha_{tl} y} e^{\mp i \boldsymbol{q} \cdot \boldsymbol{r}_{||}} \Big| \boldsymbol{k} \rangle (\mp) (n + \frac{1}{2} \pm \frac{1}{2})^{\frac{1}{2}} \end{aligned} \tag{3.22}$$

The overlap integral,

$$\begin{aligned} \langle \boldsymbol{k'} \Big| e^{-\alpha_{tl} y} e^{\mp i \boldsymbol{q} \cdot \boldsymbol{r}_{||}} \Big| \boldsymbol{k} \rangle \, = \\ \frac{b^3}{2S} \int_l^L (y \, - \, l)^2 \, e^{-\alpha_{tl} y} e^{-b(y-l)} dy \int_{-\infty}^{+\infty} e^{\mp i q_z z + i(k_z - k'_z) z} dz \int_{-\infty}^{+\infty} e^{\mp i q_x x + i(k_x - k'_x) x} dx \, = \\ \frac{b^3}{2} e^{bl} \Bigg\{ \frac{l^2 e^{-(b+\alpha_{tl})l} \, - \, L^2 e^{-(b+\alpha_{tl})L}}{(b \, + \, \alpha_{tl})} + \\ + \frac{2}{(b \, + \, \alpha_{tl})} \left[\frac{l e^{-(b+\alpha_{tl})l} \, - \, L e^{-(b+\alpha_{tl})L}}{(b \, + \, \alpha_{tl})} \, - \, \frac{e^{-(b+\alpha_{tl})L} \, - \, e^{-(b+\alpha_{tl})l}}{(b \, + \, \alpha_{tl})^2} \right] + \\ - 2l \left[\frac{l e^{-(b+\alpha_{tl})l} \, - \, L e^{-(b+\alpha_{tl})L}}{(b \, + \, \alpha_{tl})} \, - \, \frac{e^{-(b+\alpha_{tl})L} \, - \, e^{-(b+\alpha_{tl})l}}{(b \, + \, \alpha_{tl})^2} \right] + \\ l^2 \left[\frac{e^{-(b+\alpha_{tl})l} \, - \, e^{-(b+\alpha_{tl})L}}{(b \, + \, \alpha_{tl})} \right] \Bigg\} \delta_{\boldsymbol{k'}_{||} - \boldsymbol{k}_{||} \pm \boldsymbol{q}} \end{aligned} \tag{3.23}$$

where the integrals have been evaluated using,

$$\begin{aligned}
\int_l^L y^2 e^{-(\alpha_{tl}+b)y}\,dy \;=\; & \\
\frac{l^2 e^{-(b+\alpha_{tl})l} \;-\; L^2 e^{-(b+\alpha_{tl})L}}{(b\;+\;\alpha_{tl})} \;+\; & \frac{2}{(b\;+\;\alpha_{tl})}\left[\frac{l e^{-(b+\alpha_{tl})l} \;-\; L e^{-(b+\alpha_{tl})L}}{(b\;+\;\alpha_{tl})} \;-\; \frac{e^{-(b+\alpha_{tl})L} \;-\; e^{-(b+\alpha_{tl})l}}{(b\;+\;\alpha_{tl})^2}\right] \\
\int_l^L y\, e^{-(\alpha_{tl}+b)y}\,dy \;=\; & \frac{l e^{-(b+\alpha_{tl})l} \;-\; L e^{-(b+\alpha_{tl})L}}{(b\;+\;\alpha_{tl})} \;-\; \frac{e^{-(b+\alpha_{tl})L} \;-\; e^{-(b+\alpha_{tl})l}}{(b\;+\;\alpha_{tl})^2} \\
\int_l^L e^{-(b+\alpha_{tl})y}\,dy \;=\; & \frac{e^{-(b+\alpha_{tl})l} \;-\; e^{-(b+\alpha_{tl})L}}{(b\;+\;\alpha_{tl})} \\
\frac{1}{S}\int_{-\infty}^{+\infty} dx \int_{-\infty}^{+\infty} dz\, e^{iz(k_z-k'_z)} e^{ix(k_x-k'_x)} \;=\; & \delta_{\boldsymbol{k}'_{||}\,-\,\boldsymbol{k}_{||}}
\end{aligned} \tag{3.24}$$

Thus, the matrix element $M^{\{e,a\}}(q)$ is,

$$M^{\{e,a\}}(q) = \frac{-E_a\omega^2 A}{V_l^2}\sqrt{\frac{\hbar}{2\rho\omega S}}F(\mp)(n+\frac{1}{2}\pm\frac{1}{2})^{\frac{1}{2}}\delta_{\boldsymbol{k}'_{||}\,-\,\boldsymbol{k}_{||}\pm\boldsymbol{q}} \tag{3.25}$$

with the upper sign corresponding to phonons emission and the lower to phonons absorption, and where it has been substituted:

$$\begin{aligned}
F \;=\; & \frac{b^3}{2}e^{bl}\left\{\frac{l^2 e^{-(b+\alpha_{tl})l} \;-\; L^2 e^{-(b+\alpha_{tl})L}}{(b\;+\;\alpha_{tl})} + \right. \\
& + \frac{2}{(b\;+\;\alpha_{tl})}\left[\frac{l e^{-(b+\alpha_{tl})l} \;-\; L e^{-(b+\alpha_{tl})L}}{(b\;+\;\alpha_{tl})} \;-\; \frac{e^{-(b+\alpha_{tl})L} \;-\; e^{-(b+\alpha_{tl})l}}{(b\;+\;\alpha_{tl})^2}\right] + \\
& - 2l\left[\frac{l e^{-(b+\alpha_{tl})l} \;-\; L e^{-(b+\alpha_{tl})L}}{(b\;+\;\alpha_{tl})} \;-\; \frac{e^{-(b+\alpha_{tl})L} \;-\; e^{-(b+\alpha_{tl})l}}{(b\;+\;\alpha_{tl})^2}\right] + \\
& \left. l^2\left[\frac{e^{-(b+\alpha_{tl})l} \;-\; e^{-(b+\alpha_{tl})L}}{(b\;+\;\alpha_{tl})}\right]\right\}
\end{aligned} \tag{3.26}$$

Therefore, the scattering rate predicted by the Fermi Golden Rule is given by:

$$\frac{1}{\tau_{ac}} = \frac{S}{(2\pi)^2}\int d^2\boldsymbol{q}\frac{2\pi}{\hbar}\left|M^{\{e,a\}}(q)\right|^2\delta(E(\boldsymbol{k'}) - E(\boldsymbol{k}) \pm \hbar\omega_q) = \int d^2\boldsymbol{q}\frac{E_a^2\omega^3 A^2}{4\pi\rho V_l^4}F^2(n+\frac{1}{2}\pm\frac{1}{2})\delta_{\boldsymbol{k'_{||}}-\boldsymbol{k_{||}}\pm\boldsymbol{q}}\delta(\frac{\hbar}{2m^*}(q^2 \mp 2\boldsymbol{k}\cdot\boldsymbol{q}) \pm \hbar\omega) \tag{3.27}$$

where the sum over $\boldsymbol{q}$ has been converted to an integral and n is the Bose-Einstein occupation number.

CHAPTER 4

RELAXATION TIME DUE TO REMOTE INTERFACE OPTICAL-PHONONS FROM UPPER LAYER IN DIAMOND STRUCTURE

The investigation carried out in this chapter concerns the study of the leakage of remote polar phonons from the upper layer into the diamond substrate in the structure depicted in Figure 8; as a matter of fact, the presence of a polar layer, inserted, as already mentioned in the introduction, as passivation layer or for the realization of the gate dielectric, generates an evanescent interface phonon mode that decays into the diamond. In particular, structures exploiting AlN, w-BN and c-BN as layer materials are under investigation, due to their good physical and electrical properties such as wide band-gap and high breakdown voltage that make them a promising choice for the realization of diamond-based FETs.

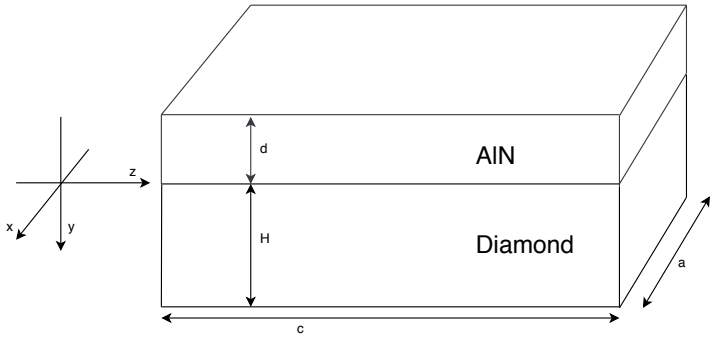

Figure 8: AlN-diamond structure.

Herein, the remote polar phonons originating from AlN (or w-BN or c-BN) are remodeled assuming a high quality surface of the material at the interface with diamond as shown in Figure 9.

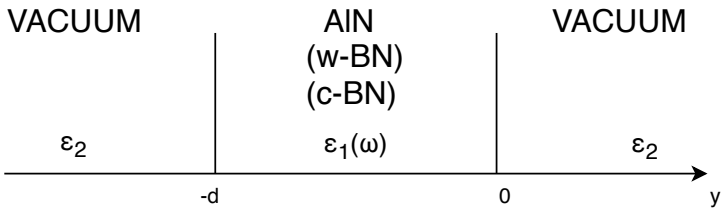

Figure 9: Upper layer configuration for evaluation of the IF phonon potential.

4.1 Crystallographic Orientation

Before starting the calculation, it is helpful to recall some knowledge about crystallographic orientation, in order to make more evident the correct interpretation of the physical structure under investigation.

First of all, it is meaningful to recall that diamond is characterized by a crystallographic structure called *diamond structure*, that consists of two interpenetrating face centered cubic (FCC) Bravais lattices, displaced along the body diagonal of the cubic cell by one quarter the length of the diagonal. The unit cell's crystallographic representation, together with a slab fragment oriented along the $\langle 111 \rangle$ direction, are reported in Figure 10.

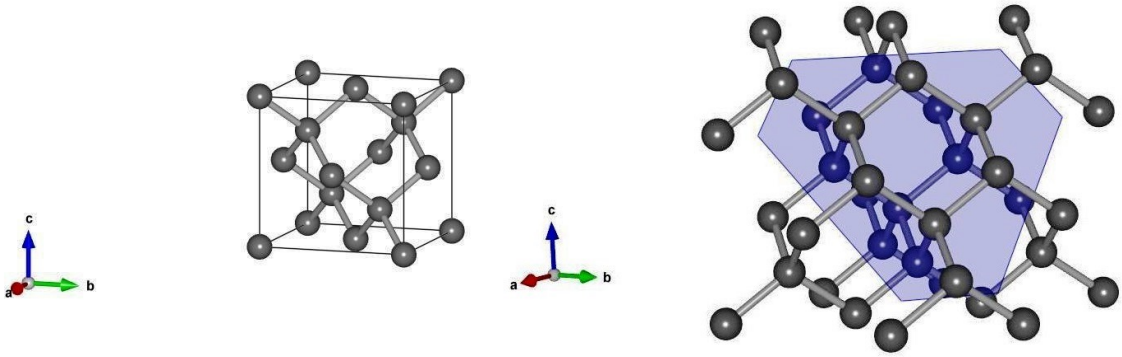

Figure 10: Diamond unit cell (left) and slab (right), with the (111) plane highlighted.

On the other hand, both AlN and w-BN belong to the family of wurtzite crystals, an hexagonal crystal system typical of various types of binary compounds: the unit cell and a slab fragment aligned along the c-axis are depicted in Figure 11 for the case of AlN. In the description reported in the following section, the c-axis of the upper layer material is assumed to be perpendicular to the diamond surface, consistent with what is reported in Ref.[36], in which the growth of AlN on diamond for the fabrication of h-FETs is reported.

Moreover, c-BN (cubic-BN) represents another interesting material for the realization of diamond-FET devices; it belongs to the family of zincblende crystals, another crystal system typical of binary compounds, in which the arrangement of atoms resembles the diamond cubic structure, with the difference that each atom of a type is surrounded by four atoms of the other type. Also in this case, the unit cell and a slab fragment aligned along the $\langle 111 \rangle$ of the material are reported in Figure 12.

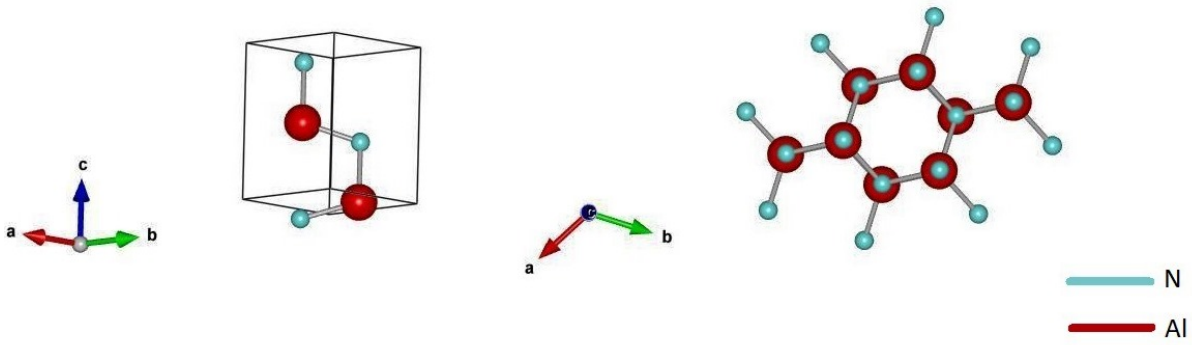

Figure 11: AlN unit cell (left) and slab (right), with the view aligned to the c-axis.

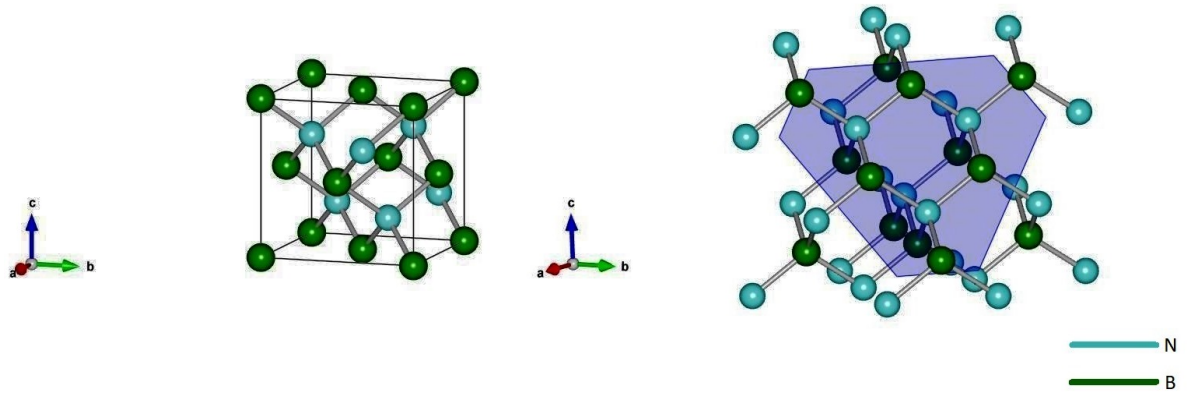

Figure 12: c-BN unit cell (left) and slab (right), with the (111) plane highlighted.

Finally, it is worth mentioning that every figure in this section is obtained through VESTA [37], a dedicated software for crystallographic representations.

4.2 Electrostatic Potential Calculation

For the calculations performed in the following analysis, it is useful to recall the classical electrostatic equations:

$$\begin{aligned} E(\boldsymbol{r}) &= -\nabla\phi(\boldsymbol{r}) \\ D(\mathbf{r}) \;=\; E(\boldsymbol{r}) \;+\; 4\pi P(\boldsymbol{r}) &= \epsilon_{\perp}(\omega)E_{\perp}(\boldsymbol{r})\hat{\rho} \;+\; \epsilon_y(\omega)E_y(\boldsymbol{r})\hat{y} \\ \nabla\cdot D(\boldsymbol{r}) \;&=\; 0 \end{aligned} \tag{4.1}$$

where $\phi(\boldsymbol{r})$ is the electrostatic potential due to optical-phonon mode, E is the electric field, D is the displacement, P is the polarization field, and $\hat{\rho}$ and $\hat{y}$ denote respectively the unit vectors perpendicular and parallel to the y axis.

The parameters $\epsilon_{\perp}$ and ϵ_y represent the frequency and direction dependent dielectric functions respectively perpendicular and parallel to the y-axis. They can be expressed as [16]:

$$\begin{aligned} \epsilon_{\perp}(\omega) \;&=\; \epsilon_{\perp}^{\infty}\,\frac{\omega^2-\omega_{\perp L}^2}{\omega^2-\omega_{\perp}^2} \\ \epsilon_y(\omega) \;&=\; \epsilon_y^{\infty}\,\frac{\omega^2-\omega_{yL}^2}{\omega^2-\omega_y^2} \end{aligned} \tag{4.2}$$

where ω_y and $\omega_{\perp}$ are the lattice dispersion frequency, ω_{yL} and $\omega_{\perp L}$ are the longitudinal-optical phonon frequency, ϵ_y^{∞} and $\epsilon_{\perp}^{\infty}$ are the high-frequency dielectric constants. Therefore, the static dielectric constants are easily derived as $\epsilon_y^0 = \epsilon_y^{\infty}\frac{\omega_{yL}^2}{\omega_y^2}$ and $\epsilon_{\perp}^0 \;=\; \epsilon_{\perp}^{\infty}\frac{\omega_{\perp L}^2}{\omega_{\perp}^2}$.

These parameters in the case of AlN, w-BN and c-BN are reported in Table III.

TABLE III: ALN, C-BN AND W-BN MATERIAL PARAMETERS

	$\epsilon_{\perp}^{\infty}$	ϵ_{y}^{∞}	$\epsilon_{\perp}^{0}$	ϵ_{y}^{0}	$\omega_{\perp L}\,(cm^{-1})$	$\omega_{\perp}\,(cm^{-1})$	$\omega_{yL}\,(cm^{-1})$	$\omega_{y}\,(cm^{-1})$
AlN[16]	4.6	4.6	8.5	8.5	916	673	893	660
w-BN[38]	4.50	4.67	6.8	5.1	1281	1053	1258	1006
c-BN[38]	4.54	4.54	7.1	7.1	1285	1040	1285	1040

At this point, it is worth mentioning that the entire procedure, developed for a wurtzite crystal double heterointerface, remains valid also in the case of a zincblende crystal such as c-BN, since the isotropic case is recovered when $\epsilon_{\perp}(\omega) = \epsilon_{y}(\omega)$.

The electrostatic potential $\phi(\boldsymbol{r})$ is taken to be of the form:

$$\phi(\boldsymbol{r}) = e^{i\boldsymbol{qp}} \times \begin{cases} Ce^{k_2(y+d)} & y < -d \\ A\cosh k_1(y + d/2) + B\sinh k_1(y + d/2) & -d \leq y \leq 0 \\ De^{-k_2 y} & y > 0 \end{cases} \tag{4.3}$$

where $\mathbf{p} = (x, z)$, $\mathbf{q} = (q_x, q_z)$, $\mathbf{r} = (x, y, z)$ and the subscript 1 and 2 are respectively, used to refer to quantities related to the polar material stratum and the vacuum.

In absence of free charge, the condition $\nabla \cdot D = 0$ holds, leading to:

$$\left[\epsilon_y \frac{\partial^2}{\partial y^2} - \epsilon_\perp q^2\right]\phi(\boldsymbol{r}) = 0 \Rightarrow \begin{cases} \left[\epsilon_{y,2}(\omega)k_2^2 - \epsilon_{\perp,2}(\omega)q^2\right]\Phi(\boldsymbol{r}) = 0 \\ \left[\epsilon_{y,1}(\omega)k_1^2 - \epsilon_{\perp,1}(\omega)q^2\right]\Phi(\boldsymbol{r}) = 0 \end{cases} \tag{4.4}$$

Thus:

$$\begin{aligned} k_1 &= \sqrt{\frac{\epsilon(\omega)_{\perp,1}}{\epsilon(\omega)_{y,1}}}q \\ k_2 &= \sqrt{\frac{\epsilon(\omega)_{\perp,2}}{\epsilon(\omega)_{y,2}}}q \end{aligned} \tag{4.5}$$

where $q = |\boldsymbol{q}|$. Imposing the continuity of the tangential component of the electric field, both at y=-d and y=0:

$$\begin{aligned} i\boldsymbol{q}e^{i\boldsymbol{qp}}Ce^{k_2(y_0+d)} &= i\boldsymbol{q}e^{i\boldsymbol{qp}}A\cosh k_1(y_0 + d/2) + B\sinh k_1(y_0 + d/2) \rightarrow C = A\cosh k_1 d/2 - B\sinh k_1 d/2 \\ i\boldsymbol{q}e^{i\boldsymbol{qp}}De^{-k_2 y_1} &= i\boldsymbol{q}e^{i\boldsymbol{qp}}A\cosh k_1(y_1 + d/2) + B\sinh k_1(y_1 + d/2) \rightarrow D = A\cosh k_1 d/2 + B\sinh k_1 d/2 \end{aligned} \tag{4.6}$$

Likewise, imposing the continuity of the normal component of electric displacement at the interfaces:

$$\begin{aligned} \epsilon(\omega)_{y,2}k_2 C &= \epsilon(\omega)_{y,1}k_1(-A\sinh k_1 d/2 + B\cosh k_1 d/2) \quad y = -d \\ -\epsilon_{y,2}k_2 D &= \epsilon(\omega)_{y,1}k_1(A\sinh k_1 d/2 + B\cosh k_1 d/2) \quad y = 0 \end{aligned} \tag{4.7}$$

Eliminating C and D from these four equations, it follows:

$$\begin{cases} \epsilon(\omega)_{y,2}k_2(A\cosh k_1 d/2 \,-\, B\sinh k_1 d/2) \,=\, \epsilon(\omega)_{y,1}k_1(-A\sinh k_1 d/2 \,+\, B\cosh k_1 d/2) \\ -\epsilon(\omega)_{y,2}k_2(A\cosh k_1 d/2 + B\sinh k_1 d/2) \,=\, \epsilon(\omega)_{y,1}k_1(A\sinh k_1 d/2 \,+\, B\cosh k_1 d/2) \end{cases} \tag{4.8}$$

So, rewriting the system in matrix form:

$$\begin{bmatrix} \epsilon(\omega)_{y,2}k_2\cosh k_1 d/2 + \epsilon(\omega)_{y,1}k_1\sinh k_1 d/2 & -\epsilon(\omega)_{y,2}k_2\sinh k_1 d/2 - \epsilon(\omega)_{y,1}k_1\cosh k_1 d/2 \\ -\epsilon(\omega)_{y,2}k_2\cosh k_1 d/2 - \epsilon(\omega)_{y,1}k_1\sinh k_1 d/2 & -\epsilon(\omega)_{y,2}k_2\sinh k_1 d/2 - \epsilon(\omega)_{y,1}k_1\cosh k_1 d/2 \end{bmatrix} \begin{bmatrix} A \\ B \end{bmatrix} = 0$$

Accordingly, the non-trivial solutions are found enforcing the non-invertibility of the coefficient matrix, or in other terms requiring the determinant of the coefficient matrix to be null:

$$2\Big(\epsilon(\omega)_{y,2}k_2\cosh k_1 d/2+\epsilon(\omega)_{y,1}k_1\sinh k_1 d/2\Big)\Big(-\epsilon(\omega)_{y,2}k_2\sinh k_1 d/2-\epsilon(\omega)_{y,1}k_1\cosh k_1 d/2\Big) = 0 \tag{4.9}$$

Thus, two cases are possible. The first, where:

$$\epsilon(\omega)_{y,1}k_1\tanh k_1 d/2 \,+\, \epsilon(\omega)_{y,2}k_2 \,=\, 0 \tag{4.10}$$

that corresponds to:

$$\begin{cases} B = 0 \\ C = D = \phi_0 \\ A = \frac{C}{\cosh k_1 d/2} = \frac{\phi_0}{\cosh k_1 d/2} \end{cases} \tag{4.11}$$

hence, the potential is symmetric and can be expressed as:

$$\phi(\boldsymbol{r}) = \phi_0 e^{i\boldsymbol{qp}} \times \begin{cases} e^{k_2(y+d)} & y < -d \\ (\cosh k_1(y + d/2))/\cosh k_1 d/2 & -d \leq y \leq 0 \\ e^{-k_2 y} & y > 0 \end{cases} \tag{4.12}$$

The second case:

$$\epsilon(\omega)_{y,1} k_1 \coth k_1 d/2 + \epsilon(\omega)_{y,2} k_2 = 0 \tag{4.13}$$

that corresponds to:

$$\begin{cases} A = 0 \\ -C = D = \phi_0 \\ B = \frac{D}{\sinh k_1 d/2} = \frac{\phi_0}{\sinh k_1 d/2} \end{cases} \tag{4.14}$$

hence, the potential is antisymmetric and can be expressed as:

$$\phi(\boldsymbol{r}) \;=\; \phi_0 e^{i\boldsymbol{qp}} \times \begin{cases} -e^{k_2(y+d)} & y < -d \\ (\sinh k_1(y \,+\, d/2))/\sinh k_1 d/2 & -d \le y \le 0 \\ e^{-k_2 y} & y > 0 \end{cases} \tag{4.15}$$

The normalization condition, illustrated in Ref.[16], is formulated as:

$$\frac{1}{L^2}\frac{\hbar}{2\omega} \;=\; \int \frac{1}{4\pi}\frac{1}{2\omega}\frac{\partial\epsilon(\omega)_{\perp,n}}{\partial\omega}|E_{\perp,n}|^2 \;+\; \frac{1}{4\pi}\frac{1}{2\omega}\frac{\partial\epsilon(\omega)_{y,n}}{\partial\omega}|E_{y,n}|^2\,dy \tag{4.16}$$

where L^2 represents the cross-sectional area of the sample. Substituting the terms $|E_{\perp,n}|^2 = q^2|\phi(z)|^2$ and $|E_{y,n}|^2 = |\frac{\partial\phi(z)}{\partial z}|^2$, it is possible to compute the integrals for both the symmetric and antisymmetric potentials. For the symmetric case:

$$\begin{gathered} \int_{-\infty}^{-d}|E_{\perp,2}|^2\,dy \;=\; \int_{0}^{+\infty}|E_{\perp,2}|^2\,dy \;=\; \phi_0^2 q^2\int_{-\infty}^{-d}e^{2k_2(y+d)}\,dy \;=\; \frac{\phi_0^2 q^2}{2k_2} \\ \int_{-d}^{0}|E_{\perp,1}|^2\,dy \;=\; \frac{\phi_0^2 q^2}{\cosh^2 k_1 d/2}\int_{-d}^{0}\cosh^2 k_1(y \,+\, d/2)\,dy \;=\; \frac{\phi_0^2 q^2}{\cosh^2 k_1 d/2}\Big(\frac{\sinh k_1 d}{2k_1} \,+\, \frac{d}{2}\Big) \\ \int_{-\infty}^{-d}|E_{y,2}|^2\,dy \;=\; \int_{0}^{+\infty}|E_{y,2}|^2\,dy \;=\; \phi_0^2 k_2^2\int_{-\infty}^{-d}e^{2k_2(y+d)}\,dy \;=\; \frac{\phi_0^2 k_2}{2} \\ \int_{-d}^{0}|E_{y,1}|^2\,dy \;=\; \frac{\phi_0^2 k_1^2}{\cosh^2 k_1 d/2}\int_{-d}^{0}\sinh^2 k_1(y \,+\, d/2)\,dy \;=\; \frac{\phi_0^2 k_1^2}{\cosh^2 k_1 d/2}\Big(\frac{\sinh k_1 d}{2k_1} \,-\, \frac{d}{2}\Big) \end{gathered} \tag{4.17}$$

For the antisymmetric case:

$$\begin{gathered}
\int_{-\infty}^{-d} |E_{\perp,2}|^2\,dy \;=\; \int_{0}^{+\infty} |E_{\perp,2}|^2\,dy \;=\; \phi_0^2 q^2 \int_{-\infty}^{-d} e^{2k_2(y+d)}\,dy \;=\; \frac{\phi_0^2 q^2}{2k_2} \\
\int_{-d}^{0} |E_{\perp,1}|^2\,dy \;=\; \frac{\phi_0^2 q^2}{\sinh^2 k_1 d/2} \int_{-d}^{0} \sinh^2 k_1(y+d/2)\,dy \;=\; \frac{\phi_0^2 q^2}{\sinh^2 k_1 d/2}\Big(\frac{\sinh k_1 d}{2k_1} - \frac{d}{2}\Big) \\
\int_{-\infty}^{-d} |E_{y,2}|^2\,dy \;=\; \int_{0}^{+\infty} |E_{y,2}|^2\,dy \;=\; \phi_0^2 k_2^2 \int_{-\infty}^{-d} e^{2k_2(y+d)}\,dy \;=\; \frac{\phi_0^2 k_2}{2} \\
\int_{-d}^{0} |E_{y,1}|^2\,dy \;=\; \frac{\phi_0^2 k_1^2}{\sinh^2 k_1 d/2} \int_{-d}^{0} \cosh^2 k_1(y+d/2)\,dy \;=\; \frac{\phi_0^2 k_1^2}{\sinh^2 k_1 d/2}\Big(\frac{\sinh k_1 d}{2k_1} + \frac{d}{2}\Big)
\end{gathered} \tag{4.18}$$

Thus, for the symmetric case:

$$\begin{aligned}
\phi_0^2 \;=\; \frac{4\pi\hbar}{2qL^2}\Bigg[& \frac{\partial\epsilon_{\perp,1}}{\partial\omega}\Big(\frac{q}{2k_1}\tanh k_1 d/2 + \frac{dq}{4\cosh^2 k_1 d/2}\Big) + \frac{1}{2}\frac{\partial\epsilon_{\perp,2}}{\partial\omega}\frac{q}{k_2} + \\
& + \frac{\partial\epsilon_{y,1}}{\partial\omega}\Big(\frac{k_1}{2q}\tanh k_1 d/2 - \frac{k_1^2 d}{4q\cosh^2 k_1 d/2}\Big) + \frac{1}{2}\frac{\partial\epsilon_{y,2}}{\partial\omega}\frac{k_2}{q}\Bigg]^{-1}
\end{aligned} \tag{4.19}$$

while for the antisymmetric case:

$$\begin{aligned}
\phi_0^2 \;=\; \frac{4\pi\hbar}{2qL^2}\Bigg[& \frac{\partial\epsilon_{\perp,1}}{\partial\omega}\Big(\frac{q}{2k_1}\coth k_1 d/2 - \frac{dq}{4\sinh^2 k_1 d/2}\Big) + \frac{1}{2}\frac{\partial\epsilon_{\perp,2}}{\partial\omega}\frac{q}{k_2} + \\
& + \frac{\partial\epsilon_{y,1}}{\partial\omega}\Big(\frac{k_1}{2q}\coth k_1 d/2 + \frac{k_1^2 d}{4q\sinh^2 k_1 d/2}\Big) + \frac{1}{2}\frac{\partial\epsilon_{y,2}}{\partial\omega}\frac{k_2}{q}\Bigg]^{-1}
\end{aligned} \tag{4.20}$$

Both of these expressions can be expressed in a more compact way exploiting the relation:

$$\begin{aligned} \Big|\frac{\partial}{\partial\omega}\Big(\sqrt{\epsilon(\omega)_{\perp,1}\epsilon(\omega)_{y.1}}-\sqrt{\epsilon(\omega)_{\perp,2}\epsilon(\omega)_{y,2}}\Big)\Big| = \\ = \frac{1}{2}\left[\Big(\frac{\partial\epsilon_{\perp,1}}{\partial\omega}\frac{q}{k_1}+\frac{\partial\epsilon_{y,1}}{\partial\omega}\frac{k_1}{q}\Big)+\Big(\frac{\partial\epsilon_{\perp,2}}{\partial\omega}\frac{q}{k_2}+\frac{\partial\epsilon_{y,2}}{\partial\omega}\frac{k_2}{q}\Big)\right] \end{aligned} \tag{4.21}$$

4.3 Hole–optical-phonon Interaction Hamiltonian and Relaxation Time

It is possible to formulate the hole–optical-phonon interaction Hamiltonian (also called Fröhlich Hamiltonian). To do this, recall that,

$$H_{Fröhlich} = \sum_{\boldsymbol{q}} e_h \cdot \Phi(\boldsymbol{r})(a_{\boldsymbol{q}} + a^{\dagger}_{-\boldsymbol{q}}) \tag{4.22}$$

For the symmetric mode, it is:

$$\begin{aligned} H^S_{IF} = \sum_{\boldsymbol{q}} \left[\frac{4\pi e_h^2\hbar L^{-2}}{|(\partial/\partial\omega)(\sqrt{\epsilon_{\perp,1}\epsilon_{y,1}}\tanh(\sqrt{\epsilon_{\perp,1}/\epsilon_{y,1}}qd/2) - \sqrt{\epsilon_{\perp,2}\epsilon_{y,2}})|}\right]^{\frac{1}{2}} \frac{1}{\sqrt{2q}} e^{i\boldsymbol{q}\cdot\boldsymbol{\rho}}(a_{\boldsymbol{q}} + a^{\dagger}_{-\boldsymbol{q}}) \\ \times \begin{cases} e^{\sqrt{\epsilon_{\perp,2}/\epsilon_{y,2}}q(y+d)} & y < -d \\ \cosh(\sqrt{\epsilon_{\perp,1}/\epsilon_{y,1}}q(y + d/2))/\cosh(\sqrt{\epsilon_{\perp,1}/\epsilon_{y,1}}qd/2) & -d \le y \le 0 \\ e^{-\sqrt{\epsilon_{\perp,2}/\epsilon_{y,2}}qy} & y > 0 \end{cases} \end{aligned} \tag{4.23}$$

The frequency ω is obtained by solving $\sqrt{\epsilon_{\perp,1}\epsilon_{y,1}}\tanh(\sqrt{\epsilon_{\perp,1}/\epsilon_{y,1}}qd/2) - \sqrt{\epsilon_{\perp,2}\epsilon_{y,2}} = 0$, within the ranges determined by the conditions $\epsilon_{y,1}\epsilon_{y,2} < 0$, $\epsilon_{\perp,1}\epsilon_{y,1} > 0$ and $\epsilon_{\perp,2}\epsilon_{y,2} > 0$.

For the antisymmetric mode, this procedure yields,

$$H_{IF}^{A} = \sum_{\boldsymbol{q}} \left[\frac{4\pi e_h^2 \hbar L^{-2}}{|(\partial/\partial\omega)(\sqrt{\epsilon_{\perp,1}\epsilon_{y,1}}\coth(\sqrt{\epsilon_{\perp,1}/\epsilon_{y,1}}qd/2) - \sqrt{\epsilon_{\perp,2}\epsilon_{y,2}})|} \right]^{\frac{1}{2}} \frac{1}{\sqrt{2q}} e^{i\boldsymbol{q}\cdot\boldsymbol{\rho}}(a_{\boldsymbol{q}} + a_{-\boldsymbol{q}}^{\dagger}) \times \begin{cases} -e^{\sqrt{\epsilon_{\perp,2}/\epsilon_{y,2}}q(y+d)} & y < -d \\ \sinh(\sqrt{\epsilon_{\perp,1}/\epsilon_{y,1}}q(y + d/2))/\sinh(\sqrt{\epsilon_{\perp,1}/\epsilon_{y,1}}qd/2) & -d \leq y \leq 0 \\ e^{-\sqrt{\epsilon_{\perp,2}/\epsilon_{y,2}}qy} & y > 0 \end{cases} \tag{4.24}$$

and the frequency ω is obtained by solving $\sqrt{\epsilon_{\perp,1}\epsilon_{y,1}}\coth(\sqrt{\epsilon_{\perp,1}/\epsilon_{y,1}}qd/2) - \sqrt{\epsilon_{\perp,2}\epsilon_{y,2}} = 0$. Finally, the dispersion relation for both symmetric and antisymmetric modes for AlN is reported in Figure 13.

With the expression for the Fröhlich interaction Hamiltonian, it is possible to proceed with the same calculation performed in the case of the IF-acoustic phonon mode, and obtain an expression for both the matrix elements and the relaxation times for each process.

The Howard-Fang wave function, exploited to describe the the 2DHG is:

$$\Psi(r) = |k\rangle = \sqrt{\frac{b^3}{2}}(y - l)e^{-\frac{1}{2}b(y-l)} \cdot \frac{e^{i\boldsymbol{k}_{||}\boldsymbol{\rho}}}{\sqrt{S}}, \quad y - l > 0 \tag{4.25}$$

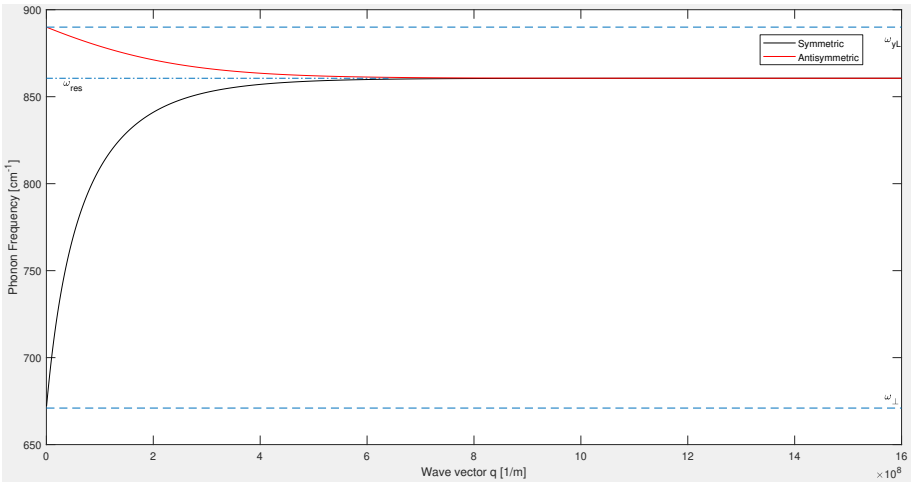

Figure 13: Dispersion Relation for symmetric and antisymmetric IF modes in AlN (5 nm thickness)

with l representing the distance of the 2DEG from the surface, S representing the area of the sample, $\boldsymbol{k}_{||} = (k_x, k_z)$, $\boldsymbol{p} = (x, z)$ and b the variational parameter determined by minimizing the total energy of the system, as in the previous case. Here it is recalled that,

$$b = \left(\frac{33 m^* e_h^2 N_h}{8 \epsilon_0 \epsilon_r \hbar^2} \right)^{\frac{1}{3}} \tag{4.26}$$

It is important to emphasize that when the exponentially decaying tail of the electrostatic potential $\Phi(\boldsymbol{r})$ reaches the diamond substrate, it is subject to a screening effect, leading to,

$$\Phi_d(\boldsymbol{r}) = \frac{\Phi(\boldsymbol{r})}{\epsilon_d}, \quad y > 0 \tag{4.27}$$

Before proceeding with the actual computations, it is worthwhile to substitute the parameters related to the vacuum layers depicted in Figure 9 in Equation 4.23 and Equation 4.24, until now expressed in the more general form suitable to describe the heterointerface between two wurtzite structures.

Recalling that vacuum is to be considered an isotropic material, $\epsilon_{\perp,2} = \epsilon_{y,2} = \epsilon_2$; furthermore, it is well know that the dieletric constant ϵ_2 for vacuum is equal to 1.

Finally, considering the leakage of the exponentially decaying tail of the electrostatic potential due to the polar layer on the diamond substrate ($y > 0$):

$$H^S_{IF,D} = \sum_{\boldsymbol{q}} \left[\frac{2\pi e_\hbar^2 \hbar \left(L^2 q \epsilon_d^2\right)^{-1}}{|(\partial/\partial\omega)(\sqrt{\epsilon_{\perp,1}\epsilon_{y,1}} \tanh(\sqrt{\epsilon_{\perp,1}/\epsilon_{y,1}} qd/2) - \epsilon_0)|} \right]^{\frac{1}{2}} e^{-qy} \left(a_{\boldsymbol{q}} e^{i\boldsymbol{q}\cdot\boldsymbol{p}} - a^\dagger_{\boldsymbol{q}} e^{-i\boldsymbol{q}\cdot\boldsymbol{p}}\right) \tag{4.28}$$

$$H^A_{IF,D} = \sum_{\boldsymbol{q}} \left[\frac{2\pi e_\hbar^2 \hbar \left(L^2 q \epsilon_d^2\right)^{-1}}{|(\partial/\partial\omega)(\sqrt{\epsilon_{\perp,1}\epsilon_{y,1}} \coth(\sqrt{\epsilon_{\perp,1}/\epsilon_{y,1}} qd/2) - \epsilon_0)|} \right]^{\frac{1}{2}} e^{-qy} \left(a_{\boldsymbol{q}} e^{i\boldsymbol{q}\cdot\boldsymbol{p}} - a^\dagger_{\boldsymbol{q}} e^{-i\boldsymbol{q}\cdot\boldsymbol{p}}\right) \tag{4.29}$$

where ϵ_0 represents the vacuum permittivity.

At this point, the Fermi Golden Rule formulation is recalled:

$$S^{\{e,a\}}(\boldsymbol{k}, \boldsymbol{k'}) = \frac{2\pi}{\hbar} |\langle \Psi_f | H_{def} | \Psi_i \rangle|^2 \delta(\epsilon_f - \epsilon_i) = \frac{2\pi}{\hbar} \sum_q |M^{\{e,a\}}(q)|^2 \delta(E(k') - E(k) \pm \hbar\omega) \tag{4.30}$$

The matrix element $M^{\{e,a\}}(q)$ for the symmetric case can be computed as,

$$M^{\{e,a\}}(q) = \langle \boldsymbol{k'}, N_n + \frac{1}{2} \pm \frac{1}{2} | H_{def} | \boldsymbol{k}, N_n + \frac{1}{2} \mp \frac{1}{2} \rangle = \left[\frac{2\pi e_h^2 \hbar \left(L^2 q \epsilon_d^2 \right)^{-1}}{|(\partial/\partial\omega)(\sqrt{\epsilon_{\perp,1}\epsilon_{y,1}} \tanh(\sqrt{\epsilon_{\perp,1}/\epsilon_{y,1}} qd/2) \, - \, \epsilon_0)|} \right]^{\frac{1}{2}} \langle \boldsymbol{k'} \Big| e^{\mp i \boldsymbol{qp}} e^{-qy} \Big| \boldsymbol{k} \rangle (\mp)(n + \frac{1}{2} \pm \frac{1}{2})^{\frac{1}{2}} \tag{4.31}$$

while for the antisymmetric case,

$$M^{\{e,a\}}(q) = \langle \boldsymbol{k'}, N_n + \frac{1}{2} \pm \frac{1}{2} | H_{def} | \boldsymbol{k}, N_n + \frac{1}{2} \mp \frac{1}{2} \rangle = \left[\frac{2\pi e_h^2 \hbar \left(L^2 q \epsilon_d^2 \right)^{-1}}{|(\partial/\partial\omega)(\sqrt{\epsilon_{\perp,1}\epsilon_{y,1}} \coth(\sqrt{\epsilon_{\perp,1}/\epsilon_{y,1}} qd/2) \, - \, \epsilon_0)|} \right]^{\frac{1}{2}} \langle \boldsymbol{k'} \Big| e^{\mp i \boldsymbol{qp}} e^{-qy} \Big| \boldsymbol{k} \rangle (\mp)(n + \frac{1}{2} \pm \frac{1}{2})^{\frac{1}{2}} \tag{4.32}$$

Using $H_{IF,D}$ as given by Equation 4.28 and Equation 4.29, one has for the overlap integral,

$$\begin{aligned} \langle \boldsymbol{k'} \Big| e^{\mp i \boldsymbol{qp}} e^{-qy} \Big| \boldsymbol{k} \rangle = \int \Psi^* H_{def} \Psi \, dx \, dy \, dz = \\ \frac{b^3}{2S} \int_l^L (y \, - \, l)^2 e^{-b(y-l)} e^{-qy} dy \cdot \int_{-\infty}^{+\infty} e^{\mp i q_z z + i(k_z - k'_z)z} dz \int_{-\infty}^{+\infty} e^{\mp i q_x x + i(k_x - k'_x)x} dx = \\ \frac{b^3}{2} e^{bl} \Bigg\{ \frac{l^2 e^{-(b+q)l} \, - \, L^2 e^{-(b+q)L}}{(b \, + \, q)} \\ + \frac{2}{(b \, + \, q)} \left[\frac{l e^{-(b+q)l} \, - \, L e^{-(b+q)L}}{(b \, + \, q)} \, - \, \frac{e^{-(b+q)L} \, - \, e^{-(b+q)l}}{(b \, + \, q)^2} \right] + \\ - 2l \left[\frac{l e^{-(b+q)l} \, - \, L e^{-(b+q)L}}{(b \, + \, q)} \, - \, \frac{e^{-(b+q)L} \, - \, e^{-(b+q)l}}{(b \, + \, q)^2} \right] \\ + l^2 \left[\frac{e^{-(b+q)l} \, - \, e^{-(b+q)L}}{(b \, + \, q)} \right] \Bigg\} \delta_{\boldsymbol{k'_{||}} - \boldsymbol{k_{||}} \pm \boldsymbol{q}} \end{aligned} \tag{4.33}$$

where the integrals have been evaluated using:

$$\int_l^L y^2 e^{-(q+b)y}\,dy = \frac{l^2 e^{-(b+q)l} - L^2 e^{-(b+q)L}}{(b+q)} + \frac{2}{(b+q)}\left[\frac{le^{-(b+q)l} - Le^{-(b+q)L}}{(b+q)} - \frac{e^{-(b+q)L} - e^{-(b+q)l}}{(b+q)^2}\right]$$

$$\int_l^L y\, e^{-(q+b)y}\,dy = \frac{le^{-(b+q)l} - Le^{-(b+q)L}}{(b+q)} - \frac{e^{-(b+q)L} - e^{-(b+q)l}}{(b+q)^2}$$

$$\int_l^L e^{-(q+b)y}\,dy = \frac{e^{-(b+q)l} - e^{-(b+q)L}}{(b+q)}$$

$$\frac{1}{S}\int_{-\infty}^{+\infty} dx \int_{-\infty}^{+\infty} dz\, e^{iz(k_z - k'_z)} e^{ix(k_x - k'_x)} = \delta_{\boldsymbol{k'_{||}} - \boldsymbol{k_{||}}} \tag{4.34}$$

with L representing the thickness of the diamond sample,

Thus, the matrix element for the symmetric case is,

$$M^{\{e,a\}}(q) = \left[\frac{2\pi e_h^2 \hbar \left(L^2 q \epsilon_d^2\right)^{-1}}{|(\partial/\partial\omega)(\sqrt{\epsilon_{\perp,1}\epsilon_{y,1}}\tanh(\sqrt{\epsilon_{\perp,1}/\epsilon_{y,1}}qd/2) - \epsilon_0)|}\right]^{\frac{1}{2}} F(q)(\mp)(n + \frac{1}{2} \pm \frac{1}{2})^{\frac{1}{2}} \delta_{\boldsymbol{k'_{||}} - \boldsymbol{k_{||}} \pm \boldsymbol{q}} \tag{4.35}$$

while for the antisymmetric case it is,

$$M^{\{e,a\}}(q) = \left[\frac{2\pi e_h^2 \hbar \left(L^2 q \epsilon_d^2\right)^{-1}}{|(\partial/\partial\omega)(\sqrt{\epsilon_{\perp,1}\epsilon_{y,1}}\coth(\sqrt{\epsilon_{\perp,1}/\epsilon_{y,1}}qd/2) - \epsilon_0)|}\right]^{\frac{1}{2}} F(q)(\mp)(n + \frac{1}{2} \pm \frac{1}{2})^{\frac{1}{2}} \delta_{\boldsymbol{k'_{||}} - \boldsymbol{k_{||}} \pm \boldsymbol{q}} \tag{4.36}$$

where the upper sign corresponds to phonon emission and the lower sign to absorption, and,

$$\begin{aligned} F(q) \;=\; \frac{b^3}{2}e^{bl}\Bigg\{ & \frac{l^2e^{-(b+q)l} \;-\; L^2e^{-(b+q)L}}{(b\;+\;q)} \\ +\frac{2}{(b\;+\;q)}\Bigg[& \frac{le^{-(b+q)l} \;-\; Le^{-(b+q)L}}{(b\;+\;q)} \;-\; \frac{e^{-(b+q)L} \;-\; e^{-(b+q)l}}{(b\;+\;q)^2}\Bigg] \;+ \\ -2l\Bigg[& \frac{le^{-(b+q)l} \;-\; Le^{-(b+q)L}}{(b\;+\;q)} \;-\; \frac{e^{-(b+q)L} \;-\; e^{-(b+q)l}}{(b\;+\;q)^2}\Bigg] \\ +l^2\Bigg[& \frac{e^{-(b+q)l} \;-\; e^{-(b+q)L}}{(b\;+\;q)}\Bigg]\Bigg\} \end{aligned} \tag{4.37}$$

It follows that:

$$\left|M^{\{e,a\}}(q)\right|^2 \;=\; |C|^2F^2(n+\frac{1}{2}\pm\frac{1}{2})\delta_{\boldsymbol{k}'_{||}\,-\,\boldsymbol{k}_{||}\,\pm\,\boldsymbol{q}} \tag{4.38}$$

where C, for the symmetric case is,

$$C \;=\; \left[\frac{2\pi e_h^2\hbar\left(L^2q\epsilon_d^2\right)^{-1}}{|(\partial/\partial\omega)(\sqrt{\epsilon_{\perp,1}\epsilon_{y,1}}\tanh(\sqrt{\epsilon_{\perp,1}/\epsilon_{y,1}}qd/2)\;-\;\epsilon_0)|}\right]^{\frac{1}{2}} \tag{4.39}$$

while for the antisymmetric case,

$$C \;=\; \left[\frac{2\pi e_h^2\hbar\left(L^2q\epsilon_d^2\right)^{-1}}{|(\partial/\partial\omega)(\sqrt{\epsilon_{\perp,1}\epsilon_{y,1}}\coth(\sqrt{\epsilon_{\perp,1}/\epsilon_{y,1}}qd/2)\;-\;\epsilon_0)|}\right]^{\frac{1}{2}} \tag{4.40}$$

Therefore, the total scattering rate predicted by the Fermi Golden Rule is given by:

$$\begin{aligned}\frac{1}{\tau} &= \frac{L^2}{(2\pi)^2}\int d^2\boldsymbol{q}\frac{2\pi}{\hbar}\,|C|^2F^2\,(n\,+\,\frac{1}{2}\pm\frac{1}{2})\delta_{\boldsymbol{k'_{||}}-\boldsymbol{k_{||}}\pm\boldsymbol{q}}\,\delta(E(\boldsymbol{k'})\,-\,E(\boldsymbol{k})\,\pm\,\hbar\omega_q)\,= \\ &\frac{L^2}{2\pi\hbar}\int d^2\boldsymbol{q}\,|C|^2F^2\,(n\,+\,\frac{1}{2}\pm\frac{1}{2})\delta_{\boldsymbol{k'_{||}}-\boldsymbol{k_{||}}\pm\boldsymbol{q}}\,\delta(E(\boldsymbol{k'})\,-\,E(\boldsymbol{k})\,\pm\,\hbar\omega_q)\,= \\ &\frac{e_h^2}{\epsilon_r^2}\int d^2\boldsymbol{q}\,\frac{D(q,\omega)}{q}\,(n\,+\,\frac{1}{2}\pm\frac{1}{2})\delta_{\boldsymbol{k'_{||}}-\boldsymbol{k_{||}}\pm\boldsymbol{q}}\,\delta(E(\boldsymbol{k'})\,-\,E(\boldsymbol{k})\,\pm\,\hbar\omega_q)\end{aligned} \tag{4.41}$$

where the term $D(q,\omega)$ is,

$$D(q,\omega)\,=\,\frac{F^2}{|(\partial/\partial\omega)(\sqrt{\epsilon_{\perp,1}\epsilon_{y,1}}\tanh(\sqrt{\epsilon_{\perp,1}/\epsilon_{y,1}}qd/2)\,-\,\epsilon_0)|} \tag{4.42}$$

In order to obtain the total contribution of both the symmetric and antisymmetric solutions, the two terms are eventually summed exploiting Matthiessen Rule:

$$\frac{1}{\tau}\,=\,\frac{1}{\tau_s}\,+\,\frac{1}{\tau_a} \tag{4.43}$$

As shown in Figure 13, a strong relationship between the phonon wavenumber and frequency exists, that has to be taken into account explicitly when deriving the scattering rate through Fermi Golden Rule. For this reason, a set of transformation analogous to the one reported in [39] is applied to the formulation obtained in Equation 4.41.

Considering $P(q,\omega)\,=\,\frac{e_h^2}{\epsilon_r^2}D(q,\omega)(n\,+\frac{1}{2}\,\pm\,\frac{1}{2})$ and $L(q,\omega,\theta)\,=\,E_{\boldsymbol{k}\mp\boldsymbol{q}}\,-\,E_{\boldsymbol{k}}\,\pm\,\hbar\omega$, it holds:

$$\frac{1}{\tau}\,=\,\int\frac{P}{q}\delta(L)d\boldsymbol{q}\,=\,\int P\delta(L)dq\,d\theta\,=\,\int P\left|\frac{dL}{dq}\right|^{-1}d\theta\,=\,\int P\left|\frac{dL}{dq}\right|^{-1}\left|\frac{d\theta}{d\omega}\right|d\omega \tag{4.44}$$

Momentum conservation is enforced as well, in the form:

$$E_{\boldsymbol{k}\mp\boldsymbol{q}} - E_{\boldsymbol{k}} \pm \hbar\omega = \frac{\hbar^2\left(\boldsymbol{k}-\boldsymbol{q}\right)^2}{2m^*} - \frac{\hbar^2\boldsymbol{k}^2}{2m^*} \pm \hbar\omega = q^2 - 2qkcos\theta \pm \frac{2m^*\omega}{\hbar} = 0$$
$$cos\theta = \frac{q}{2k} \pm \frac{m^*\omega}{qk\hbar} \tag{4.45}$$
$$\theta = \arccos\left(\frac{q}{2k} \pm \frac{m^*\omega}{qk\hbar}\right)$$

where parabolic carrier bands are assumed. Thus, it holds:

$$\frac{d\theta}{d\omega} = \frac{-1}{\sqrt{1-\left(\frac{q}{2k} \pm \frac{m^*\omega}{qk\hbar}\right)^2}}\left[\frac{1}{2k}\frac{\partial q}{\partial\omega} \pm \frac{m^*}{k\hbar}\left(\frac{q-\omega\frac{\partial q}{\partial\omega}}{q^2}\right)\right] =$$
$$\frac{-\frac{m^*}{k\hbar}\left(\frac{\hbar}{2m^*}\frac{1}{V_g} \pm \frac{1}{q} \mp \frac{V_p}{q}\frac{1}{V_g}\right)}{\frac{m^*}{k\hbar}\sqrt{\frac{1}{m^*}\left(2E_k - \frac{E_q}{2} \mp \hbar\omega\right) - V_p^2}} = \frac{\left[\left(\pm\frac{V_p}{q} - \frac{\hbar}{2m^*}\right)\frac{1}{V_g} \mp \frac{1}{q}\right]}{\sqrt{\frac{1}{m^*}\left(2E_k - \frac{E_q}{2} \mp \hbar\omega\right) - V_p^2}} \tag{4.46}$$

where $V_g = \frac{\partial\omega}{\partial q}$ and $V_p = \frac{\omega}{q}$ represent respectively phonon's Group and Phase velocity.

It is immediate to derive,

$$\frac{dL}{dq} = \frac{\hbar^2 q}{m^*} - \frac{\hbar^2 k}{m^*}cos\theta \pm \hbar\frac{\partial\omega}{\partial q} = \frac{\hbar^2}{m^*}\left(q - kcos\theta \pm \frac{m^*}{\hbar}\frac{\partial\omega}{\partial q}\right) \tag{4.47}$$

Recalling Equation 4.45, the derivative reported in Equation 4.47 can be expressed as:

$$\frac{dL}{dq} = \frac{\hbar^2}{m^*}\left[q - k\left(\frac{q}{2k} \pm \frac{m^*\omega}{qk\hbar}\right) \pm \frac{m^*}{\hbar}\frac{\partial\omega}{\partial q}\right] =$$
$$\frac{\hbar^2}{m^*}\left(q \mp \frac{m^*\omega}{\hbar q} - \frac{q}{2} \pm \frac{m^*}{\hbar}\frac{\partial\omega}{\partial q}\right) = \frac{\hbar^2}{m^*}\left[\frac{q}{2} - \frac{m^*}{\hbar}\left(\pm V_p \mp V_g\right)\right] \tag{4.48}$$

It is finally obtained:

$$\frac{1}{\tau_{(a)}^{(e)}} = \mp\frac{m^* e_h^2}{\epsilon_r^2 \hbar^2} \int_{\omega_1}^{\omega_2} \frac{\left(n + \frac{1}{2} \pm \frac{1}{2}\right) D(q,\omega)\sigma \left[\left(\frac{V_p}{q} \mp \frac{\hbar}{2m^*}\right)\frac{1}{V_g} - \frac{1}{q}\right]}{\left[\frac{q}{2} \mp \frac{m^*}{\hbar}\left(V_p - V_g\right)\right]\sqrt{\frac{1}{m^*}\left(2E_k - \frac{E_q}{2} \mp \hbar\omega\right) - V_p^2}}\, d\omega \tag{4.49}$$

$$\sigma = \begin{cases} 0 & \text{if } \frac{1}{m^*}\left(2E_k - \frac{E_q}{2} \mp \hbar\omega\right) - V_p^2 < 0 \\ 1 & \text{otherwise} \end{cases} \tag{4.50}$$

where the conditional variable σ has been introduced to ensure energy and momentum conservation accordingly to what reported in [40], and the range $[\omega_1, \omega_2]$ is determined by the region of existence of the IF modes depicted in Figure 13.

CHAPTER 5

NUMERICAL EVALUATION

The numerical results obtained for the formulation of the scattering rate for Remote IF optical-phonons of Equation 4.49 are reported in this section.

A Matlab code based on the one developed in [41] has been used for the purpose of performing the numerical integration: the built-in function *trapz* is exploited to numerically evaluate the required integration. The results for both AlN and w-BN are reported in the following section: for both the cases, the upper layer is characterized by a thickness $d = 5\,nm$, and the density of charges in the 2DHG is considered to be $N_h = 2 \times 10^{13}\,cm^{-2}$, localized at $l = 0\,nm$.

5.1 AlN layer

The dispersion curve for the IF modes in AlN are already reported in Figure 13, while Phase and Group velocities for the optical phonons are reported in Figure 14.

As noticeable, the lowest velocities happen to be in the surrounding of the resonance frequency of symmetric and antisymmetric modes: according to Equation 4.50, this leads to the fulfillment of the momentum and energy conservation condition, leading to an higher emission associated to the resonance frequency; this behavior is depicted in Figure 15, in which the number of phonons emitted in respect to the frequency is represented for three different values of holes energy E_k. The localization of the emission of phonons in a narrow range of values close to the resonant frequency is also related to the relatively high effective mass m^* of diamond.

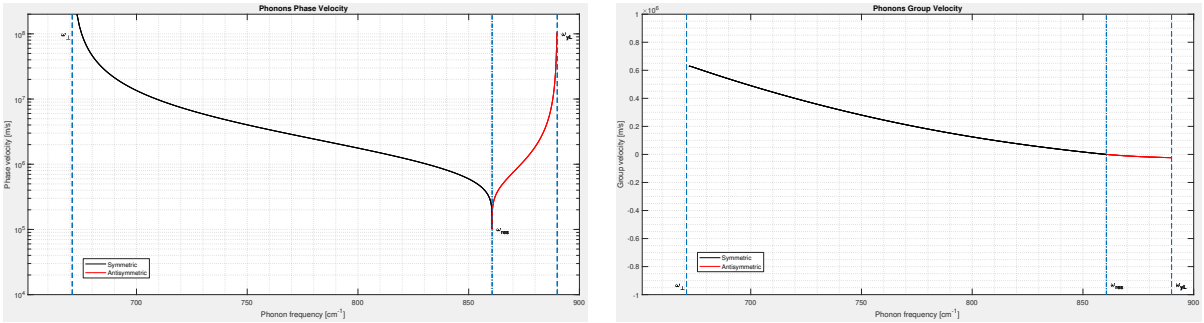

Figure 14: Phase (left) and Group (right) velocity for the IF polar-phonons in AlN layer.

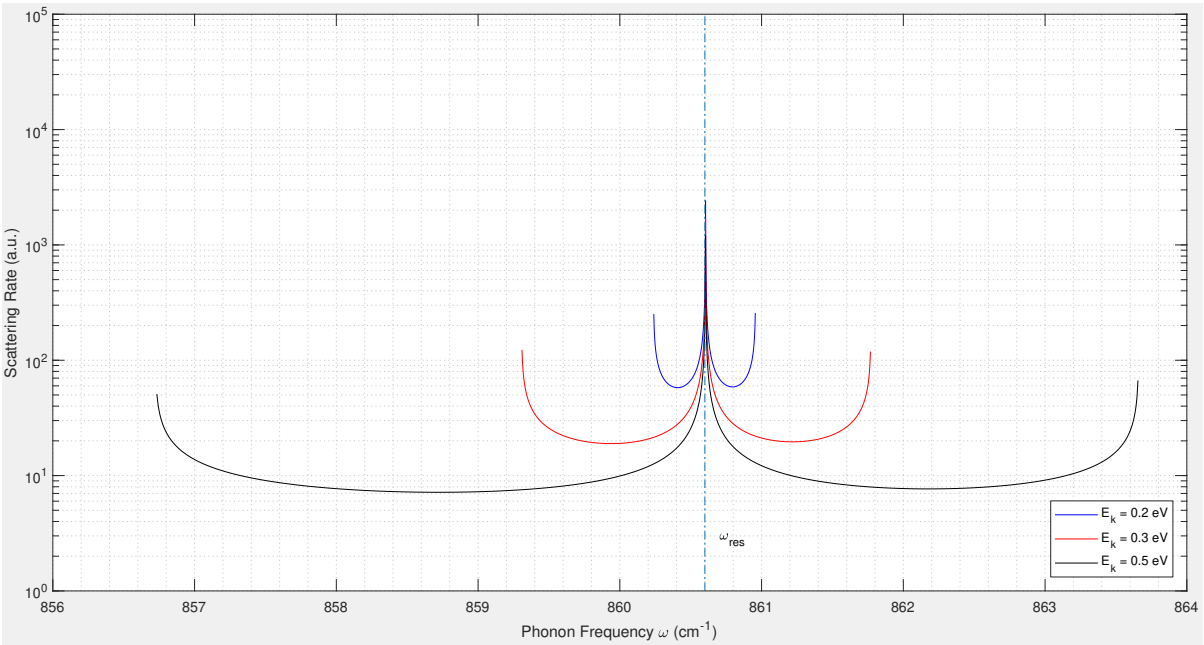

Figure 15: Frequency distribution of the phonon emission for the case of an AlN layer.

The scattering rates obtained after the numerical integration are reported in Figure 16: as noticeable, the emission contributions appear for a value of hole energy equivalent to the resonance frequency of the IF modes.

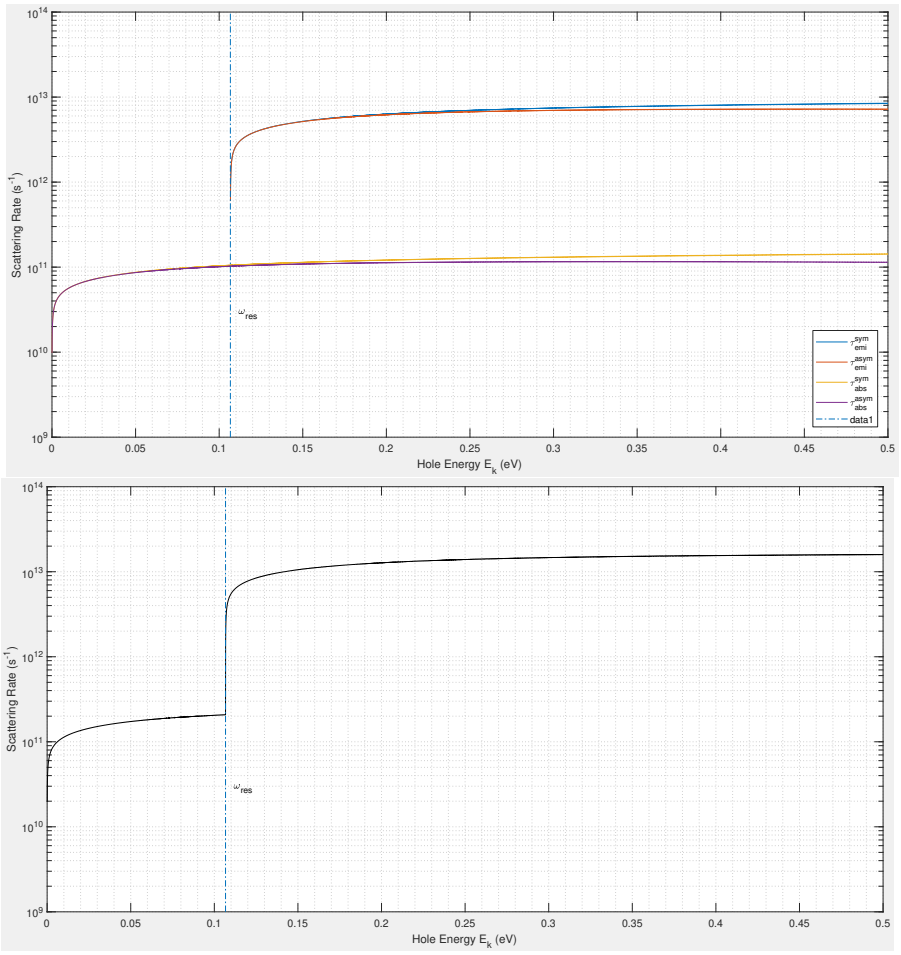

Figure 16: Scattering rate for symmetric and antisymmetric absorption and emission (top) and their summation (bottom) for the AlN case.

5.2 w-BN layer

The dispersion curve for the IF modes in w-BN are reported in Figure 17: it is worth noticing that, in comparison to the curves obtained for the case of AlN layer, the resonant frequency for the w-BN layer happens for an higher value of phonon frequency.

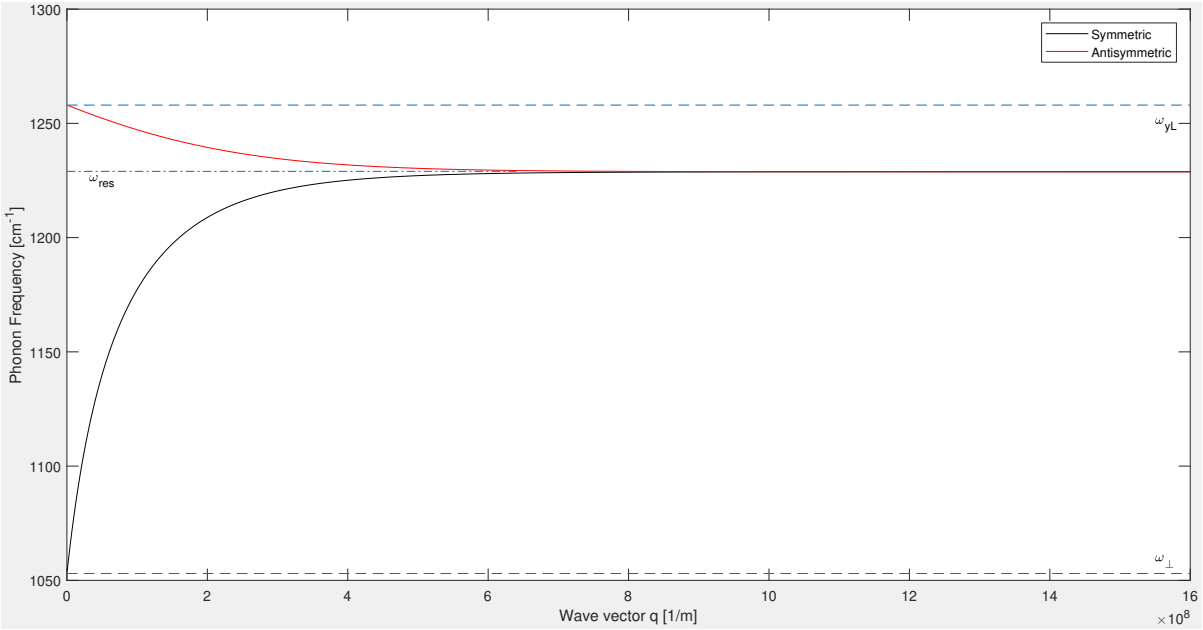

Figure 17: Dispersion Relation for symmetric and antisymmetric IF modes in w-BN (5 nm thickness)

From the dispersion curve reported above, the Phase and Group velocities for the IF optical -phonons are obtained and reported in Figure 18.

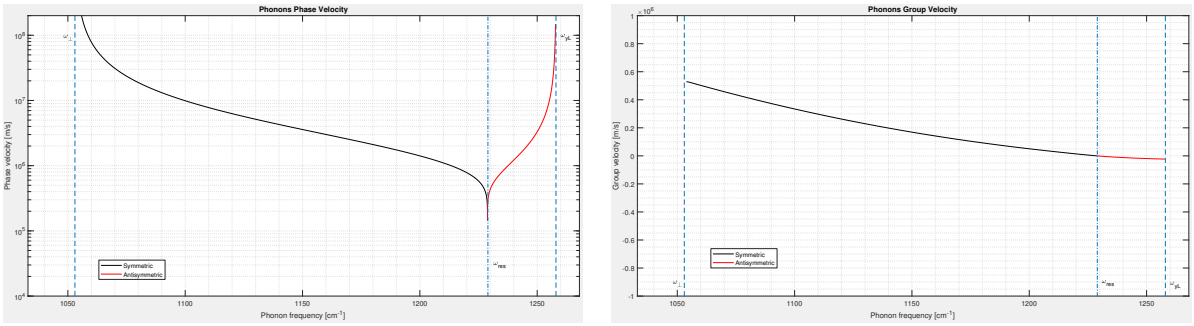

Figure 18: Phase (left) and Group (right) velocity for the IF polar-phonons in w-BN layer.

Also in this case, the lowest velocities happen to be in the surrounding of the resonance frequency of symmetric and antisymmetric modes, leading to an higher emission associated to the resonance frequency, as depicted in Figure 19.

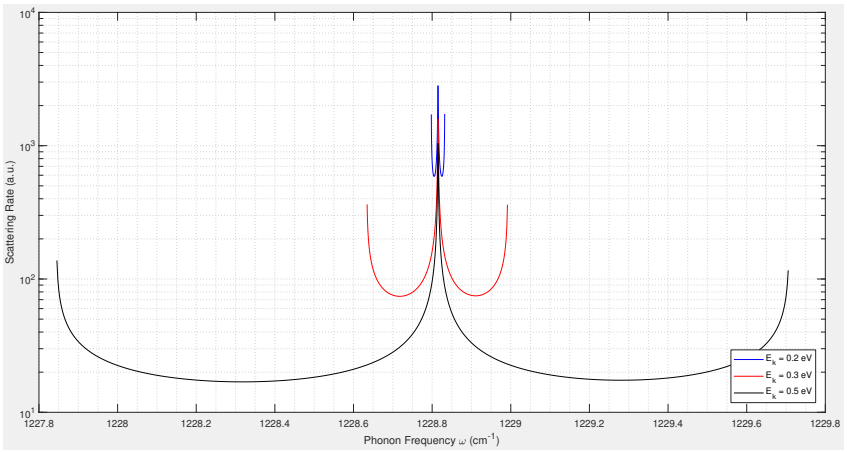

Figure 19: Frequency distribution of the phonon emission for the case of a w-BN layer.

In comparison to the AlN case, the emission of phonons appears to be more localized in a narrow range of values close to the resonant frequency; this could be explained with the higher phonons' phase velocity in the case of w-BN .

The scattering rates obtained after the numerical integration are reported in Figure 20: as noticeable, also in this case the emission contribute appears for hole energies equivalent to the resonance frequency of the IF modes: this leads to a sharp increase of the scattering rate localized at higher energies in respect to the AlN case.

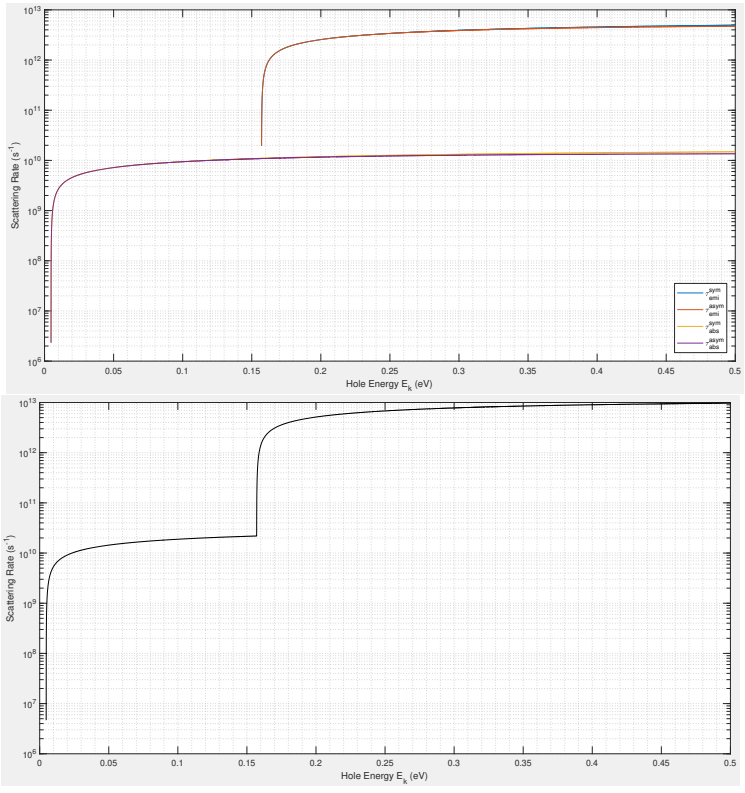

Figure 20: Scattering rate for symmetric and antisymmetric absorption and emission (top) and their summation (bottom) for the w-BN case.

5.3 Discussion

The numerical evaluation performed for the Remote IF polar-phonons shows some interesting results: it is however worthy to underline that different configurations of the simulation parameters may lead to a modification in the scattering rate. In particular, different materials, characterized by different resonant frequencies, may lead to emissions of Remote-IF polar phonons localized at higher or reduced hole energies.

The layer thickness modifies the wave number of the IF polar-phonons: as a matter of fact, an increase in d would result in a reduction of the wave number q, leading to higher Phase and Group velocities; this would consequently lead to an emission of polar phonons more localized in the vicinity of the resonance frequency.

On the other hand, an higher density of holes localized at the diamond surface would lead to an increase in the scattering rate, consistently with what has been reported in the evaluation of the same contribution for the case of SiO_2/Si [24][25]. Concerning this topic, it is important to underline that the depth of the 2DHG has been fixed to be $l = 0\,nm$. This choice is related to the representation of the 2DHG through Fang-Howard wavefunction: as depicted in Figure 21, for such a configuration the probability to find the holes ($|\Psi|^2$) is already localized a few Ångström below the surface of diamond, in accordance with what has been measured and reported in the literature [2].

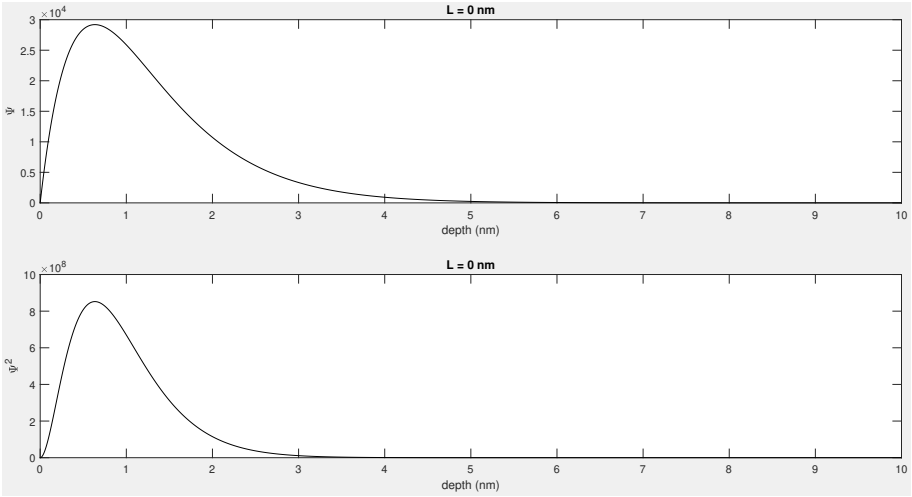

Figure 21: Representation of the Fang-Howard wavefunction (top) and absolute squared value (bottom) for $l = 0\,nm$.

In order to obtain a useful comparison with the existent models trying to obtain an estimation of the 2DHG mobility in H-terminated diamond, as the one reported in [18], the mobility related to the obtained scattering rates is computed. Therefore, the conduction mass m_c^* is introduced accordingly to [18]:

$$m_c^* = \frac{\left(m_{lh}^{*3/2} + m_{hh}^{*3/2} + m_{so}^{*3/2}\right)}{\left(m_{lh}^{*1/2} + m_{hh}^{*1/2} + m_{so}^{*1/2}\right)} \tag{5.1}$$

and the 2DHG mobility is obtained as:

$$\mu = \frac{e_h \tau}{m_c^*} \tag{5.2}$$

The mobility results obtained for the AlN case are reported in Figure 22: the dependence of the mobility to the hole energy and to the hole density (for $E_k = 0.5\,eV$) is shown.

Comparing the obtained results with the one reported in [18], it appears evident that the obtained contribution is of the same order of magnitude of the ones reported there: thus, the importance of the model under analysis is clear, allowing to obtain a more faithful representation of the overall mobility in diamond-based devices realized through the insertion of polar materials.

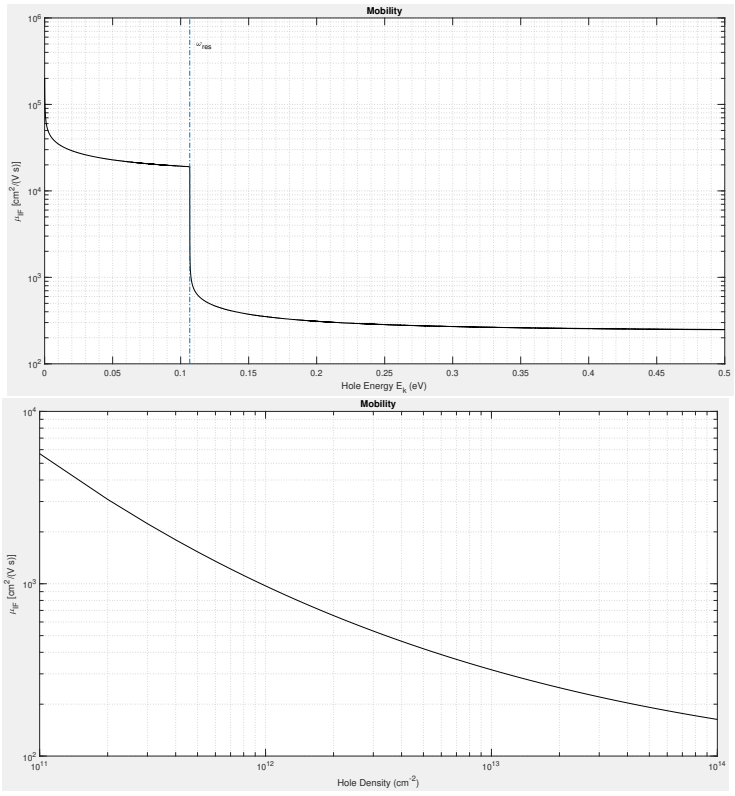

Figure 22: 2DHG mobility considering only the IF Remote polar-phonons coming from the layer of AlN. The dependence to holes energy (TOP) and holes density (BOTTOM) is shown.

CHAPTER 6

CONCLUSION AND FUTURE WORK

6.1 Conclusion

The scattering rates of holes by surface-acoustic phonons and remote-IF-polar phonons in the diamond structure are formulated for the first time.

An introduction on the current research trends in the realization of diamond-FETs is given, together with a recapitulation on the possible doping and passivation mechanisms.

The analysis of the SAWs in the structure led to an extensive study of Rayleigh wave and its higher modes, with particular attention on the Sezawa waves; the obtained dispersion curves confirms the existence of Rayleigh wave as a single mode in the diamond substrate.

On the other hand, the model adopted in the case of remote-IF-polar phonons is suitable to describe several promising polar materials, such as AlN, w-BN and c-BN, MoO3 and WO3, currently adopted for the realization of diamond based MISFETs and HFET due to their wide-band gap.

The obtained formulations facilitate taking into account these scattering mechanisms in the calculation of holes mobility in diamond, affording a more complete view of the involved contributions.

6.2 Future Work

Numerical computations of the obtained expression for the surface acoustic phonons would represent a useful evaluation, in order to obtain a comparison with the calculated Remote IF polar-phonons contribution.

Furthermore, an extensive work taking into account these newly formulated contributions together with the already known scattering mechanisms is desirable, for the purpose of evaluating if the obtained model is able to predict the hole mobility in diamond-based devices with a satisfactory accuracy or if further study involving other mechanisms should be performed.

Finally, the general formulation of the remote-polar-optical phonons scattering mechanism presented herein facilitates the analysis of other polar materials which are not considered in this work, permitting an easy comparison of the effects related to the insertion of certain materials in respect to others and providing insight useful for the selection of the material.

APPENDIX

SEZAWA WAVE QUANTIZATION

Sezawa waves represents one of the possible and more interesting surface modes existing in the structure depicted in Figure 23. In the following description, the ′ symbol will be used to denote quantities related to the upper layer, while unprimed symbols will be used to refer to quantities related to the subjacent structure.

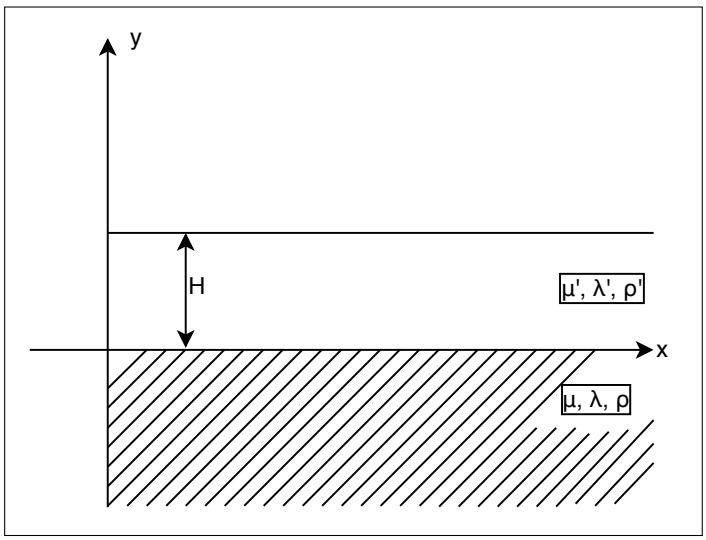

Figure 23: Physical structure under analysis for the Sezawa waves study.

APPENDIX (continued)

One starts with the expression of the horizontal and vertical displacement within a stratum (Equation A.1) and in the subjacent medium (Equation A.2) for the Sezawa waves obtained and reported by Sezawa and Kanai [31]. After the enforcement of the Boundary Conditions requiring the continuity of displacement and stress at the interface, and the absence of stress at the surface of the structure, it is obtained:

$$\begin{cases} u'_x = -A\frac{s'}{f}\left[-iB - 2iC + i\frac{r's}{f^2}D + i\frac{r's}{f^2}E - i\frac{rs'}{f^2}F + iG \right] \\ u'_y = -iA\left[i\frac{r's'}{f^2}H + i\frac{s'}{f}I - iL - i\frac{r's'}{f^2}M + i\frac{r'}{f}N \right] \end{cases} \tag{A.1}$$

$$\begin{cases} u_x = \frac{iA\mu' s' k'^2}{\mu f^3}\left(Pe^{ry} + \frac{s}{f}Qe^{sy} \right) \\ u_y = \frac{-A\mu' s' k'^2}{\mu f^3}\left(\frac{r}{f}Pe^{ry} + Qe^{sy} \right) \end{cases} \tag{A.2}$$

where:

APPENDIX (continued)

$$
\begin{cases}
B = (\frac{k'^2}{f^2} - 2)\eta cosh(r'y)sinh(r'H) - cosh(r'H)sinh(r'y) \quad C = \frac{r's'}{f^2}\eta sin(s'(H-y)) \\
D = \varphi\Big\{(\frac{k'^2}{f^2} - 2)cosh(r'H)cos(s'y) + 2cos(s'H)cosh(r'y)\Big\} \\
E = \zeta\Big\{(\frac{k'^2}{f^2} - 2)cosh(r'H)sin(s'y) + 2sin(s'H)cosh(r'y)\Big\} \\
F = \varphi\Big\{2sin(s'H)sinh(r'y) + (\frac{k'^2}{f^2} - 2)sinh(r'H)sin(s'y)\Big\} \\
G = \theta\Big\{(\frac{k'^2}{f^2} - 2)sinh(r'H)cos(s'y) + 2cos(s'H)sinh(r'y)\Big\} \\
H = \eta\Big\{(\frac{k'^2}{f^2} - 2)cosh(r'y)cosh(r'H) - sinh(r'H)sinh(r'y) - 2cos(s'(H-y))\Big\} \\
I = \varphi\Big\{\frac{r}{f}(\frac{k'^2}{f^2} - 2)sinh(r'H)cos(s'y) + \frac{2r'^2s}{f^3}cos(s'H)sinh(r'y)\Big\} \\
L = \frac{2r'^2s'^2}{f^4}\zeta sin(s'H)sinh(r'y) + (\frac{k'^2}{f^2} - 2)\theta sinh(r'H)sin(s'y) \\
M = 2\theta cos(s'H)cosh(r'y) - (\frac{k'^2}{f^2} - 2)\zeta cosh(r'H)cos(s'y) \\
N = \varphi\Big\{ - \frac{s}{f}(\frac{k'^2}{f^2} - 2)cosh(r'H)sin(s'y) + 2\frac{rs'^2}{f^3}sin(s'H)cosh(r'y)\Big\} \\
P = \frac{2sr'}{f^2}\beta cos(s'H) + 2\frac{r's'}{f^2}\alpha sin(s'H) - \frac{2sr'}{f^2}(2 - \frac{k'^2}{f^2})(\frac{\mu'}{\mu} - 1)cosh(r'H) + (2 - \frac{k'^2}{f^2})\gamma sinh(r'H) \\
Q = -\frac{2r'}{f}\gamma cos(s'H) - 4\frac{rr's'}{f^3}(\frac{\mu'}{\mu} - 1)sin(s'H) + \frac{r'}{f}(2 - \frac{k'^2}{f^2})\alpha cosh(r'H) - \frac{r}{f}(2 - \frac{k'^2}{f^2})\beta sinh(r'H) \\
\varphi = \frac{\mu' k^2 k'^2}{\mu f'} \quad \zeta = \frac{4rs}{f^2}\Big(\frac{\mu'}{\mu} - 1\Big)^2 - \alpha^2 \\
\eta = \frac{2rs}{f^2}\Big(\frac{\mu'}{\mu} - 1\Big)\beta - \alpha\gamma \quad \theta = \frac{rs}{f^2}\beta^2 - \gamma^2 \\
\alpha = \frac{2\mu'}{\mu} - \Big(2 - \frac{k^2}{f^2}\Big) \quad \beta = \frac{2\mu'}{\mu}\Big(2 - \frac{k^2}{f^2}\Big) - 2 \quad \gamma = \frac{\mu'}{\mu}\Big(2 - \frac{k'^2}{f^2}\Big) - \Big(2 - \frac{k^2}{f^2}\Big) \\
r^2 = f^2 - h^2 \quad s^2 = f^2 - k^2 \\
r'^2 = f^2 - h'^2 \quad s'^2 = k'^2 - f^2 \\
h^2 = \frac{\rho p^2}{\lambda + 2\mu} \quad k^2 = \frac{\rho p^2}{\mu} \\
h'^2 = \frac{\rho' p^2}{\lambda' + 2\mu'} \quad k'^2 = \frac{\rho' p^2}{\mu'}
\end{cases}
\tag{A.3}
$$

APPENDIX (continued)

where ρ and ρ', μ and μ', λ and λ' represent the densities and elastic constants of the materials, p represents the wave's angular frequency, and f its wave vector.

Before proceeding further, it is important to notice that even if the displacement expressions differ according to the layer under study, the amplitude of the constant A is undetermined and equal for both the expressions: for this reason, in order to identify it unequivocally, second quantization must be enforced to the whole expression. It is now possible, as a preliminary step, to define generic displacements u_x and u_y, whose actual expressions coincide with the one reported in Equation A.1 and Equation A.2 according to the layer under consideration.
Indeed, the normalization condition requires:

$$\frac{1}{aL}\int_0^a \int_{-\infty}^{H} u_x u_x^* + u_y u_y^* \, dxdy = \frac{\hbar}{2m\omega_k} \tag{A.4}$$

In both the expressions of the displacements, no dependencies along the x direction is present: therefore, it possible to eliminate the integral in the x variable, obtaining:

$$\frac{1}{L}\int_{-\infty}^{H} u_x u_x^* + u_y u_y^* \, dy = \frac{\hbar}{2m\omega_k} \tag{A.5}$$

It is now possible to divide the integrals according to the layer under consideration, obtaining:

$$\frac{1}{L}\int_{-\infty}^{0} u_x u_x^* + u_y u_y^* \, dy + \frac{1}{H}\int_0^{H} u'_x u'^*_x + u'_y u'^*_y \, dy = \frac{\hbar}{2m\omega_k} \tag{A.6}$$

APPENDIX (continued)

Thus, developing the integrals for the second quantization, a condition for A is found: the expression obtained is here reported in this appendix since it is cumbersome, and it is intended to be used directly during the numeric computations for specific cases.

For the resolution of the quantization procedure, a MATLAB code has been developed in order to verify the correctness of the performed calculations. The exploited code does not use all the constants reported in Kanai, in order to avoid obtaining a too extended formulation: however, a version with the complete formulation has been developed without success, since the integral calculations required an excessive quantity of memory. Even introducing by hand the results obtained after the integration on paper, no useful simplifications were achieved, leading to a cumbersome result due to the excessive length of the final expression. The obtained result is reported below.

APPENDIX (continued)

```
(A^2((s_p^2((k^4k_p^4mu_p^2((r_p^3s^2sinh(2Hr_p)(cos(2Hs_p) + 1))/2 -
(Hr^2(cosh(2Hr_p)/2 - 1/2)(cos(2Hs_p)/2 - 1/2)(2f^2 - k_p^2)^2)/2 +
(Hr_p^4s^2(cosh(2Hr_p) - 1)(cos(2Hs_p) + 1))/2 + (Hr^2(2f^2 - k_p^2)^2(cosh(2Hr_p) -
1)(cos(2Hs_p) + 1))/8 - 2Hr_p^4s^2cos(Hs_p)^2(cosh(2Hr_p)/2 + 1/2) +
(r^2sin(2Hs_p)(2f^2 - k_p^2)^2(cosh(2Hr_p) - 1))/(8s_p) + (rr_p^3ssinh(2Hr_p)(f^22i -
k_p^21i)(cos(2Hs_p) + 1)1i)/(r_p^2 + s_p^2) - (rr_p^2ss_psin(2Hs_p)(2f^2 -
k_p^2)(cosh(2Hr_p) - 1))/(r_p^2 + s_p^2))))/(f^14mu^2) -
(k^4k_p^4mu_p^2rr_p^3scos(Hs_p)sinh(Hr_p)(f^22i - k_p^21i)4i)/(f^14mu^2(r_p^2 +
s_p^2))))/f^2 + (2s_p((2k^2k_p^2mu_pr(cosh(2Hr_p)/2 - 1/2)(cos(Hs_p)^2 - 1)((2f^2mu -
2f^2mu_p - k^2mu + k_p^2mu_p)^2/(f^4mu^2) - (rs(2f^2mu - 2f^2mu_p +
k_p^2mu_p)^2)/(f^6mu^2)))/(f^5mus_p) - (2k^2k_p^4mu_pr(cosh(2Hr_p)/2 - 1/2)(cos(Hs_p)^2
- 1)((2f^2mu - 2f^2mu_p - k^2mu + k_p^2mu_p)^2/(f^4mu^2) - (rs(2f^2mu - 2f^2mu_p +
k_p^2mu_p)^2)/(f^6mu^2)))/(f^7mus_p) + (k^2k_p^6mu_pr(cosh(2Hr_p)/2 - 1/2)(cos(Hs_p)^2
- 1)((2f^2mu - 2f^2mu_p - k^2mu + k_p^2mu_p)^2/(f^4mu^2) - (rs(2f^2mu - 2f^2mu_p +
k_p^2mu_p)^2)/(f^6mu^2)))/(2f^9mus_p) - (k^2k_p^2mu_pr_p^3ss_p^2sin(2Hs_p)(sinh(2Hr_p)
- 2Hr_p)((4(2f^2mu_p - 2f^2mu + k^2mu)^2)/(f^4mu^2) - (16rs(mu -
mu_p)^2)/(f^2mu^2)))/(8f^11mu) +
(4k^2k_p^2mu_pr_p^2scos(Hs_p)sinh(Hr_p)(r_pcosh(Hr_p)sin(Hs_p) -
s_pcos(Hs_p)sinh(Hr_p))((2f^2mu - 2f^2mu_p - k^2mu + k_p^2mu_p)^2/(f^4mu^2) -
(rs(2f^2mu - 2f^2mu_p + k_p^2mu_p)^2)/(f^6mu^2)))/(f^7mu(r_p^2 + s_p^2)) -
(2k^2k_p^4mu_pr_p^2scos(Hs_p)sinh(Hr_p)(r_pcosh(Hr_p)sin(Hs_p) -
s_pcos(Hs_p)sinh(Hr_p))((2f^2mu - 2f^2mu_p - k^2mu + k_p^2mu_p)^2/(f^4mu^2) -
(rs(2f^2mu - 2f^2mu_p + k_p^2mu_p)^2)/(f^6mu^2)))/(f^9mu(r_p^2 + s_p^2)) +
(4k^2k_p^2mu_prr_p^2s_p^2sinh(Hr_p)sin(Hs_p)((2f^2mu_p - 2f^2mu + k^2mu)^2/(f^4mu^2) -
(4rs(mu - mu_p)^2)/(f^2mu^2))(r_pcosh(Hr_p)cos(Hs_p) - r_p +
s_psinh(Hr_p)sin(Hs_p)))/(f^9mu(r_p^2 + s_p^2)) -
(2k^2k_p^4mu_prr_p^2s_p^2sinh(Hr_p)sin(Hs_p)((2f^2mu_p - 2f^2mu + k^2mu)^2/(f^4mu^2) -
(4rs(mu - mu_p)^2)/(f^2mu^2))(r_pcosh(Hr_p)cos(Hs_p) - r_p +
s_psinh(Hr_p)sin(Hs_p)))/(f^11mu(r_p^2 + s_p^2))))/f -
(r_p^2((k^4k_p^4mu_p^2((Hr^2s_p^4(cosh(2Hr_p) + 1)(cos(2Hs_p) - 1))/2 + (Hs^2(2f^2 -
k_p^2)^2(cosh(2Hr_p) + 1)(cos(2Hs_p) - 1))/8 + (s^2sin(2Hs_p)(2f^2 -
k_p^2)^2(cosh(2Hr_p) + 1))/(8s_p) + (r^2s_p^4sinh(2Hr_p)(cos(2Hs_p)/2 - 1/2))/r_p -
(Hs^2cos(Hs_p)^2(cosh(2Hr_p)/2 + 1/2)(2f^2 - k_p^2)^2)/2 - 2Hr^2s_p^4(cosh(2Hr_p)/2 -
1/2)(cos(2Hs_p)/2 - 1/2) + (2rss_p^3cosh(Hr_p)^2sin(2Hs_p)(2f^2 - k_p^2))/(r_p^2 +
s_p^2) + (rr_pss_p^2sinh(2Hr_p)(2f^2 - k_p^2)(cos(2Hs_p) - 1))/(r_p^2 +
s_p^2)))/(f^14mu^2) - (4k^4k_p^4mu_p^2rss_p^3cosh(Hr_p)sin(Hs_p)(2f^2 -
k_p^2))/(f^14mu^2(r_p^2 + s_p^2))))/f^2 + (2r_p((k^2k_p^2mu_pssinh(2Hr_p)(sin(2Hs_p) -
2Hs_p)((2f^2mu - 2f^2mu_p - k^2mu + k_p^2mu_p)^2/(f^4mu^2) - (rs(2f^2mu - 2f^2mu_p +
k_p^2mu_p)^2)/(f^6mu^2)))/(2f^5mus_p) - (k^2k_p^4mu_pssinh(2Hr_p)(sin(2Hs_p) -
2Hs_p)((2f^2mu - 2f^2mu_p - k^2mu + k_p^2mu_p)^2/(f^4mu^2) - (rs(2f^2mu - 2f^2mu_p +
k_p^2mu_p)^2)/(f^6mu^2)))/(2f^7mus_p) + (k^2k_p^6mu_pssinh(2Hr_p)(sin(2Hs_p) -
2Hs_p)((2f^2mu - 2f^2mu_p - k^2mu + k_p^2mu_p)^2/(f^4mu^2) - (rs(2f^2mu - 2f^2mu_p +
k_p^2mu_p)^2)/(f^6mu^2)))/(8f^9mus_p) - (k^2k_p^2mu_prr_ps_p^4(cosh(2Hr_p)/2 -
1/2)(cos(2Hs_p)/2 - 1/2)((2(2f^2mu_p - 2f^2mu + k^2mu)^2)/(f^4mu^2) - (8rs(mu -
mu_p)^2)/(f^2mu^2)))/(f^11mu) - (4k^2k_p^2mu_prs_p^2sinh(Hr_p)sin(Hs_p)((2f^2mu -
2f^2mu_p - k^2mu + k_p^2mu_p)^2/(f^4mu^2) - (rs(2f^2mu - 2f^2mu_p +
k_p^2mu_p)^2)/(f^6mu^2))(s_p - s_pcosh(Hr_p)cos(Hs_p) +
r_psinh(Hr_p)sin(Hs_p)))/(f^7mu(r_p^2 + s_p^2)) +
(2k^2k_p^4mu_prs_p^2sinh(Hr_p)sin(Hs_p)((2f^2mu - 2f^2mu_p - k^2mu +
k_p^2mu_p)^2/(f^4mu^2) - (rs(2f^2mu - 2f^2mu_p + k_p^2mu_p)^2)/(f^6mu^2))(s_p -
s_pcosh(Hr_p)cos(Hs_p) + r_psinh(Hr_p)sin(Hs_p)))/(f^9mu(r_p^2 + s_p^2)) -
(k^2k_p^4mu_pr_p^2ss_p^2cosh(Hr_p)sin(Hs_p)(r_pcosh(Hr_p)sin(Hs_p) -
s_pcos(Hs_p)sinh(Hr_p))((2(2f^2mu_p - 2f^2mu + k^2mu)^2)/(f^4mu^2) - (8rs(mu -
mu_p)^2)/(f^2mu^2)))/(f^11mu(r_p^2 + s_p^2)) +
(k^2k_p^2mu_pr_p^2ss_p^2cosh(Hr_p)sin(Hs_p)(r_pcosh(Hr_p)sin(Hs_p) -
s_pcos(Hs_p)sinh(Hr_p))((4(2f^2mu_p - 2f^2mu + k^2mu)^2)/(f^4mu^2) - (16rs(mu -
mu_p)^2)/(f^2mu^2)))/(f^9mu(r_p^2 + s_p^2))))/f + (r_p^2s_p^2(2Hcos(Hs_p)^2((2f^2mu -
2f^2mu_p - k^2mu + k_p^2mu_p)^2/(f^4mu^2) - (rs(2f^2mu - 2f^2mu_p +
k_p^2mu_p)^2)/(f^6mu^2))^2 + 2H(cosh(2Hr_p)/2 + 1/2)((2f^2mu_p - 2f^2mu +
```

APPENDIX (continued)

```
k^2mu)^2/(f^4mu^2) - (4rs(mu - mu_p)^2)/(f^2mu^2))^2 + (sin(2Hs_p)((2f^2mu_p - 2f^2mu +
k^2mu)^2/(f^4mu^2) - (4rs(mu - mu_p)^2)/(f^2mu^2))^2(cosh(2Hr_p) + 1))/(2s_p) +
(cos(Hs_p)^2sinh(2Hr_p)((2f^2mu - 2f^2mu_p - k^2mu + k_p^2mu_p)^2/(f^4mu^2) -
(rs(2f^2mu - 2f^2mu_p + k_p^2mu_p)^2)/(f^6mu^2))^2)/r_p - (2Hk_p^2(cosh(2Hr_p)/2 +
1/2)((2f^2mu_p - 2f^2mu + k^2mu)^2/(f^4mu^2) - (4rs(mu - mu_p)^2)/(f^2mu^2))^2)/f^2 +
(Hk_p^4(cosh(2Hr_p)/2 + 1/2)((2f^2mu_p - 2f^2mu + k^2mu)^2/(f^4mu^2) - (4rs(mu -
mu_p)^2)/(f^2mu^2))^2)/(2f^4) - (k_p^2sin(2Hs_p)((2f^2mu_p - 2f^2mu +
k^2mu)^2/(f^4mu^2) - (4rs(mu - mu_p)^2)/(f^2mu^2))^2(cosh(2Hr_p) + 1))/(2f^2s_p) +
(k_p^4sin(2Hs_p)((2f^2mu_p - 2f^2mu + k^2mu)^2/(f^4mu^2) - (4rs(mu -
mu_p)^2)/(f^2mu^2))^2(cosh(2Hr_p) + 1))/(8f^4s_p) +
(4r_pcos(Hs_p)^2sinh(2Hr_p)((2f^2mu_p - 2f^2mu + k^2mu)^2/(f^4mu^2) - (4rs(mu -
mu_p)^2)/(f^2mu^2))((2f^2mu - 2f^2mu_p - k^2mu + k_p^2mu_p)^2/(f^4mu^2) - (rs(2f^2mu -
2f^2mu_p + k_p^2mu_p)^2)/(f^6mu^2)))/(r_p^2 + s_p^2) + (s_psin(2Hs_p)((8(2f^2mu_p -
2f^2mu + k^2mu)^2)/(f^4mu^2) - (32rs(mu - mu_p)^2)/(f^2mu^2))((2f^2mu - 2f^2mu_p -
k^2mu + k_p^2mu_p)^2/(f^4mu^2) - (rs(2f^2mu - 2f^2mu_p +
k_p^2mu_p)^2)/(f^6mu^2))(cosh(2Hr_p) + 1))/(4(r_p^2 + s_p^2)) -
(2k_p^2r_pcos(Hs_p)^2sinh(2Hr_p)((2f^2mu_p - 2f^2mu + k^2mu)^2/(f^4mu^2) - (4rs(mu -
mu_p)^2)/(f^2mu^2))((2f^2mu - 2f^2mu_p - k^2mu + k_p^2mu_p)^2/(f^4mu^2) - (rs(2f^2mu -
2f^2mu_p + k_p^2mu_p)^2)/(f^6mu^2)))/(f^2(r_p^2 + s_p^2)) -
(k_p^2s_psin(2Hs_p)((4(2f^2mu_p - 2f^2mu + k^2mu)^2)/(f^4mu^2) - (16rs(mu -
mu_p)^2)/(f^2mu^2))((2f^2mu - 2f^2mu_p - k^2mu + k_p^2mu_p)^2/(f^4mu^2) - (rs(2f^2mu -
2f^2mu_p + k_p^2mu_p)^2)/(f^6mu^2))(cosh(2Hr_p) + 1))/(4f^2(r_p^2 + s_p^2))))/f^4 -
(2r_ps_p((k^4k_p^4mu_p^2rssinh(2Hr_p)(cos(Hs_p)^2 - 1))/(f^10mu^2s_p) -
(k^4k_p^6mu_p^2rssinh(2Hr_p)(cos(Hs_p)^2 - 1))/(f^12mu^2s_p) +
(k^4k_p^8mu_p^2rssinh(2Hr_p)(cos(Hs_p)^2 - 1))/(4f^14mu^2s_p) +
(k^4k_p^4mu_p^2rr_pss_p^2sin(2Hs_p)(cosh(2Hr_p)/2 - 1/2))/(f^14mu^2) +
(4k^4k_p^4mu_p^2r_p^2s^2cosh(Hr_p)cos(Hs_p)(r_pcosh(Hr_p)sin(Hs_p) -
s_pcos(Hs_p)sinh(Hr_p)))/(f^12mu^2(r_p^2 + s_p^2)) -
(2k^4k_p^6mu_p^2r_p^2s^2cosh(Hr_p)cos(Hs_p)(r_pcosh(Hr_p)sin(Hs_p) -
s_pcos(Hs_p)sinh(Hr_p)))/(f^14mu^2(r_p^2 + s_p^2)) -
(4k^4k_p^4mu_p^2r^2s_p^2sinh(Hr_p)sin(Hs_p)(r_pcos(Hs_p)sinh(Hr_p) +
s_pcosh(Hr_p)sin(Hs_p)))/(f^12mu^2(r_p^2 + s_p^2)) +
(2k^4k_p^6mu_p^2r^2s_p^2sinh(Hr_p)sin(Hs_p)(r_pcos(Hs_p)sinh(Hr_p) +
s_pcosh(Hr_p)sin(Hs_p)))/(f^14mu^2(r_p^2 + s_p^2))))/f^2 -
(2r_p^2s_p((k^2k_p^2mu_ps((2(2f^2mu_p - 2f^2mu + k^2mu)^2)/(f^4mu^2) - (8rs(mu -
mu_p)^2)/(f^2mu^2))(2cos(Hs_p)^2 - 2)(cosh(2Hr_p) + 1))/(4f^5mus_p) +
(k^2k_p^6mu_ps((2f^2mu_p - 2f^2mu + k^2mu)^2/(f^4mu^2) - (4rs(mu -
mu_p)^2)/(f^2mu^2))(2cos(Hs_p)^2 - 2)(cosh(2Hr_p) + 1))/(8f^9mus_p) -
(k^2k_p^4mu_ps((2(2f^2mu_p - 2f^2mu + k^2mu)^2)/(f^4mu^2) - (8rs(mu -
mu_p)^2)/(f^2mu^2))(2cos(Hs_p)^2 - 2)(cosh(2Hr_p) + 1))/(4f^7mus_p) -
(4k^2k_p^2mu_pscosh(Hr_p)cos(Hs_p)((2f^2mu - 2f^2mu_p - k^2mu + k_p^2mu_p)^2/(f^4mu^2)
- (rs(2f^2mu - 2f^2mu_p + k_p^2mu_p)^2)/(f^6mu^2))(s_p - s_pcosh(Hr_p)cos(Hs_p) +
r_psinh(Hr_p)sin(Hs_p)))/(f^5mu(r_p^2 + s_p^2)) +
(2k^2k_p^4mu_pscosh(Hr_p)cos(Hs_p)((2f^2mu - 2f^2mu_p - k^2mu + k_p^2mu_p)^2/(f^4mu^2)
- (rs(2f^2mu - 2f^2mu_p + k_p^2mu_p)^2)/(f^6mu^2))(s_p - s_pcosh(Hr_p)cos(Hs_p) +
r_psinh(Hr_p)sin(Hs_p)))/(f^7mu(r_p^2 + s_p^2)) +
(k^2k_p^4mu_prs_p^2cosh(Hr_p)sin(Hs_p)(r_pcos(Hs_p)sinh(Hr_p) +
s_pcosh(Hr_p)sin(Hs_p))((2(2f^2mu_p - 2f^2mu + k^2mu)^2)/(f^4mu^2) - (8rs(mu -
mu_p)^2)/(f^2mu^2)))/(f^9mu(r_p^2 + s_p^2)) -
(k^2k_p^2mu_prs_p^2cosh(Hr_p)sin(Hs_p)(r_pcos(Hs_p)sinh(Hr_p) +
s_pcosh(Hr_p)sin(Hs_p))((4(2f^2mu_p - 2f^2mu + k^2mu)^2)/(f^4mu^2) - (16rs(mu -
mu_p)^2)/(f^2mu^2)))/(f^7mu(r_p^2 + s_p^2)) -
(k^2k_p^2mu_prs_p^2cos(Hs_p)sin(Hs_p)(sinh(2Hr_p) + 2Hr_p)((2f^2mu - 2f^2mu_p - k^2mu +
k_p^2mu_p)^2/(f^4mu^2) - (rs(2f^2mu - 2f^2mu_p +
k_p^2mu_p)^2)/(f^6mu^2)))/(f^7mur_p)))/f^3 + (2r_ps_p((k_p^2(r_pcosh(Hr_p)sin(Hs_p) -
s_pcos(Hs_p)sinh(Hr_p))(cosh(2Hr_p)/2 - 1/2)(((2f^2mu_p - 2f^2mu + k^2mu)(2f^2mu -
2f^2mu_p - k^2mu + k_p^2mu_p))/(f^4mu^2) + (2rs(mu - mu_p)(2f^2mu - 2f^2mu_p +
k_p^2mu_p))/(f^4mu^2))((2f^2mu - 2f^2mu_p - k^2mu + k_p^2mu_p)^2/(f^4mu^2) - (rs(2f^2mu
- 2f^2mu_p + k_p^2mu_p)^2)/(f^6mu^2)))/(f^2(r_p^2 + s_p^2)) - ((r_pcosh(Hr_p)sin(Hs_p)
```

APPENDIX (continued)

```
- s_pcos(Hs_p)sinh(Hr_p))(cosh(2Hr_p)/2 - 1/2)((2(2f^2mu_p - 2f^2mu + k^2mu)(2f^2mu -
2f^2mu_p - k^2mu + k_p^2mu_p))/(f^4mu^2) + (4rs(mu - mu_p)(2f^2mu - 2f^2mu_p +
k_p^2mu_p))/(f^4mu^2))((2f^2mu - 2f^2mu_p - k^2mu + k_p^2mu_p)^2/(f^4mu^2) - (rs(2f^2mu
- 2f^2mu_p + k_p^2mu_p)^2)/(f^6mu^2)))/(r_p^2 + s_p^2) -
(4cosh(Hr_p)sinh(Hr_p)(((2f^2mu_p - 2f^2mu + k^2mu)(2f^2mu - 2f^2mu_p - k^2mu +
k_p^2mu_p))/(f^4mu^2) + (2rs(mu - mu_p)(2f^2mu - 2f^2mu_p +
k_p^2mu_p))/(f^4mu^2))((2f^2mu - 2f^2mu_p - k^2mu + k_p^2mu_p)^2/(f^4mu^2) - (rs(2f^2mu
- 2f^2mu_p + k_p^2mu_p)^2)/(f^6mu^2))(s_p - s_pcosh(Hr_p)cos(Hs_p) +
r_psinh(Hr_p)sin(Hs_p)))/(r_p^2 + s_p^2) - 2Hsinh(Hr_p)sin(Hs_p)(((2f^2mu_p - 2f^2mu +
k^2mu)(2f^2mu - 2f^2mu_p - k^2mu + k_p^2mu_p))/(f^4mu^2) + (2rs(mu - mu_p)(2f^2mu -
2f^2mu_p + k_p^2mu_p))/(f^4mu^2))((2f^2mu - 2f^2mu_p - k^2mu + k_p^2mu_p)^2/(f^4mu^2) -
(rs(2f^2mu - 2f^2mu_p + k_p^2mu_p)^2)/(f^6mu^2)) +
(Hk_p^2sinh(Hr_p)sin(Hs_p)(((2f^2mu_p - 2f^2mu + k^2mu)(2f^2mu - 2f^2mu_p - k^2mu +
k_p^2mu_p))/(f^4mu^2) + (2rs(mu - mu_p)(2f^2mu - 2f^2mu_p +
k_p^2mu_p))/(f^4mu^2))((2f^2mu - 2f^2mu_p - k^2mu + k_p^2mu_p)^2/(f^4mu^2) - (rs(2f^2mu
- 2f^2mu_p + k_p^2mu_p)^2)/(f^6mu^2)))/f^2 + (4k_p^2cosh(Hr_p)sinh(Hr_p)(((2f^2mu_p -
2f^2mu + k^2mu)(2f^2mu - 2f^2mu_p - k^2mu + k_p^2mu_p))/(f^4mu^2) + (2rs(mu -
mu_p)(2f^2mu - 2f^2mu_p + k_p^2mu_p))/(f^4mu^2))((2f^2mu - 2f^2mu_p - k^2mu +
k_p^2mu_p)^2/(f^4mu^2) - (rs(2f^2mu - 2f^2mu_p + k_p^2mu_p)^2)/(f^6mu^2))(s_p -
s_pcosh(Hr_p)cos(Hs_p) + r_psinh(Hr_p)sin(Hs_p)))/(f^2(r_p^2 + s_p^2)) -
(k_p^4cosh(Hr_p)sinh(Hr_p)(((2f^2mu_p - 2f^2mu + k^2mu)(2f^2mu - 2f^2mu_p - k^2mu +
k_p^2mu_p))/(f^4mu^2) + (2rs(mu - mu_p)(2f^2mu - 2f^2mu_p +
k_p^2mu_p))/(f^4mu^2))((2f^2mu - 2f^2mu_p - k^2mu + k_p^2mu_p)^2/(f^4mu^2) - (rs(2f^2mu
- 2f^2mu_p + k_p^2mu_p)^2)/(f^6mu^2))(s_p - s_pcosh(Hr_p)cos(Hs_p) +
r_psinh(Hr_p)sin(Hs_p)))/(f^4(r_p^2 + s_p^2)) + (r_p^3s_p^2sin(Hs_p)((4(2f^2mu_p -
2f^2mu + k^2mu)^2)/(f^4mu^2) - (16rs(mu - mu_p)^2)/(f^2mu^2))(((2f^2mu_p - 2f^2mu +
k^2mu)(2f^2mu - 2f^2mu_p - k^2mu + k_p^2mu_p))/(f^4mu^2) + (2rs(mu - mu_p)(2f^2mu -
2f^2mu_p + k_p^2mu_p))/(f^4mu^2))(cosh(Hr_p) - cos(Hs_p)))/(f^4(r_p^2 + s_p^2)) +
(r_ps_p^2sinh(Hr_p)sin(Hs_p)(sinh(2Hr_p) - 2Hr_p)((2f^2mu_p - 2f^2mu +
k^2mu)^2/(f^4mu^2) - (4rs(mu - mu_p)^2)/(f^2mu^2))(((2f^2mu_p - 2f^2mu + k^2mu)(2f^2mu
- 2f^2mu_p - k^2mu + k_p^2mu_p))/(f^4mu^2) + (2rs(mu - mu_p)(2f^2mu - 2f^2mu_p +
k_p^2mu_p))/(f^4mu^2)))/(2f^4) + (r_ps_p^2cosh(Hr_p)sin(Hs_p)(cosh(Hr_p)^2 -
1)((2(2f^2mu_p - 2f^2mu + k^2mu)^2)/(f^4mu^2) - (8rs(mu -
mu_p)^2)/(f^2mu^2))(((2f^2mu_p - 2f^2mu + k^2mu)(2f^2mu - 2f^2mu_p - k^2mu +
k_p^2mu_p))/(f^4mu^2) + (2rs(mu - mu_p)(2f^2mu - 2f^2mu_p + k_p^2mu_p))/(f^4mu^2)))/f^4
- (k_p^2r_ps_p^2cosh(Hr_p)sin(Hs_p)(cosh(Hr_p)^2 - 1)((2f^2mu_p - 2f^2mu +
k^2mu)^2/(f^4mu^2) - (4rs(mu - mu_p)^2)/(f^2mu^2))(((2f^2mu_p - 2f^2mu + k^2mu)(2f^2mu
- 2f^2mu_p - k^2mu + k_p^2mu_p))/(f^4mu^2) + (2rs(mu - mu_p)(2f^2mu - 2f^2mu_p +
k_p^2mu_p))/(f^4mu^2)))/f^6))/f^2 + (2r_ps_p((sinh(2Hr_p)(cos(Hs_p)^2 - 1)((2f^2mu_p -
2f^2mu + k^2mu)^2/(f^4mu^2) - (4rs(mu - mu_p)^2)/(f^2mu^2))((2f^2mu - 2f^2mu_p - k^2mu
+ k_p^2mu_p)^2/(f^4mu^2) - (rs(2f^2mu - 2f^2mu_p + k_p^2mu_p)^2)/(f^6mu^2)))/s_p -
(4cos(Hs_p)sinh(Hr_p)((2f^2mu - 2f^2mu_p - k^2mu + k_p^2mu_p)^2/(f^4mu^2) - (rs(2f^2mu
- 2f^2mu_p + k_p^2mu_p)^2)/(f^6mu^2))^2(s_p - s_pcosh(Hr_p)cos(Hs_p) +
r_psinh(Hr_p)sin(Hs_p)))/(r_p^2 + s_p^2) + (2k_p^2cos(Hs_p)sinh(Hr_p)((2f^2mu -
2f^2mu_p - k^2mu + k_p^2mu_p)^2/(f^4mu^2) - (rs(2f^2mu - 2f^2mu_p +
k_p^2mu_p)^2)/(f^6mu^2))^2(s_p - s_pcosh(Hr_p)cos(Hs_p) +
r_psinh(Hr_p)sin(Hs_p)))/(f^2(r_p^2 + s_p^2)) + (r_ps_p^2sin(2Hs_p)(cosh(2Hr_p)/2 -
1/2)((2(2f^2mu_p - 2f^2mu + k^2mu)^2)/(f^4mu^2) - (8rs(mu - mu_p)^2)/(f^2mu^2))((2f^2mu
- 2f^2mu_p - k^2mu + k_p^2mu_p)^2/(f^4mu^2) - (rs(2f^2mu - 2f^2mu_p +
k_p^2mu_p)^2)/(f^6mu^2)))/(2f^4) - (k_p^2sinh(2Hr_p)(cos(Hs_p)^2 - 1)((2f^2mu_p -
2f^2mu + k^2mu)^2/(f^4mu^2) - (4rs(mu - mu_p)^2)/(f^2mu^2))((2f^2mu - 2f^2mu_p - k^2mu
+ k_p^2mu_p)^2/(f^4mu^2) - (rs(2f^2mu - 2f^2mu_p + k_p^2mu_p)^2)/(f^6mu^2)))/(f^2s_p) +
(k_p^4sinh(2Hr_p)(cos(Hs_p)^2 - 1)((2f^2mu_p - 2f^2mu + k^2mu)^2/(f^4mu^2) - (4rs(mu -
mu_p)^2)/(f^2mu^2))((2f^2mu - 2f^2mu_p - k^2mu + k_p^2mu_p)^2/(f^4mu^2) - (rs(2f^2mu -
2f^2mu_p + k_p^2mu_p)^2)/(f^6mu^2)))/(4f^4s_p) +
(4r_p^2s_p^2cosh(Hr_p)sin(Hs_p)((2f^2mu_p - 2f^2mu + k^2mu)^2/(f^4mu^2) - (4rs(mu -
mu_p)^2)/(f^2mu^2))^2(r_pcosh(Hr_p)cos(Hs_p) - r_p +
s_psinh(Hr_p)sin(Hs_p)))/(f^4(r_p^2 + s_p^2)) -
(2k_p^2r_p^2s_p^2cosh(Hr_p)sin(Hs_p)((2f^2mu_p - 2f^2mu + k^2mu)^2/(f^4mu^2) - (4rs(mu
```

APPENDIX (continued)

```
- mu_p)^2)/(f^2mu^2))^2(r_pcosh(Hr_p)cos(Hs_p) - r_p +
s_psinh(Hr_p)sin(Hs_p)))/(f^6(r_p^2 + s_p^2))))/f^2 -
(2r_ps_p^2((k^2k_p^2mu_pr_ps((2f^2mu - 2f^2mu_p - k^2mu + k_p^2mu_p)^2/(f^4mu^2) -
(rs(2f^2mu - 2f^2mu_p + k_p^2mu_p)^2)/(f^6mu^2))(cosh(2Hr_p) - 1)(cos(2Hs_p) +
1))/(2f^7mu) - (k^2k_p^2mu_prsinh(2Hr_p)(sin(2Hs_p) + 2Hs_p)((2f^2mu_p - 2f^2mu +
k^2mu)^2/(f^4mu^2) - (4rs(mu - mu_p)^2)/(f^2mu^2)))/(2f^5mus_p) +
(k^2k_p^4mu_prsinh(2Hr_p)(sin(2Hs_p) + 2Hs_p)((2f^2mu_p - 2f^2mu + k^2mu)^2/(f^4mu^2) -
(4rs(mu - mu_p)^2)/(f^2mu^2)))/(2f^7mus_p) - (k^2k_p^6mu_prsinh(2Hr_p)(sin(2Hs_p) +
2Hs_p)((2f^2mu_p - 2f^2mu + k^2mu)^2/(f^4mu^2) - (4rs(mu -
mu_p)^2)/(f^2mu^2)))/(8f^9mus_p) -
(4k^2k_p^2mu_prcos(Hs_p)sinh(Hr_p)(r_pcos(Hs_p)sinh(Hr_p) +
s_pcosh(Hr_p)sin(Hs_p))((2f^2mu - 2f^2mu_p - k^2mu + k_p^2mu_p)^2/(f^4mu^2) -
(rs(2f^2mu - 2f^2mu_p + k_p^2mu_p)^2)/(f^6mu^2)))/(f^5mu(r_p^2 + s_p^2)) +
(2k^2k_p^4mu_prcos(Hs_p)sinh(Hr_p)(r_pcos(Hs_p)sinh(Hr_p) +
s_pcosh(Hr_p)sin(Hs_p))((2f^2mu - 2f^2mu_p - k^2mu + k_p^2mu_p)^2/(f^4mu^2) -
(rs(2f^2mu - 2f^2mu_p + k_p^2mu_p)^2)/(f^6mu^2)))/(f^7mu(r_p^2 + s_p^2)) -
(k^2k_p^4mu_pr_p^2scosh(Hr_p)cos(Hs_p)((2(2f^2mu_p - 2f^2mu + k^2mu)^2)/(f^4mu^2) -
(8rs(mu - mu_p)^2)/(f^2mu^2))(r_pcosh(Hr_p)cos(Hs_p) - r_p +
s_psinh(Hr_p)sin(Hs_p)))/(f^9mu(r_p^2 + s_p^2)) +
(k^2k_p^2mu_pr_p^2scosh(Hr_p)cos(Hs_p)((4(2f^2mu_p - 2f^2mu + k^2mu)^2)/(f^4mu^2) -
(16rs(mu - mu_p)^2)/(f^2mu^2))(r_pcosh(Hr_p)cos(Hs_p) - r_p +
s_psinh(Hr_p)sin(Hs_p)))/(f^7mu(r_p^2 + s_p^2))))/f^3 +
(2r_p^2s_p^2((cosh(Hr_p)^2(r_pcos(Hs_p)sinh(Hr_p) + s_pcosh(Hr_p)sin(Hs_p))((4(2f^2mu_p
- 2f^2mu + k^2mu)^2)/(f^4mu^2) - (16rs(mu - mu_p)^2)/(f^2mu^2))(((2f^2mu_p - 2f^2mu +
k^2mu)(2f^2mu - 2f^2mu_p - k^2mu + k_p^2mu_p))/(f^4mu^2) + (2rs(mu - mu_p)(2f^2mu -
2f^2mu_p + k_p^2mu_p))/(f^4mu^2)))/(r_p^2 + s_p^2) + (cosh(Hr_p)(sin(Hs_p) +
Hs_pcos(Hs_p))((4(2f^2mu_p - 2f^2mu + k^2mu)^2)/(f^4mu^2) - (16rs(mu -
mu_p)^2)/(f^2mu^2))(((2f^2mu_p - 2f^2mu + k^2mu)(2f^2mu - 2f^2mu_p - k^2mu +
k_p^2mu_p))/(f^4mu^2) + (2rs(mu - mu_p)(2f^2mu - 2f^2mu_p +
k_p^2mu_p))/(f^4mu^2)))/(2s_p) + (cos(Hs_p)(r_psinh(Hr_p) + s_psin(Hs_p))((4(2f^2mu_p -
2f^2mu + k^2mu)(2f^2mu - 2f^2mu_p - k^2mu + k_p^2mu_p))/(f^4mu^2) + (8rs(mu -
mu_p)(2f^2mu - 2f^2mu_p + k_p^2mu_p))/(f^4mu^2))((2f^2mu - 2f^2mu_p - k^2mu +
k_p^2mu_p)^2/(f^4mu^2) - (rs(2f^2mu - 2f^2mu_p + k_p^2mu_p)^2)/(f^6mu^2)))/(r_p^2 +
s_p^2) + (cos(Hs_p)sinh(Hr_p)^3(((2f^2mu_p - 2f^2mu + k^2mu)(2f^2mu - 2f^2mu_p - k^2mu
+ k_p^2mu_p))/(f^4mu^2) + (2rs(mu - mu_p)(2f^2mu - 2f^2mu_p +
k_p^2mu_p))/(f^4mu^2))((2f^2mu - 2f^2mu_p - k^2mu + k_p^2mu_p)^2/(f^4mu^2) - (rs(2f^2mu
- 2f^2mu_p + k_p^2mu_p)^2)/(f^6mu^2)))/r_p + (2cosh(Hr_p)sinh(Hr_p)((2f^2mu_p - 2f^2mu
+ k^2mu)^2/(f^4mu^2) - (4rs(mu - mu_p)^2)/(f^2mu^2))(((2f^2mu_p - 2f^2mu +
k^2mu)(2f^2mu - 2f^2mu_p - k^2mu + k_p^2mu_p))/(f^4mu^2) + (2rs(mu - mu_p)(2f^2mu -
2f^2mu_p + k_p^2mu_p))/(f^4mu^2))(r_pcosh(Hr_p)cos(Hs_p) - r_p +
s_psinh(Hr_p)sin(Hs_p)))/(r_p^2 + s_p^2) + (cosh(Hr_p)cos(Hs_p)(sinh(2Hr_p) +
2Hr_p)((4(2f^2mu_p - 2f^2mu + k^2mu)(2f^2mu - 2f^2mu_p - k^2mu + k_p^2mu_p))/(f^4mu^2)
+ (8rs(mu - mu_p)(2f^2mu - 2f^2mu_p + k_p^2mu_p))/(f^4mu^2))((2f^2mu - 2f^2mu_p - k^2mu
+ k_p^2mu_p)^2/(f^4mu^2) - (rs(2f^2mu - 2f^2mu_p + k_p^2mu_p)^2)/(f^6mu^2)))/(4r_p) -
(k_p^2cosh(Hr_p)(sin(Hs_p) + Hs_pcos(Hs_p))((2(2f^2mu_p - 2f^2mu + k^2mu)^2)/(f^4mu^2)
- (8rs(mu - mu_p)^2)/(f^2mu^2))(((2f^2mu_p - 2f^2mu + k^2mu)(2f^2mu - 2f^2mu_p - k^2mu
+ k_p^2mu_p))/(f^4mu^2) + (2rs(mu - mu_p)(2f^2mu - 2f^2mu_p +
k_p^2mu_p))/(f^4mu^2)))/(2f^2s_p) + (k_p^4cosh(Hr_p)^2(r_pcos(Hs_p)sinh(Hr_p) +
s_pcosh(Hr_p)sin(Hs_p))((2f^2mu_p - 2f^2mu + k^2mu)^2/(f^4mu^2) - (4rs(mu -
mu_p)^2)/(f^2mu^2))(((2f^2mu_p - 2f^2mu + k^2mu)(2f^2mu - 2f^2mu_p - k^2mu +
k_p^2mu_p))/(f^4mu^2) + (2rs(mu - mu_p)(2f^2mu - 2f^2mu_p +
k_p^2mu_p))/(f^4mu^2)))/(f^4(r_p^2 + s_p^2)) -
(k_p^2cosh(Hr_p)^2(r_pcos(Hs_p)sinh(Hr_p) + s_pcosh(Hr_p)sin(Hs_p))((4(2f^2mu_p -
2f^2mu + k^2mu)^2)/(f^4mu^2) - (16rs(mu - mu_p)^2)/(f^2mu^2))(((2f^2mu_p - 2f^2mu +
k^2mu)(2f^2mu - 2f^2mu_p - k^2mu + k_p^2mu_p))/(f^4mu^2) + (2rs(mu - mu_p)(2f^2mu -
2f^2mu_p + k_p^2mu_p))/(f^4mu^2)))/(f^2(r_p^2 + s_p^2)) -
(k_p^2cosh(Hr_p)cos(Hs_p)(sinh(2Hr_p) + 2Hr_p)((2(2f^2mu_p - 2f^2mu + k^2mu)(2f^2mu -
2f^2mu_p - k^2mu + k_p^2mu_p))/(f^4mu^2) + (4rs(mu - mu_p)(2f^2mu - 2f^2mu_p +
k_p^2mu_p))/(f^4mu^2))((2f^2mu - 2f^2mu_p - k^2mu + k_p^2mu_p)^2/(f^4mu^2) - (rs(2f^2mu
```

APPENDIX (continued)

```
- 2f^2mu_p + k_p^2mu_p)^2)/(f^6mu^2)))/(4f^2r_p) - (k_p^2cosh(Hr_p)sinh(Hr_p)((2f^2mu_p
- 2f^2mu + k^2mu)^2/(f^4mu^2) - (4rs(mu - mu_p)^2)/(f^2mu^2))(((2f^2mu_p - 2f^2mu +
k^2mu)(2f^2mu - 2f^2mu_p - k^2mu + k_p^2mu_p))/(f^4mu^2) + (2rs(mu - mu_p)(2f^2mu -
2f^2mu_p + k_p^2mu_p))/(f^4mu^2))(r_pcosh(Hr_p)cos(Hs_p) - r_p +
s_psinh(Hr_p)sin(Hs_p))))/(f^2(r_p^2 + s_p^2))))/f^4 +
(k^4k_p^4mu_p^2((r_p^3s^2sinh(2Hr_p)(cos(2Hs_p) + 1))/2 - (Hr^2(cosh(2Hr_p)/2 -
1/2)(cos(2Hs_p)/2 - 1/2)(2f^2 - k_p^2)^2)/2 + (Hr_p^4s^2(cosh(2Hr_p) - 1)(cos(2Hs_p) +
1))/2 + (Hr^2(2f^2 - k_p^2)^2(cosh(2Hr_p) - 1)(cos(2Hs_p) + 1))/8 -
2Hr_p^4s^2cos(Hs_p)^2(cosh(2Hr_p)/2 + 1/2) + (r^2sin(2Hs_p)(2f^2 - k_p^2)^2(cosh(2Hr_p)
- 1))/(8s_p) + (rr_p^3ssinh(2Hr_p)(f^22i - k_p^21i)(cos(2Hs_p) + 1)1i)/(r_p^2 + s_p^2)
- (rr_p^2ss_psin(2Hs_p)(2f^2 - k_p^2)(cosh(2Hr_p) - 1))/(r_p^2 + s_p^2))))/(f^14mu^2) +
(r_ps_p(4f^4mu^2 + 4f^4mu_p^2 + k^4mu^2 - 4f^2k^2mu^2 - 2f^2k_p^2mu_p^2 - 8f^4mumu_p +
4f^2k^2mumu_p + 2f^2k_p^2mumu_p - k^2k_p^2mumu_p - 4f^2mu^2rs - 4f^2mu_p^2rs +
2k_p^2mu_p^2rs + 8f^2mumu_prs - 2k_p^2mumu_prs)^2(8f^4r_p^3sin(2Hs_p) -
10f^4s_p^3sinh(2Hr_p) + 4f^2k_p^2s_p^3sinh(2Hr_p) + 36f^4s_p^3cosh(Hr_p)^3sinh(Hr_p) +
4k_p^4s_p^3cosh(Hr_p)^3sinh(Hr_p) + 20Hf^4r_ps_p^3 + 20Hf^4r_p^3s_p +
38f^4r_p^2s_psinh(2Hr_p) + 8f^4r_ps_p^2sin(2Hs_p) -
24f^2k_p^2s_p^3cosh(Hr_p)^3sinh(Hr_p) + 64f^4r_ps_p^2cosh(Hr_p)sin(Hs_p) -
32f^4r_p^2s_pcos(Hs_p)sinh(Hr_p) + 12Hf^4r_ps_p^3cosh(Hr_p)^2 +
12Hf^4r_p^3s_pcosh(Hr_p)^2 + 4Hk_p^4r_ps_p^3cosh(Hr_p)^2 + 4Hk_p^4r_p^3s_pcosh(Hr_p)^2
- 12f^2k_p^2r_p^2s_psinh(2Hr_p) + 36f^4r_p^2s_pcosh(Hr_p)^3sinh(Hr_p) +
4k_p^4r_p^2s_pcosh(Hr_p)^3sinh(Hr_p) - 32f^2k_p^2r_ps_p^2cosh(Hr_p)sin(Hs_p) -
16Hf^2k_p^2r_ps_p^3cosh(Hr_p)^2 - 16Hf^2k_p^2r_p^3s_pcosh(Hr_p)^2 -
24f^2k_p^2r_p^2s_pcosh(Hr_p)^3sinh(Hr_p)))/(8f^16mu^4(r_p^2 + s_p^2)) -
(k^2k_p^2mu_pr_ps_p(4f^4mu^2 + 4f^4mu_p^2 + k^4mu^2 - 4f^2k^2mu^2 - 2f^2k_p^2mu_p^2 -
8f^4mumu_p + 4f^2k^2mumu_p + 2f^2k_p^2mumu_p - k^2k_p^2mumu_p - 4f^2mu^2rs -
4f^2mu_p^2rs + 2k_p^2mu_p^2rs + 8f^2mumu_prs - 2k_p^2mumu_prs)(8f^2rr_ps_p^3 +
8f^4r_pss_pcosh(Hr_p)^2 + 2k_p^4r_pss_pcosh(Hr_p)^2 - 2f^2rs_p^4sinh(Hr_p)sin(Hs_p) -
8f^2rr_ps_p^3cos(Hs_p)^2 - 8f^2k_p^2r_pss_pcosh(Hr_p)^2 +
6f^2rr_p^2s_p^2sinh(Hr_p)sin(Hs_p) + 6f^2rs_p^4cosh(Hr_p)^2sinh(Hr_p)sin(Hs_p) +
12f^4r_p^2scosh(Hr_p)^2sinh(Hr_p)sin(Hs_p) -
2k_p^2rs_p^4cosh(Hr_p)^2sinh(Hr_p)sin(Hs_p) +
2k_p^4r_p^2scosh(Hr_p)^2sinh(Hr_p)sin(Hs_p) + 4f^4r_pss_pcosh(Hr_p)cos(Hs_p) +
4Hf^4r_p^3scosh(Hr_p)sin(Hs_p) - 12f^4r_pss_pcosh(Hr_p)^3cos(Hs_p) -
2k_p^4r_pss_pcosh(Hr_p)^3cos(Hs_p) - 10f^2k_p^2r_p^2scosh(Hr_p)^2sinh(Hr_p)sin(Hs_p) +
4Hf^2rr_ps_p^4cosh(Hr_p)sin(Hs_p) + 4Hf^4r_pss_p^2cosh(Hr_p)sin(Hs_p) +
6f^2rr_p^2s_p^2cosh(Hr_p)^2sinh(Hr_p)sin(Hs_p) - 2Hk_p^2rr_ps_p^4cosh(Hr_p)sin(Hs_p) -
2k_p^2rr_p^2s_p^2cosh(Hr_p)^2sinh(Hr_p)sin(Hs_p) - 2f^2k_p^2r_pss_pcosh(Hr_p)cos(Hs_p)
- 2Hf^2k_p^2r_p^3scosh(Hr_p)sin(Hs_p) + 4Hf^2rr_p^3s_p^2cosh(Hr_p)sin(Hs_p) -
2Hk_p^2rr_p^3s_p^2cosh(Hr_p)sin(Hs_p) + 10f^2k_p^2r_pss_pcosh(Hr_p)^3cos(Hs_p) -
2Hf^2k_p^2r_pss_p^2cosh(Hr_p)sin(Hs_p)))/(f^16mu^3(r_p^2 + s_p^2)) +
(k^2k_p^2mu_pr_ps_p(4f^4mu^2 + 4f^4mu_p^2 + k^4mu^2 - 4f^2k^2mu^2 - 2f^2k_p^2mu_p^2 -
8f^4mumu_p + 4f^2k^2mumu_p + 2f^2k_p^2mumu_p - k^2k_p^2mumu_p - 4f^2mu^2rs -
4f^2mu_p^2rs + 2k_p^2mu_p^2rs + 8f^2mumu_prs - 2k_p^2mumu_prs)(f^4rr_ps_p4i -
f^2k_p^2rr_ps_p2i - f^4rr_ps_pcosh(Hr_p)^24i + f^4rr_p^2sinh(Hr_p)sin(Hs_p)4i +
f^2r_p^3ss_pcos(Hs_p)^28i + f^2k_p^2rr_ps_pcosh(Hr_p)^22i -
f^2r_pss_p^3cosh(Hr_p)^3cos(Hs_p)6i - f^2r_p^3ss_pcosh(Hr_p)^3cos(Hs_p)6i +
k_p^2r_pss_p^3cosh(Hr_p)^3cos(Hs_p)2i + k_p^2r_p^3ss_pcosh(Hr_p)^3cos(Hs_p)2i -
f^2k_p^2rr_p^2sinh(Hr_p)sin(Hs_p)2i + f^4rs_p^2cosh(Hr_p)^2sinh(Hr_p)sin(Hs_p)12i +
k_p^4rs_p^2cosh(Hr_p)^2sinh(Hr_p)sin(Hs_p)2i - f^4rr_ps_pcosh(Hr_p)cos(Hs_p)12i -
k_p^4rr_ps_pcosh(Hr_p)cos(Hs_p)2i + Hf^4rs_p^3cos(Hs_p)sinh(Hr_p)4i +
f^4rr_ps_pcosh(Hr_p)^3cos(Hs_p)12i + f^2r_pss_p^3cosh(Hr_p)cos(Hs_p)6i -
f^2r_p^3ss_pcosh(Hr_p)cos(Hs_p)2i + k_p^4rr_ps_pcosh(Hr_p)^3cos(Hs_p)2i -
k_p^2r_pss_p^3cosh(Hr_p)cos(Hs_p)2i - k_p^2r_p^3ss_pcosh(Hr_p)cos(Hs_p)2i -
f^2k_p^2rs_p^2cosh(Hr_p)^2sinh(Hr_p)sin(Hs_p)10i + Hf^4rr_p^2s_pcos(Hs_p)sinh(Hr_p)4i +
Hf^2r_p^4ss_pcos(Hs_p)sinh(Hr_p)2i + f^2k_p^2rr_ps_pcosh(Hr_p)cos(Hs_p)10i -
Hf^2k_p^2rs_p^3cos(Hs_p)sinh(Hr_p)2i + Hf^2r_p^2ss_p^3cos(Hs_p)sinh(Hr_p)2i -
f^2k_p^2rr_ps_pcosh(Hr_p)^3cos(Hs_p)10i -
Hf^2k_p^2rr_p^2s_pcos(Hs_p)sinh(Hr_p)2i)1i)/(f^16mu^3(r_p^2 + s_p^2)) -
```

APPENDIX (continued)

```
(k^4k_p^4mu_p^2rr_p^3scos(Hs_p)sinh(Hr_p)(f^22i - k_p^21i)4i)/(f^14mu^2(r_p^2 +
s_p^2))))/H + (A^2s_p^2(((mu_p(k_p^2/f^2 - 2))/mu - k^2/f^2 + 2)^2 -
(rs((mu_p(k_p^2/f^2 - 2))/mu + 2)^2)/f^2)^2((H(cosh(2Hr_p) - 1)(cos(2Hs_p) + 1))/2 +
(sinh(2Hr_p)(cos(2Hs_p) + 1))/(2r_p) - 2Hcos(Hs_p)^2(cosh(2Hr_p)/2 + 1/2) + (H(2f^2 -
k_p^2)^2(cosh(2Hr_p) - 1)(cos(2Hs_p) + 1))/(8f^4) + (sin(2Hs_p)(2f^2 -
k_p^2)^2(cosh(2Hr_p) - 1))/(8f^4s_p) - (H(cosh(2Hr_p)/2 - 1/2)(cos(2Hs_p)/2 - 1/2)(2f^2
- k_p^2)^2)/(2f^4) - (r_psinh(2Hr_p)(2f^2 - k_p^2)(cos(2Hs_p) + 1))/(f^2(r_p^2 +
s_p^2)) - (s_psin(2Hs_p)(2f^2 - k_p^2)(cosh(2Hr_p) - 1))/(f^2(r_p^2 + s_p^2)) +
(4r_pcos(Hs_p)sinh(Hr_p)(2f^2 - k_p^2))/(f^2(r_p^2 + s_p^2)))))/(Hf^2) -
(A^2r_p^2s_p^3(sin(2Hs_p) - 2Hs_p)(((mu_p(k_p^2/f^2 - 2))/mu - k^2/f^2 + 2)((2mu_p)/mu
+ k^2/f^2 - 2) - (2rs((mu_p(k_p^2/f^2 - 2))/mu + 2)(mu_p/mu - 1))/f^2)^2)/(Hf^6) -
(A^2r_p^2s^2s_p^2(((2mu_p)/mu + k^2/f^2 - 2)^2 - (4rs(mu_p/mu -
1)^2)/f^2)^2((H(cosh(2Hr_p) + 1)(cos(2Hs_p) - 1))/2 - 2H(cosh(2Hr_p)/2 -
1/2)(cos(2Hs_p)/2 - 1/2) + (sinh(2Hr_p)(cos(2Hs_p)/2 - 1/2))/r_p + (H(2f^2 -
k_p^2)^2(cosh(2Hr_p) + 1)(cos(2Hs_p) - 1))/(8f^4) + (sin(2Hs_p)(2f^2 -
k_p^2)^2(cosh(2Hr_p) + 1))/(8f^4s_p) - (Hcos(Hs_p)^2(cosh(2Hr_p)/2 + 1/2)(2f^2 -
k_p^2)^2)/(2f^4) - (r_psinh(2Hr_p)(2f^2 - k_p^2)(cos(2Hs_p) - 1))/(f^2(r_p^2 + s_p^2))
- (2s_pcosh(Hr_p)^2sin(2Hs_p)(2f^2 - k_p^2))/(f^2(r_p^2 + s_p^2)) +
(4s_pcosh(Hr_p)sin(Hs_p)(2f^2 - k_p^2))/(f^2(r_p^2 + s_p^2))))/(Hf^6) +
(A^2s_p^2(sinh(2Hr_p) - 2Hr_p)(((mu_p(k_p^2/f^2 - 2))/mu - k^2/f^2 + 2)((2mu_p)/mu +
k^2/f^2 - 2) - (2rs((mu_p(k_p^2/f^2 - 2))/mu + 2)(mu_p/mu - 1))/f^2)^2(2f^2 -
k_p^2)^2)/(4Hf^6r_p) - (8A^2r_ps_p^3(r_pcosh(Hr_p)sin(Hs_p) -
s_pcos(Hs_p)sinh(Hr_p))(((mu_p(k_p^2/f^2 - 2))/mu - k^2/f^2 + 2)((2mu_p)/mu + k^2/f^2 -
2) - (2rs((mu_p(k_p^2/f^2 - 2))/mu + 2)(mu_p/mu - 1))/f^2)^2)/(Hf^4(r_p^2 + s_p^2)) +
(A^2k_p^4mu_p^2s_p^2(((s^2/f^2 + 1)((r_pcosh(Hr_p)(k_p^2/f^2 - 2)((2mu_p)/mu + k^2/f^2
- 2))/f - (2r_pcos(Hs_p)((mu_p(k_p^2/f^2 - 2))/mu - k^2/f^2 + 2))/f +
(rsinh(Hr_p)((mu_p(k_p^2/f^2 - 2))/mu + 2)(k_p^2/f^2 - 2))/f +
(4rr_ps_psin(Hs_p)(mu_p/mu - 1))/f^3)^2)/(2s) + ((r^2/f^2 + 1)(sinh(Hr_p)(k_p^2/f^2 -
2)((mu_p(k_p^2/f^2 - 2))/mu - k^2/f^2 + 2) + (2r_ps_psin(Hs_p)((2mu_p)/mu + k^2/f^2 -
2))/f^2 - (2r_pscos(Hs_p)((mu_p(k_p^2/f^2 - 2))/mu + 2))/f^2 +
(2r_pscosh(Hr_p)(k_p^2/f^2 - 2)(mu_p/mu - 1))/f^2)^2)/(2r) - ((r/f +
s/f)((r_pcosh(Hr_p)(k_p^2/f^2 - 2)((2mu_p)/mu + k^2/f^2 - 2))/f -
(2r_pcos(Hs_p)((mu_p(k_p^2/f^2 - 2))/mu - k^2/f^2 + 2))/f +
(rsinh(Hr_p)((mu_p(k_p^2/f^2 - 2))/mu + 2)(k_p^2/f^2 - 2))/f +
(4rr_ps_psin(Hs_p)(mu_p/mu - 1))/f^3)(2sinh(Hr_p)(k_p^2/f^2 - 2)((mu_p(k_p^2/f^2 -
2))/mu - k^2/f^2 + 2) + (4r_ps_psin(Hs_p)((2mu_p)/mu + k^2/f^2 - 2))/f^2 -
(4r_pscos(Hs_p)((mu_p(k_p^2/f^2 - 2))/mu + 2))/f^2 + (4r_pscosh(Hr_p)(k_p^2/f^2 -
2)(mu_p/mu - 1))/f^2))/(r + s)))/(Lf^6mu^2) -
(4A^2r_ps_p^3sinh(Hr_p)sin(Hs_p)(((mu_p(k_p^2/f^2 - 2))/mu - k^2/f^2 + 2)((2mu_p)/mu +
k^2/f^2 - 2) - (2rs((mu_p(k_p^2/f^2 - 2))/mu + 2)(mu_p/mu - 1))/f^2)(((mu_p(k_p^2/f^2 -
2))/mu - k^2/f^2 + 2)^2 - (rs((mu_p(k_p^2/f^2 - 2))/mu + 2)^2)/f^2))/f^4 +
(2A^2ss_p^2sin(2Hs_p)(((2mu_p)/mu + k^2/f^2 - 2)^2 - (4rs(mu_p/mu -
1)^2)/f^2)(cosh(2Hr_p)/2 - 1/2)(((mu_p(k_p^2/f^2 - 2))/mu - k^2/f^2 + 2)^2 -
(rs((mu_p(k_p^2/f^2 - 2))/mu + 2)^2)/f^2))/(Hf^4) +
(4A^2k_p^2r_ps_p^3(r_pcosh(Hr_p)sin(Hs_p) - s_pcos(Hs_p)sinh(Hr_p))(((mu_p(k_p^2/f^2 -
2))/mu - k^2/f^2 + 2)((2mu_p)/mu + k^2/f^2 - 2) - (2rs((mu_p(k_p^2/f^2 - 2))/mu +
2)(mu_p/mu - 1))/f^2)^2)/(Hf^6(r_p^2 + s_p^2)) +
(2A^2k_p^2r_ps_p^3sinh(Hr_p)sin(Hs_p)(((mu_p(k_p^2/f^2 - 2))/mu - k^2/f^2 +
2)((2mu_p)/mu + k^2/f^2 - 2) - (2rs((mu_p(k_p^2/f^2 - 2))/mu + 2)(mu_p/mu -
1))/f^2)(((mu_p(k_p^2/f^2 - 2))/mu - k^2/f^2 + 2)^2 - (rs((mu_p(k_p^2/f^2 - 2))/mu +
2)^2)/f^2))/f^6 - (4A^2r_pss_p^2sinh(Hr_p)sin(Hs_p)(((2mu_p)/mu + k^2/f^2 - 2)^2 -
(4rs(mu_p/mu - 1)^2)/f^2)((mu_p(k_p^2/f^2 - 2))/mu - k^2/f^2 + 2)((2mu_p)/mu + k^2/f^2
- 2) - (2rs((mu_p(k_p^2/f^2 - 2))/mu + 2)(mu_p/mu - 1))/f^2))/f^4 +
(4A^2s_p^2cos(Hs_p)(((mu_p(k_p^2/f^2 - 2))/mu - k^2/f^2 + 2)((2mu_p)/mu + k^2/f^2 - 2)
- (2rs((mu_p(k_p^2/f^2 - 2))/mu + 2)(mu_p/mu - 1))/f^2)(sinh(Hr_p) -
Hr_pcosh(Hr_p))(((mu_p(k_p^2/f^2 - 2))/mu - k^2/f^2 + 2)^2 - (rs((mu_p(k_p^2/f^2 -
2))/mu + 2)^2)/f^2))/(Hf^2r_p) + (8A^2r_ps_p^2sinh(Hr_p)(((mu_p(k_p^2/f^2 - 2))/mu -
k^2/f^2 + 2)((2mu_p)/mu + k^2/f^2 - 2) - (2rs((mu_p(k_p^2/f^2 - 2))/mu + 2)(mu_p/mu -
1))/f^2)(((mu_p(k_p^2/f^2 - 2))/mu - k^2/f^2 + 2)^2 - (rs((mu_p(k_p^2/f^2 - 2))/mu +
```

APPENDIX (continued)

```
2)^2)/f^2)(cosh(Hr_p) - cos(Hs_p)))/(Hf^2(r_p^2 + s_p^2)) -
(2A^2r_pss_psinh(2Hr_p)(((2mu_p)/mu + k^2/f^2 - 2)^2 - (4rs(mu_p/mu -
1)^2)/f^2)(cos(2Hs_p)/2 - 1/2)(((mu_p(k_p^2/f^2 - 2))/mu - k^2/f^2 + 2)^2 -
(rs((mu_p(k_p^2/f^2 - 2))/mu + 2)^2)/f^2))/(Hf^4) - (8A^2r_ps_p^3cos(Hs_p)(r_psin(Hs_p)
- s_psinh(Hr_p))(((mu_p(k_p^2/f^2 - 2))/mu - k^2/f^2 + 2)((2mu_p)/mu + k^2/f^2 - 2) -
(2rs((mu_p(k_p^2/f^2 - 2))/mu + 2)(mu_p/mu - 1))/f^2)(((mu_p(k_p^2/f^2 - 2))/mu -
k^2/f^2 + 2)^2 - (rs((mu_p(k_p^2/f^2 - 2))/mu + 2)^2)/f^2))/(Hf^4(r_p^2 + s_p^2)) -
(A^2k^4k_p^4mu_p^2r^2s_p^4(2H(cosh(2Hr_p)/2 - 1/2)(cos(2Hs_p)/2 - 1/2) - (H(cosh(2Hr_p)
+ 1)(cos(2Hs_p) - 1))/2 + (sinh(2Hr_p)(cos(2Hs_p) - 1))/(2r_p) - (H(2f^2 -
k_p^2)^2(cosh(2Hr_p) - 1)(cos(2Hs_p) + 1))/(8f^4) + (sin(2Hs_p)(2f^2 -
k_p^2)^2(cosh(2Hr_p) - 1))/(8f^4s_p) + (H(cosh(2Hr_p)/2 - 1/2)(cos(2Hs_p)/2 - 1/2)(2f^2
- k_p^2)^2)/(2f^4) - (r_psinh(2Hr_p)(2f^2 - k_p^2)(cos(2Hs_p) - 1))/(f^2(r_p^2 +
s_p^2)) - (2s_psinh(Hr_p)^2sin(2Hs_p)(2f^2 - k_p^2))/(f^2(r_p^2 + s_p^2))))/(Hf^14mu^2)
+ (2A^2k_p^2r_pss_p^2sinh(Hr_p)sin(Hs_p)(((2mu_p)/mu + k^2/f^2 - 2)^2 - (4rs(mu_p/mu -
1)^2)/f^2)(((mu_p(k_p^2/f^2 - 2))/mu - k^2/f^2 + 2)((2mu_p)/mu + k^2/f^2 - 2) -
(2rs((mu_p(k_p^2/f^2 - 2))/mu + 2)(mu_p/mu - 1))/f^2))/f^6 -
(2A^2k_p^2s_p^2cos(Hs_p)(((mu_p(k_p^2/f^2 - 2))/mu - k^2/f^2 + 2)((2mu_p)/mu + k^2/f^2
- 2) - (2rs((mu_p(k_p^2/f^2 - 2))/mu + 2)(mu_p/mu - 1))/f^2)(sinh(Hr_p) -
Hr_pcosh(Hr_p))(((mu_p(k_p^2/f^2 - 2))/mu - k^2/f^2 + 2)^2 - (rs((mu_p(k_p^2/f^2 -
2))/mu + 2)^2)/f^2))/(Hf^4r_p) - (2A^2r_p^2ss_p^2cosh(Hr_p)(((2mu_p)/mu + k^2/f^2 -
2)^2 - (4rs(mu_p/mu - 1)^2)/f^2)(((mu_p(k_p^2/f^2 - 2))/mu - k^2/f^2 + 2)((2mu_p)/mu +
k^2/f^2 - 2) - (2rs((mu_p(k_p^2/f^2 - 2))/mu + 2)(mu_p/mu - 1))/f^2)(sin(Hs_p) -
Hs_pcos(Hs_p)))/(Hf^6) + (2A^2k_p^2r_pss_psinh(2Hr_p)(((2mu_p)/mu + k^2/f^2 - 2)^2 -
(4rs(mu_p/mu - 1)^2)/f^2)(cos(2Hs_p)/2 - 1/2)(((mu_p(k_p^2/f^2 - 2))/mu - k^2/f^2 +
2)^2 - (rs((mu_p(k_p^2/f^2 - 2))/mu + 2)^2)/f^2))/(Hf^6) -
(A^2k_p^4r_pss_psinh(2Hr_p)(((2mu_p)/mu + k^2/f^2 - 2)^2 - (4rs(mu_p/mu -
1)^2)/f^2)(cos(2Hs_p)/2 - 1/2)(((mu_p(k_p^2/f^2 - 2))/mu - k^2/f^2 + 2)^2 -
(rs((mu_p(k_p^2/f^2 - 2))/mu + 2)^2)/f^2))/(2Hf^8) -
(8A^2r_pss_p^2cosh(Hr_p)(((2mu_p)/mu + k^2/f^2 - 2)^2 - (4rs(mu_p/mu -
1)^2)/f^2)(r_psin(Hs_p) - s_psinh(Hr_p))(((mu_p(k_p^2/f^2 - 2))/mu - k^2/f^2 +
2)((2mu_p)/mu + k^2/f^2 - 2) - (2rs((mu_p(k_p^2/f^2 - 2))/mu + 2)(mu_p/mu -
1))/f^2))/(Hf^4(r_p^2 + s_p^2)) + (4A^2r_p^2ss_p^4sin(Hs_p)(((2mu_p)/mu + k^2/f^2 -
2)^2 - (4rs(mu_p/mu - 1)^2)/f^2)(((mu_p(k_p^2/f^2 - 2))/mu - k^2/f^2 + 2)((2mu_p)/mu +
k^2/f^2 - 2) - (2rs((mu_p(k_p^2/f^2 - 2))/mu + 2)(mu_p/mu - 1))/f^2)(cosh(Hr_p) -
cos(Hs_p)))/(Hf^6(r_p^2 + s_p^2)) + (A^2k_p^2r_p^2ss_p^2cosh(Hr_p)(((2mu_p)/mu +
k^2/f^2 - 2)^2 - (4rs(mu_p/mu - 1)^2)/f^2)(((mu_p(k_p^2/f^2 - 2))/mu - k^2/f^2 +
2)((2mu_p)/mu + k^2/f^2 - 2) - (2rs((mu_p(k_p^2/f^2 - 2))/mu + 2)(mu_p/mu -
1))/f^2)(sin(Hs_p) - Hs_pcos(Hs_p)))/(Hf^8) +
(A^2k^4k_p^4mu_p^2r_p^2s^2s_p^2(H(cosh(2Hr_p) + 1) + 2Hcos(Hs_p)^2 +
(sinh(2Hr_p)(cos(2Hs_p) + 1))/(2r_p) + (sin(2Hs_p)(cosh(2Hr_p) + 1))/(2s_p) -
(Hk_p^2(cosh(2Hr_p) + 1))/f^2 + (Hk_p^4(cosh(2Hr_p) + 1))/(4f^4) -
(2r_psinh(2Hr_p)(cos(2Hs_p) + 1))/(r_p^2 + s_p^2) - (2s_psin(2Hs_p)(cosh(2Hr_p) +
1))/(r_p^2 + s_p^2) - (k_p^2sin(2Hs_p)(cosh(2Hr_p) + 1))/(2f^2s_p) +
(k_p^4sin(2Hs_p)(cosh(2Hr_p) + 1))/(8f^4s_p) + (k_p^2r_psinh(2Hr_p)(cos(2Hs_p) +
1))/(f^2(r_p^2 + s_p^2)) + (k_p^2s_psin(2Hs_p)(cosh(2Hr_p) + 1))/(f^2(r_p^2 +
s_p^2))))/(Hf^14mu^2) - (8A^2k_p^2r_ps_p^2sinh(Hr_p)(((mu_p(k_p^2/f^2 - 2))/mu -
k^2/f^2 + 2)((2mu_p)/mu + k^2/f^2 - 2) - (2rs((mu_p(k_p^2/f^2 - 2))/mu + 2)(mu_p/mu -
1))/f^2)(((mu_p(k_p^2/f^2 - 2))/mu - k^2/f^2 + 2)^2 - (rs((mu_p(k_p^2/f^2 - 2))/mu +
2)^2)/f^2)(cosh(Hr_p) - cos(Hs_p)))/(Hf^4(r_p^2 + s_p^2)) +
(2A^2k_p^4r_ps_p^2sinh(Hr_p)(((mu_p(k_p^2/f^2 - 2))/mu - k^2/f^2 + 2)((2mu_p)/mu +
k^2/f^2 - 2) - (2rs((mu_p(k_p^2/f^2 - 2))/mu + 2)(mu_p/mu - 1))/f^2)(((mu_p(k_p^2/f^2 -
2))/mu - k^2/f^2 + 2)^2 - (rs((mu_p(k_p^2/f^2 - 2))/mu + 2)^2)/f^2)(cosh(Hr_p) -
cos(Hs_p)))/(Hf^6(r_p^2 + s_p^2)) - (2A^2k^4k_p^4mu_p^2rss_p^3sin(2Hs_p)(cosh(2Hr_p)/2
- 1/2))/(Hf^14mu^2) + (8A^2k_p^2r_pss_p^2cosh(Hr_p)(((2mu_p)/mu + k^2/f^2 - 2)^2 -
(4rs(mu_p/mu - 1)^2)/f^2)(r_psin(Hs_p) - s_psinh(Hr_p))(((mu_p(k_p^2/f^2 - 2))/mu -
k^2/f^2 + 2)((2mu_p)/mu + k^2/f^2 - 2) - (2rs((mu_p(k_p^2/f^2 - 2))/mu + 2)(mu_p/mu -
1))/f^2))/(Hf^6(r_p^2 + s_p^2)) - (2A^2k_p^4r_pss_p^2cosh(Hr_p)(((2mu_p)/mu + k^2/f^2 -
2)^2 - (4rs(mu_p/mu - 1)^2)/f^2)(r_psin(Hs_p) - s_psinh(Hr_p))(((mu_p(k_p^2/f^2 -
2))/mu - k^2/f^2 + 2)((2mu_p)/mu + k^2/f^2 - 2) - (2rs((mu_p(k_p^2/f^2 - 2))/mu +
```

APPENDIX (continued)

```
2)(mu_p/mu - 1))/f^2))/(Hf^8(r_p^2 + s_p^2)) -
(8A^2r_pss_p^2cosh(Hr_p)cos(Hs_p)(((2mu_p)/mu + k^2/f^2 - 2)^2 - (4rs(mu_p/mu -
1)^2)/f^2)(r_pcosh(Hr_p)sin(Hs_p) - s_pcos(Hs_p)sinh(Hr_p))(((mu_p(k_p^2/f^2 - 2))/mu -
k^2/f^2 + 2)^2 - (rs((mu_p(k_p^2/f^2 - 2))/mu + 2)^2)/f^2))/(Hf^4(r_p^2 + s_p^2)) -
(8A^2r_pss_p^2sinh(Hr_p)sin(Hs_p)(((2mu_p)/mu + k^2/f^2 - 2)^2 - (4rs(mu_p/mu -
1)^2)/f^2)(r_pcos(Hs_p)sinh(Hr_p) + s_pcosh(Hr_p)sin(Hs_p))(((mu_p(k_p^2/f^2 - 2))/mu -
k^2/f^2 + 2)^2 - (rs((mu_p(k_p^2/f^2 - 2))/mu + 2)^2)/f^2))/(Hf^4(r_p^2 + s_p^2)) +
(4A^2k^2k_p^2mu_pr_pss_p^2cos(Hs_p)sinh(Hr_p)(((mu_p(k_p^2/f^2 - 2))/mu - k^2/f^2 +
2)((2mu_p)/mu + k^2/f^2 - 2) - (2rs((mu_p(k_p^2/f^2 - 2))/mu + 2)(mu_p/mu -
1))/f^2))/(f^8mu) - (2A^2k^2k_p^4mu_pr_pss_p^2cos(Hs_p)sinh(Hr_p)(((mu_p(k_p^2/f^2 -
2))/mu - k^2/f^2 + 2)((2mu_p)/mu + k^2/f^2 - 2) - (2rs((mu_p(k_p^2/f^2 - 2))/mu +
2)(mu_p/mu - 1))/f^2))/(f^10mu) - (4A^2k^2k_p^2mu_prs_p^2(cosh(2Hr_p)/2 -
1/2)(cos(2Hs_p)/2 - 1/2)(((mu_p(k_p^2/f^2 - 2))/mu - k^2/f^2 + 2)^2 -
(rs((mu_p(k_p^2/f^2 - 2))/mu + 2)^2)/f^2))/(Hf^10mu) +
(4A^2k^2k_p^4mu_prs_p^2(cosh(2Hr_p)/2 - 1/2)(cos(2Hs_p)/2 - 1/2)(((mu_p(k_p^2/f^2 -
2))/mu - k^2/f^2 + 2)^2 - (rs((mu_p(k_p^2/f^2 - 2))/mu + 2)^2)/f^2))/(Hf^12mu) -
(A^2k^2k_p^6mu_prs_p^2(cosh(2Hr_p)/2 - 1/2)(cos(2Hs_p)/2 - 1/2)(((mu_p(k_p^2/f^2 -
2))/mu - k^2/f^2 + 2)^2 - (rs((mu_p(k_p^2/f^2 - 2))/mu + 2)^2)/f^2))/(Hf^14mu) +
(4A^2k^2k_p^2mu_pr_p^2ss_p^3cosh(Hr_p)sin(Hs_p)(((mu_p(k_p^2/f^2 - 2))/mu - k^2/f^2 +
2)((2mu_p)/mu + k^2/f^2 - 2) - (2rs((mu_p(k_p^2/f^2 - 2))/mu + 2)(mu_p/mu -
1))/f^2))/(f^10mu) - (2A^2k^2k_p^4mu_pr_p^2ss_p^3cosh(Hr_p)sin(Hs_p)(((mu_p(k_p^2/f^2 -
2))/mu - k^2/f^2 + 2)((2mu_p)/mu + k^2/f^2 - 2) - (2rs((mu_p(k_p^2/f^2 - 2))/mu +
2)(mu_p/mu - 1))/f^2))/(f^12mu) - (A^2k^2k_p^2mu_pss_p^2(((mu_p(k_p^2/f^2 - 2))/mu -
k^2/f^2 + 2)^2 - (rs((mu_p(k_p^2/f^2 - 2))/mu + 2)^2)/f^2)(cosh(2Hr_p) - 1)(cos(2Hs_p)
+ 1))/(Hf^8mu) + (A^2k^2k_p^2mu_pr_p^2s^2s_p(((2mu_p)/mu + k^2/f^2 - 2)^2 -
(4rs(mu_p/mu - 1)^2)/f^2)(cosh(2Hr_p) + 1)(cos(2Hs_p) - 1))/(Hf^10mu) -
(A^2k^2k_p^4mu_pr_p^2s^2s_p(((2mu_p)/mu + k^2/f^2 - 2)^2 - (4rs(mu_p/mu -
1)^2)/f^2)(cosh(2Hr_p) + 1)(cos(2Hs_p) - 1))/(Hf^12mu) +
(A^2k^2k_p^6mu_pr_p^2s^2s_p(((2mu_p)/mu + k^2/f^2 - 2)^2 - (4rs(mu_p/mu -
1)^2)/f^2)(cosh(2Hr_p) + 1)(cos(2Hs_p) - 1))/(4Hf^14mu) +
(4A^2k_p^2r_pss_p^2cosh(Hr_p)cos(Hs_p)(((2mu_p)/mu + k^2/f^2 - 2)^2 - (4rs(mu_p/mu -
1)^2)/f^2)(r_pcosh(Hr_p)sin(Hs_p) - s_pcos(Hs_p)sinh(Hr_p))(((mu_p(k_p^2/f^2 - 2))/mu -
k^2/f^2 + 2)^2 - (rs((mu_p(k_p^2/f^2 - 2))/mu + 2)^2)/f^2))/(Hf^6(r_p^2 + s_p^2)) -
(4A^2k^2k_p^2mu_prr_ps_p^3sinh(Hr_p)(((mu_p(k_p^2/f^2 - 2))/mu - k^2/f^2 +
2)((2mu_p)/mu + k^2/f^2 - 2) - (2rs((mu_p(k_p^2/f^2 - 2))/mu + 2)(mu_p/mu -
1))/f^2)(sin(Hs_p) - Hs_pcos(Hs_p)))/(Hf^10mu) +
(2A^2k^2k_p^4mu_prr_ps_p^3sinh(Hr_p)(((mu_p(k_p^2/f^2 - 2))/mu - k^2/f^2 +
2)((2mu_p)/mu + k^2/f^2 - 2) - (2rs((mu_p(k_p^2/f^2 - 2))/mu + 2)(mu_p/mu -
1))/f^2)(sin(Hs_p) - Hs_pcos(Hs_p)))/(Hf^12mu) +
(4A^2k_p^2r_pss_p^2sinh(Hr_p)sin(Hs_p)(((2mu_p)/mu + k^2/f^2 - 2)^2 - (4rs(mu_p/mu -
1)^2)/f^2)(r_pcos(Hs_p)sinh(Hr_p) + s_pcosh(Hr_p)sin(Hs_p))(((mu_p(k_p^2/f^2 - 2))/mu -
k^2/f^2 + 2)^2 - (rs((mu_p(k_p^2/f^2 - 2))/mu + 2)^2)/f^2))/(Hf^6(r_p^2 + s_p^2)) -
(4A^2k^2k_p^2mu_prss_p^3(((2mu_p)/mu + k^2/f^2 - 2)^2 - (4rs(mu_p/mu -
1)^2)/f^2)(cosh(2Hr_p)/2 - 1/2)(cos(2Hs_p)/2 - 1/2))/(Hf^10mu) +
(4A^2k^2k_p^2mu_prs_p^3sin(Hs_p)(((mu_p(k_p^2/f^2 - 2))/mu - k^2/f^2 + 2)((2mu_p)/mu +
k^2/f^2 - 2) - (2rs((mu_p(k_p^2/f^2 - 2))/mu + 2)(mu_p/mu - 1))/f^2)(sinh(Hr_p) -
Hr_pcosh(Hr_p)))/(Hf^8mur_p) - (2A^2k^2k_p^4mu_prs_p^3sin(Hs_p)(((mu_p(k_p^2/f^2 -
2))/mu - k^2/f^2 + 2)((2mu_p)/mu + k^2/f^2 - 2) - (2rs((mu_p(k_p^2/f^2 - 2))/mu +
2)(mu_p/mu - 1))/f^2)(sinh(Hr_p) - Hr_pcosh(Hr_p)))/(Hf^10mur_p) +
(A^2k^2k_p^2mu_prs_p^3sin(2Hs_p)(sinh(2Hr_p) - 2Hr_p)(((mu_p(k_p^2/f^2 - 2))/mu -
k^2/f^2 + 2)^2 - (rs((mu_p(k_p^2/f^2 - 2))/mu + 2)^2)/f^2))/(Hf^10mur_p) +
(2A^2k^4k_p^4mu_p^2rr_pss_p^2sinh(2Hr_p)(cos(2Hs_p)/2 - 1/2))/(Hf^14mu^2) -
(2A^2k^4k_p^6mu_p^2rr_pss_p^2sinh(2Hr_p)(cos(2Hs_p)/2 - 1/2))/(Hf^16mu^2) +
(A^2k^4k_p^8mu_p^2rr_pss_p^2sinh(2Hr_p)(cos(2Hs_p)/2 - 1/2))/(2Hf^18mu^2) -
(8A^2k^2k_p^2mu_prs_p^3sinh(Hr_p)(r_psin(Hs_p) - s_psinh(Hr_p))(((mu_p(k_p^2/f^2 -
2))/mu - k^2/f^2 + 2)((2mu_p)/mu + k^2/f^2 - 2) - (2rs((mu_p(k_p^2/f^2 - 2))/mu +
2)(mu_p/mu - 1))/f^2))/(Hf^8mu(r_p^2 + s_p^2)) +
(8A^2k^2k_p^4mu_prs_p^3sinh(Hr_p)(r_psin(Hs_p) - s_psinh(Hr_p))(((mu_p(k_p^2/f^2 -
2))/mu - k^2/f^2 + 2)((2mu_p)/mu + k^2/f^2 - 2) - (2rs((mu_p(k_p^2/f^2 - 2))/mu +
```

APPENDIX (continued)

```
2)(mu_p/mu - 1))/f^2))/(Hf^10mu(r_p^2 + s_p^2)) -
(2A^2k^2k_p^6mu_prs_p^3sinh(Hr_p)(r_psin(Hs_p) - s_psinh(Hr_p))(((mu_p(k_p^2/f^2 -
2))/mu - k^2/f^2 + 2)((2mu_p)/mu + k^2/f^2 - 2) - (2rs((mu_p(k_p^2/f^2 - 2))/mu +
2)(mu_p/mu - 1))/f^2))/(Hf^12mu(r_p^2 + s_p^2)) -
(A^2k^2k_p^2mu_pr_pss_psinh(2Hr_p)(sin(2Hs_p) + 2Hs_p)(((mu_p(k_p^2/f^2 - 2))/mu -
k^2/f^2 + 2)^2 - (rs((mu_p(k_p^2/f^2 - 2))/mu + 2)^2)/f^2))/(Hf^8mu) +
(A^2k^2k_p^4mu_pr_pss_psinh(2Hr_p)(sin(2Hs_p) + 2Hs_p)(((mu_p(k_p^2/f^2 - 2))/mu -
k^2/f^2 + 2)^2 - (rs((mu_p(k_p^2/f^2 - 2))/mu + 2)^2)/f^2))/(Hf^10mu) -
(A^2k^2k_p^6mu_pr_pss_psinh(2Hr_p)(sin(2Hs_p) + 2Hs_p)(((mu_p(k_p^2/f^2 - 2))/mu -
k^2/f^2 + 2)^2 - (rs((mu_p(k_p^2/f^2 - 2))/mu + 2)^2)/f^2))/(4Hf^12mu) -
(A^2k^2k_p^2mu_pr_ps^2s_p^2sin(2Hs_p)(sinh(2Hr_p) + 2Hr_p)(((2mu_p)/mu + k^2/f^2 - 2)^2
- (4rs(mu_p/mu - 1)^2)/f^2))/(Hf^10mu) -
(A^2k^2k_p^2mu_prr_pss_p^2sinh(2Hr_p)(sin(2Hs_p) - 2Hs_p)(((2mu_p)/mu + k^2/f^2 - 2)^2
- (4rs(mu_p/mu - 1)^2)/f^2))/(Hf^10mu) +
(A^2k^2k_p^4mu_prr_pss_p^2sinh(2Hr_p)(sin(2Hs_p) - 2Hs_p)(((2mu_p)/mu + k^2/f^2 - 2)^2
- (4rs(mu_p/mu - 1)^2)/f^2))/(Hf^12mu) -
(A^2k^2k_p^6mu_prr_pss_p^2sinh(2Hr_p)(sin(2Hs_p) - 2Hs_p)(((2mu_p)/mu + k^2/f^2 - 2)^2
- (4rs(mu_p/mu - 1)^2)/f^2))/(4Hf^14mu) -
(8A^2k^2k_p^2mu_pr_p^2ss_p^2cosh(Hr_p)(((mu_p(k_p^2/f^2 - 2))/mu - k^2/f^2 +
2)((2mu_p)/mu + k^2/f^2 - 2) - (2rs((mu_p(k_p^2/f^2 - 2))/mu + 2)(mu_p/mu -
1))/f^2)(cosh(Hr_p) - cos(Hs_p)))/(Hf^8mu(r_p^2 + s_p^2)) +
(8A^2k^2k_p^4mu_pr_p^2ss_p^2cosh(Hr_p)(((mu_p(k_p^2/f^2 - 2))/mu - k^2/f^2 +
2)((2mu_p)/mu + k^2/f^2 - 2) - (2rs((mu_p(k_p^2/f^2 - 2))/mu + 2)(mu_p/mu -
1))/f^2)(cosh(Hr_p) - cos(Hs_p)))/(Hf^10mu(r_p^2 + s_p^2)) -
(2A^2k^2k_p^6mu_pr_p^2ss_p^2cosh(Hr_p)(((mu_p(k_p^2/f^2 - 2))/mu - k^2/f^2 +
2)((2mu_p)/mu + k^2/f^2 - 2) - (2rs((mu_p(k_p^2/f^2 - 2))/mu + 2)(mu_p/mu -
1))/f^2)(cosh(Hr_p) - cos(Hs_p)))/(Hf^12mu(r_p^2 + s_p^2)) -
(8A^2k^2k_p^2mu_pr_p^2ss_p^4cos(Hs_p)(((mu_p(k_p^2/f^2 - 2))/mu - k^2/f^2 +
2)((2mu_p)/mu + k^2/f^2 - 2) - (2rs((mu_p(k_p^2/f^2 - 2))/mu + 2)(mu_p/mu -
1))/f^2)(cosh(Hr_p) - cos(Hs_p)))/(Hf^10mu(r_p^2 + s_p^2)) -
(8A^2k^2k_p^2mu_prr_ps_p^4sin(Hs_p)(r_psin(Hs_p) - s_psinh(Hr_p))(((mu_p(k_p^2/f^2 -
2))/mu - k^2/f^2 + 2)((2mu_p)/mu + k^2/f^2 - 2) - (2rs((mu_p(k_p^2/f^2 - 2))/mu +
2)(mu_p/mu - 1))/f^2))/(Hf^10mu(r_p^2 + s_p^2)) -
(8A^2k^2k_p^2mu_prs_p^3sinh(Hr_p)sin(Hs_p)(((mu_p(k_p^2/f^2 - 2))/mu - k^2/f^2 + 2)^2 -
(rs((mu_p(k_p^2/f^2 - 2))/mu + 2)^2)/f^2)(r_pcosh(Hr_p)cos(Hs_p) - r_p +
s_psinh(Hr_p)sin(Hs_p)))/(Hf^10mu(r_p^2 + s_p^2)) +
(4A^2k^2k_p^4mu_prs_p^3sinh(Hr_p)sin(Hs_p)(((mu_p(k_p^2/f^2 - 2))/mu - k^2/f^2 + 2)^2 -
(rs((mu_p(k_p^2/f^2 - 2))/mu + 2)^2)/f^2)(r_pcosh(Hr_p)cos(Hs_p) - r_p +
s_psinh(Hr_p)sin(Hs_p)))/(Hf^12mu(r_p^2 + s_p^2)) -
(8A^2k^2k_p^2mu_prs_p^3cos(Hs_p)sinh(Hr_p)(r_pcosh(Hr_p)sin(Hs_p) -
s_pcos(Hs_p)sinh(Hr_p))(((mu_p(k_p^2/f^2 - 2))/mu - k^2/f^2 + 2)^2 -
(rs((mu_p(k_p^2/f^2 - 2))/mu + 2)^2)/f^2))/(Hf^10mu(r_p^2 + s_p^2)) +
(4A^2k^2k_p^4mu_prs_p^3cos(Hs_p)sinh(Hr_p)(r_pcosh(Hr_p)sin(Hs_p) -
s_pcos(Hs_p)sinh(Hr_p))(((mu_p(k_p^2/f^2 - 2))/mu - k^2/f^2 + 2)^2 -
(rs((mu_p(k_p^2/f^2 - 2))/mu + 2)^2)/f^2))/(Hf^12mu(r_p^2 + s_p^2)) +
(8A^2k^4k_p^4mu_p^2rr_pss_p^3cosh(Hr_p)sin(Hs_p)(r_pcosh(Hr_p)cos(Hs_p) - r_p +
s_psinh(Hr_p)sin(Hs_p)))/(Hf^14mu^2(r_p^2 + s_p^2)) -
(4A^2k^4k_p^6mu_p^2rr_pss_p^3cosh(Hr_p)sin(Hs_p)(r_pcosh(Hr_p)cos(Hs_p) - r_p +
s_psinh(Hr_p)sin(Hs_p)))/(Hf^16mu^2(r_p^2 + s_p^2)) +
(8A^2k^2k_p^2mu_pr_pss_p^2cos(Hs_p)sinh(Hr_p)(r_pcos(Hs_p)sinh(Hr_p) +
s_pcosh(Hr_p)sin(Hs_p))(((mu_p(k_p^2/f^2 - 2))/mu - k^2/f^2 + 2)^2 -
(rs((mu_p(k_p^2/f^2 - 2))/mu + 2)^2)/f^2))/(Hf^8mu(r_p^2 + s_p^2)) -
(4A^2k^2k_p^4mu_pr_pss_p^2cos(Hs_p)sinh(Hr_p)(r_pcos(Hs_p)sinh(Hr_p) +
s_pcosh(Hr_p)sin(Hs_p))(((mu_p(k_p^2/f^2 - 2))/mu - k^2/f^2 + 2)^2 -
(rs((mu_p(k_p^2/f^2 - 2))/mu + 2)^2)/f^2))/(Hf^10mu(r_p^2 + s_p^2)) +
(8A^2k^2k_p^2mu_pr_p^2s^2s_p^2cosh(Hr_p)sin(Hs_p)(((2mu_p)/mu + k^2/f^2 - 2)^2 -
(4rs(mu_p/mu - 1)^2)/f^2)(r_pcos(Hs_p)sinh(Hr_p) +
s_pcosh(Hr_p)sin(Hs_p)))/(Hf^10mu(r_p^2 + s_p^2)) -
(4A^2k^2k_p^4mu_pr_p^2s^2s_p^2cosh(Hr_p)sin(Hs_p)(((2mu_p)/mu + k^2/f^2 - 2)^2 -
```

APPENDIX (continued)

```
(4rs(mu_p/mu - 1)^2)/f^2)(r_pcos(Hs_p)sinh(Hr_p) +
s_pcosh(Hr_p)sin(Hs_p)))/(Hf^12mu(r_p^2 + s_p^2)) +
(8A^2k^2k_p^2mu_pr_p^2s^2s_p^2cosh(Hr_p)cos(Hs_p)(((2mu_p)/mu + k^2/f^2 - 2)^2 -
(4rs(mu_p/mu - 1)^2)/f^2)(s_p - s_pcosh(Hr_p)cos(Hs_p) +
r_psinh(Hr_p)sin(Hs_p)))/(Hf^10mu(r_p^2 + s_p^2)) -
(4A^2k^2k_p^4mu_pr_p^2s^2s_p^2cosh(Hr_p)cos(Hs_p)(((2mu_p)/mu + k^2/f^2 - 2)^2 -
(4rs(mu_p/mu - 1)^2)/f^2)(s_p - s_pcosh(Hr_p)cos(Hs_p) +
r_psinh(Hr_p)sin(Hs_p)))/(Hf^12mu(r_p^2 + s_p^2)) +
(8A^2k^4k_p^4mu_p^2rr_pss_p^3cos(Hs_p)sinh(Hr_p)(s_p - s_pcosh(Hr_p)cos(Hs_p) +
r_psinh(Hr_p)sin(Hs_p)))/(Hf^14mu^2(r_p^2 + s_p^2)) -
(4A^2k^4k_p^6mu_p^2rr_pss_p^3cos(Hs_p)sinh(Hr_p)(s_p - s_pcosh(Hr_p)cos(Hs_p) +
r_psinh(Hr_p)sin(Hs_p)))/(Hf^16mu^2(r_p^2 + s_p^2)) +
(8A^2k^2k_p^2mu_pr_pss_p^2cosh(Hr_p)cos(Hs_p)(((mu_p(k_p^2/f^2 - 2))/mu - k^2/f^2 +
2)^2 - (rs((mu_p(k_p^2/f^2 - 2))/mu + 2)^2)/f^2)(r_pcosh(Hr_p)cos(Hs_p) - r_p +
s_psinh(Hr_p)sin(Hs_p)))/(Hf^8mu(r_p^2 + s_p^2)) -
(4A^2k^2k_p^4mu_pr_pss_p^2cosh(Hr_p)cos(Hs_p)(((mu_p(k_p^2/f^2 - 2))/mu - k^2/f^2 +
2)^2 - (rs((mu_p(k_p^2/f^2 - 2))/mu + 2)^2)/f^2)(r_pcosh(Hr_p)cos(Hs_p) - r_p +
s_psinh(Hr_p)sin(Hs_p)))/(Hf^10mu(r_p^2 + s_p^2)) -
(8A^2k^2k_p^2mu_prr_pss_p^3sinh(Hr_p)sin(Hs_p)(((2mu_p)/mu + k^2/f^2 - 2)^2 -
(4rs(mu_p/mu - 1)^2)/f^2)(s_p - s_pcosh(Hr_p)cos(Hs_p) +
r_psinh(Hr_p)sin(Hs_p)))/(Hf^10mu(r_p^2 + s_p^2)) +
(4A^2k^2k_p^4mu_prr_pss_p^3sinh(Hr_p)sin(Hs_p)(((2mu_p)/mu + k^2/f^2 - 2)^2 -
(4rs(mu_p/mu - 1)^2)/f^2)(s_p - s_pcosh(Hr_p)cos(Hs_p) +
r_psinh(Hr_p)sin(Hs_p)))/(Hf^12mu(r_p^2 + s_p^2)) -
(8A^2k^2k_p^2mu_prr_pss_p^3cosh(Hr_p)sin(Hs_p)(((2mu_p)/mu + k^2/f^2 - 2)^2 -
(4rs(mu_p/mu - 1)^2)/f^2)(r_pcosh(Hr_p)sin(Hs_p) -
s_pcos(Hs_p)sinh(Hr_p)))/(Hf^10mu(r_p^2 + s_p^2)) +
(4A^2k^2k_p^4mu_prr_pss_p^3cosh(Hr_p)sin(Hs_p)(((2mu_p)/mu + k^2/f^2 - 2)^2 -
(4rs(mu_p/mu - 1)^2)/f^2)(r_pcosh(Hr_p)sin(Hs_p) -
s_pcos(Hs_p)sinh(Hr_p)))/(Hf^12mu(r_p^2 + s_p^2))=hbar/(2 m omega)
```

CITED LITERATURE

1. Russell, S. A. O., Sharabi, S., Tallaire, A., and Moran, D. A. J.: Hydrogen-terminated diamond field-effect transistors with cutoff frequency of 53 GHz. IEEE Electron Device Letters, 33(10):1471–1473, Oct 2012.

2. Imura, M., Hayakawa, R., Ohsato, H., Watanabe, E., Tsuya, D., Nagata, T., Liao, M., Koide, Y., Yamamoto, J., Ban, K., Iwaya, M., and Amano, H.: Development of AlN/diamond heterojunction field effect transistors. Diamond and Related Materials, 24:206 – 209, 2012.

3. Benetti, M., Cannata, D., Di Pictrantonio, F., and Verona, E.: Growth of AlN piezoelectric film on diamond for high-frequency surface acoustic wave devices. IEEE Transactions on Ultrasonics, Ferroelectrics, and Frequency Control, 52(10):1806–1811, Oct 2005.

4. Kueck, D., Scharpf, J., Ebert, W., Fikry, M., Scholz, F., and Kohn, E.: Passivation of H-terminated diamond with MOCVD-aluminium nitride - a key to understand and stabilize its surface conductivity. Physica Status Solidi (a), 207:2035 – 2039, Sep 2010.

5. Imura, M., Hayakawa, R., Watanabe, E., Liao, M., Koide, Y., and Amano, H.: Demonstration of diamond field effect transistors by AlN/diamond heterostructure. Physica Status Solidi (RRL) - Rapid Research Letters, 5:125 – 127, Mar 2011.

6. Sasama, Y., Komatsu, K., Moriyama, S., Imura, M., Teraji, T., Watanabe, K., Taniguchi, T., Uchihashi, T., and Takahide, Y.: High-mobility diamond field effect transistor with a monocrystalline h-BN gate dielectric. APL Materials, 6(11):111105, 2018.

7. Maier, F., Riedel, M., Mantel, B., Ristein, J., and Ley, L.: Origin of surface conductivity in diamond. Physical Review Letters, 85:3472–5, Nov 2000.

8. Takeuchi, D., Kato, H., Ri, G. S., Yamada, T., Vinod, P. R., Hwang, D., Nebel, C. E., Okushi, H., and Yamasaki, S.: Direct observation of negative electron affinity in hydrogen-terminated diamond surfaces. Applied Physics Letters, 86(15):152103, 2005.

CITED LITERATURE (continued)

9. Strobel, P., Riedel, M., Ristein, J., and Ley, L.: Surface transfer doping of diamond. Nature, 430:439–41, Aug 2004.

10. Strobel, P., Ristein, J., Ley, L., Seppelt, K., Goldt, I., and Boltalina, O.: Surface conductivity induced by fullerenes on diamond: Passivation and thermal stability. Diamond and Related Materials, 15(4):720 – 724, 2006.

11. Crawford, K. G., Cao, L., Qi, D., Tallaire, A., Limiti, E., Verona, C., Wee, A. T. S., and Moran, D. A. J.: Enhanced surface transfer doping of diamond by V_2O_5 with improved thermal stability. Applied Physics Letters, 108(4):042103, 2016.

12. Russell, S. A. O., Cao, L., Qi, D., Tallaire, A., Crawford, K. G., Wee, A. T. S., and Moran, D. A. J.: Surface transfer doping of diamond by MoO_3: A combined spectroscopic and hall measurement study. Applied Physics Letters, 103(20):202112, 2013.

13. Kubovic, M. and Kasu, M.: Enhancement and stabilization of hole concentration of Hydrogen-terminated diamond surface using ozone adsorbates. Japanese Journal of Applied Physics, 49(11):110208, Nov 2010.

14. Kubovic, M., Kasu, M., and Kageshima, H.: Sorption properties of NO_2 gas and its strong influence on hole concentration of H-terminated diamond surfaces. Applied Physics Letters, 96(5):052101, 2010.

15. Daicho, A., Saito, T., Kurihara, S., Hiraiwa, A., and Kawarada, H.: High-reliability passivation of hydrogen-terminated diamond surface by atomic layer deposition of Al_2O_3. Journal of Applied Physics, 115(22):223711, 2014.

16. Stroscio, M. A. and Dutta, M.: Phonons in Nanostructures. Cambridge University Press, 2001.

17. Pernot, J., Volpe, P. N., Omnès, F., Muret, P., Mortet, V., Haenen, K., and Teraji, T.: Hall hole mobility in boron-doped homoepitaxial diamond. Phys. Rev. B, 81:205203, May 2010.

18. Li, Y., Zhang, J., Liu, G.-P., Ren, Z.-Y., Zhang, J.-C., and Hao, Y.: Mobility of Two-Dimensional Hole Gas in H-terminated diamond. Physica Status Solidi (RRL) - Rapid Research Letters, 12:1700401, Jan 2018.

CITED LITERATURE (continued)

19. Willatzen, M., Cardona, M., and Christensen, N. E.: Linear muffin-tin-orbital and k·p calculations of effective masses and band structure of semiconducting diamond. Phys. Rev. B, 50:18054–18059, Dec 1994.

20. Yu, S., Kim, K. W., Stroscio, M. A., Iafrate, G. J., and Ballato, A.: Electron–acoustic-phonon scattering rates in rectangular quantum wires. Phys. Rev. B, 50:1733–1738, Jul 1994.

21. Yu, S., Kim, K. W., Stroscio, M. A., Iafrate, G. J., and Ballato, A.: Electron interaction with confined acoustic phonons in cylindrical quantum wires via deformation potential. Journal of Applied Physics, 80(5):2815–2822, 1996.

22. Bannov, N., Aristov, V., Mitin, V., and Stroscio, M. A.: Electron relaxation times due to the deformation-potential interaction of electrons with confined acoustic phonons in a free-standing quantum well. Phys. Rev. B, 51:9930–9942, Apr 1995.

23. Donetti, L., Gmiz, F., Roldn, J. B., and Godoy, A.: Acoustic phonon confinement in silicon nanolayers: Effect on electron mobility. Journal of Applied Physics, 100(1):013701, 2006.

24. Hess, K. and Vogl, P.: Remote polar phonon scattering in silicon inversion layers. Solid State Communications, 30(12):797 – 799, 1979.

25. Moore, B. T. and Ferry, D. K.: Remote polar phonon scattering in Si inversion layers. Journal of Applied Physics, 51(5):2603–2605, 1980.

26. Reggiani, L., Waechter, D., and Zukotynski, S.: Hall-coefficient factor and inverse valence-band parameters of holes in natural diamond. Phys. Rev. B, 28:3550–3555, Sep 1983.

27. Electrochemical Society, Spear, K. E., and Dismukes, J. P.: Synthetic Diamond: Emerging CVD Science and Technology. Wiley, 1994.

28. Nava, F., Canali, C., Jacoboni, C., Reggiani, L., and Kozlov, S.: Electron effective masses and lattice scattering in natural diamond. Solid State Communications, 33(4):475 – 477, 1980.

29. Auld, B.: Acoustic Fields and Waves in Solids, volume 2. Krieger Publishing Company, 1990.

CITED LITERATURE (continued)

30. Kanai, K.: On the M_2-waves (Sezawa waves). Earthquake Research Institute - Tokyo University, 29:39–48, 1951.

31. Sezawa, K. and Kanai, K.: Discontinuity in the Dispersion Curves of Rayleigh Waves. Earthquake Research Institute - Tokyo University, 13:237–244, 1935.

32. Graff, K. F.: Wave Motion in Elastic Solids. Courier Corporation, 1991.

33. Fang, F. F. and Howard, W. E.: Negative field-effect mobility on (100) Si surfaces. Phys. Rev. Lett., 16:797–799, May 1966.

34. Davies, J. H.: The Physics of Low-dimensional Semiconductors: An Introduction. Cambridge University Press, 1997.

35. Ando, T., Fowler, A. B., and Stern, F.: Electronic properties of two-dimensional systems. Rev. Mod. Phys., 54:437–672, Apr 1982.

36. Imura, M., Nakajima, K., Liao, M., Koide, Y., and Amano, H.: Growth mechanism of c-axis-oriented AlN on (111) diamond substrates by metal-organic vapor phase epitaxy. Journal of Crystal Growth, 312(8):1325 – 1328, 2010.

37. Momma, K. and Izumi, F.: Vesta 3 for three-dimensional visualization of crystal, volumetric and morphology data. J. Appl. Crystallogr., 44:1272–1276, 2011.

38. Karch, K. and Bechstedt, F.: Ab initio lattice dynamics of BN and AlN: Covalent versus ionic forces. Phys. Rev. B, 56:7404–7415, Sep 1997.

39. M. Komirenko, S., W. Kim, K., Stroscio, M., and Dutta, M.: Energy-dependent electron scattering via interaction with optical phonons in wurtzite crystals and quantum wells. Phys. Rev. B, 61, 01 2000.

40. Park, K., Mohamed, A., Dutta, M., Stroscio, M., and Bayram, C.: Electron Scattering via Interface Optical Phonons with High Group Velocity in Wurtzite GaN-based Quantum Well Heterostructure. Scientific Reports, 8, 12 2018.

41. Mohamed, A., Park, K., Bayram, C., Dutta, M., and Stroscio, M.: Confined and interface optical phonon emission in gan/ingan double barrier quantum well heterostructures. PLOS ONE, 14(4):1–12, 04 2019.

CITED LITERATURE (continued)

42. Lee, B. C., Kim, K. W., Stroscio, M. A., and Dutta, M.: Optical-phonon confinement and scattering in wurtzite heterostructures. Phys. Rev. B, 58:4860–4865, Aug 1998.

VITA

NAME	Giorgio Bonomo
EDUCATION	
	B.S. in Electronic engineering, July 2017, Politecnico of Turin, Italy
	M.S. in Electrical and Computer Engineering, University of Illinois at Chicago, May 2019 (Expected), USA
	Specialization Degree in Electronic Micro and Nano electronics , July 2019 (Expected), Politecnico of Turin, Italy
LANGUAGE SKILLS	
Italian	Native speaker
English	Full working proficiency
	2017 - IELTS examination (7.5)
	A.Y. 2018/19 One Year of study abroad in Chicago, Illinois
	A.Y. 2017/18. 50% of lessons and exams attended exclusively in English
SCHOLARSHIPS	
Fall 2018	Full tuition waiver from UIC for merit
Fall 2018	Italian scholarship for TOP-UIC students
TECHNICAL SKILLS	
Basic level	Python, C#, Verilog, Avogadro, VESTA, LABview
Average level	C, C++, Simulink, Microsoft office, VHDL-AMS, LaTex
Advanced level	Matlab, LTSpice, ModelSim, Quartus, Arduino, VHDL
Analog Devices	PLL, VCO, Tone-Decoder, Amplifiers, ADC/DAC converters, AC/DC converter
Digital Devices	FPGA, Microcontrollers
Laboratory Instrumentation	Oscilloscope (Analog/Digital), Multimeter, Power Supply, Signal generator
NOTABLE PROJECTS	

VITA (continued)

Dec 2018	AES Hardware Trojan Attack
	Realization of two Hardware Trojan against AES encryption system through two different topologies: the first exploits toggling signals, to charge a capacitor and stealthy force a certain value to the encryption key; the second, exploits a non-reliable realization of a Control Unit to insert an malicious state, reached through the insertion of spikes of high frequency on the Clock-signal line, such that it violates the required time constraints.
November 2018	MNIST classification
	Realization of a Neural Network able to recognize the digits represented in pictures taken from the MNIST dataset using the backpropagation algorithm. A 95 % of success rate on the test set has been achieved.
July 2018	Ripple Carry adder in NML technology
	Design through a specific tool (MagCAD) of basic digital circuits such as Half Adders, Full-Adders and Ripple Carry adders, both in iNML and pNML technology. The correct behavior of the designed circuits has been proven through ModelSim simulations.
February 2018	JPEG XT Dedicated Hardware
	Design of a dedicated Datapath and Control Unit in VHDL for the implementation of the algorithm based on the Discrete Cosine Transform described in the JPEG_XT format. ModelSim' simulations have been used to prove the correct functioning.
January 2018	Efficiency measurement of an incandescent light bulb
	Realization of a fully-automated system based on Arduino, capable to gradually light up a small incandescent bulb and measure the variation of efficiency. Matlab code and C# interface have been developed for the storage of data and the required computations.